FY 2008

EVALUATION OF THE 2007 TOYOTA CAMRY HYBRID SYNERGY DRIVE SYSTEM

Prepared by:

Oak Ridge National Laboratory

Mitch Olszewski, Program Manager

Submitted to:

Energy Efficiency and Renewable Energy
FreedomCAR and Vehicle Technologies
Vehicle Systems Team

Susan A. Rogers, Technology Development Manager

April 2008

Engineering Science and Technology Division

EVALUATION OF THE 2007 TOYOTA CAMRY HYBRID SYNERGY DRIVE SYSTEM

T. A. Burress
C. L. Coomer
S. L. Campbell
L. E. Seiber
L. D. Marlino
R. H. Staunton
J. P. Cunningham

ORNL-27 (4-00)

TABLE OF CONTENTS

TABLE OF CONTENTS (cont'd)

Page

LIST OF FIGURES

LIST OF FIGURES (cont'd)

LIST OF TABLES

ACRONYMS AND ABBREVIATIONS

A/C	air conditioning	ID	inner diameter
ac	alternating current	IGBT	insulated-gate bipolar transistor
ANL	Argonne National Laboratory	IPM	intelligent power module
AWG	America wire gauge	LV	low voltage
CAN	controller area network	MG	motor-generator
CT	current transformer	NdFeB	neodymium iron boron
DAQ	data acquisition system	Nm	Newton meter
dc	direct current	NTRC	National Transportation Research Center
DF	dissipation factor	OD	outer diameter
DOE	U.S. Department of Energy	ORNL	Oak Ridge National Laboratory
ECU	electronic control unit	PC	personal computer
ECVT	electronically controlled continuously variable transmission	PCU	power control unit
		PEEMRC	Power Electronics and Electric Machinery Research Center
emf	electromotive force (measured in volts)		
EMI	electromagnetic interference	PI	proportional-integral
ESR	equivalent series resistance	PM	permanent magnet
EV	electric vehicle	PMSM	permanent magnet synchronous motor
FCVT	FreedomCAR and Vehicle Technologies	rms	root mean square
HEV	hybrid electric vehicle	rpm	revolutions per minute
HV	high voltage	Si	silicon
IC	integrated circuit	TC	thermocouple
ICE	internal combustion engine	THS	Toyota Hybrid System

1. INTRODUCTION

The U.S. Department of Energy (DOE) and American automotive manufacturers General Motors, Ford, and DaimlerChrysler began a five-year, cost-shared partnership in 1993. Currently, hybrid electric vehicle (HEV) research and development is conducted by DOE through its FreedomCAR and Vehicle Technologies (FCVT) program. The mission of the FCVT program is to develop more energy efficient and environmentally friendly highway transportation technologies. Program activities include research, development, demonstration, testing, technology validation, and technology transfer. These activities are aimed at developing technologies that can be domestically produced in a clean and cost-competitive manner.

Under the FCVT program, support is provided through a three-phase approach [1] which is intended to:

- Identify overall propulsion and vehicle-related needs by analyzing programmatic goals and reviewing industry's recommendations and requirements, then develop the appropriate technical targets for systems, subsystems, and component research and development activities;

- Develop and validate individual subsystems and components, including electric motors, emission control devices, battery systems, power electronics, accessories, and devices to reduce parasitic losses; and

- Determine how well the components and subassemblies work together in a vehicle environment or as a complete propulsion system and whether the efficiency and performance targets at the vehicle level have been achieved.

The research performed in this area will help remove technical and cost barriers to enable technology for use in such advanced vehicles as hybrid electric, plug-in hybrid electric, electric, and fuel-cell-powered vehicles.

The Oak Ridge National Laboratory's (ORNL) Power Electronics and Electric Machinery Research Center (PEEMRC) performed benchmark assessments and subsystem testing of the 2004 Toyota Prius in 2004–2005. This work has been fully reported in two reports [2,3]. In 2006, the PEEMRC performed similar work on the hybrid version of the 2005 Honda Accord [4]. This report presents the results of benchmark testing of the 2007 Toyota Camry electric drive subsystems.

Subsystem-level testing was conducted by the PEEMRC at ORNL, which is a broad-based research center for power electronics and electric machinery (motor) development. Located in the national user facility known as the National Transportation Research Center (NTRC), the PEEMRC has more than 9000 square feet of space for developing and building the next generation prototypes of power electronics and electric machine technologies.

The 2007 Toyota Camry hybrid is equipped with the Hybrid Synergy Drive system which includes an internal combustion engine (ICE), an electric motor, and a generator. These components are integrated with a power splitting planetary gear which provides various power flow configurations for different modes of operation. The electric motor assists the ICE in providing mechanical drive power for the vehicle and also acts as a generator to recharge the battery during regenerative braking. According to published specifications, Toyota claims the motor can deliver a peak power output of 105 kW (143 hp) at 4500 revolutions per minute (rpm). Toyota has not published a rated torque (or power) versus speed graph for the Camry electric motor and no specifications have been published for the generator. The hybrid version of the Camry features a 2.4-liter 4-cylinder, 16-valve engine, which has a specified peak power output of 110 kW (147 hp) at 6000 rpm [5].

The Camry electric drive system has several features in common with the Toyota Prius system as they both use the Toyota Hybrid System (THS) II. Both make use of the electric motor to provide all of the traction power during acceleration from a stop. This continues until the engine is needed for any of several reasons (more torque, low battery state of charge, high battery temperature, etc.) Both vehicles have a dedicated generator, which is used to route power from the ICE to the electric motor. Both use a clutch-less, electronically controlled continuously variable transmission (ECVT) which uses a planetary gear to manage power flow from the ICE and motor to the differential gear unit. The planetary gear configuration of the ECVT provides the opportunity to operate the ICE throughout a more efficient torque-speed range, depending on the torques and speeds of the generator and electric motor.

Unlike the Toyota Camry and Prius, which are both considered to be full hybrids, the Honda Accord hybrid with its smaller motor is considered to be a "mild hybrid" since the motor never propels the vehicle without engine power. In operation, the 2005 Accord hybrid exhibits enhanced performance compared to the conventionally powered Accord, but little or no gain in fuel economy.

In order to fully benchmark the HEV technology used in the 2007 Camry, a design characterization study was conducted to evaluate the vehicle's hybrid electric drive subsystem. A flow diagram which portrays the baseline benchmarking approach is shown in Fig. 1.1. The characterization study included (1) a design review, (2) a packaging and fabrication assessment, (3) bench-top electrical tests, (4) back-electromotive force (emf) and locked rotor tests, (5) performance and efficiency tests on the motor and inverter, (6) efficiency tests on the bi-directional boost converter, and (7) continuous duration tests of the drive motor and inverter. The design and packaging review includes comparisons to the 2004 Toyota Prius, which was evaluated during previous years. Results from the performance and efficiency tests were used to map electrical and thermal data for motor/inverter operation over the full range of speeds and shaft loads that the motor is capable of producing. The results of the design and packaging assessments are presented in Section 2 and the performance and efficiency tests results are presented in Section 3.
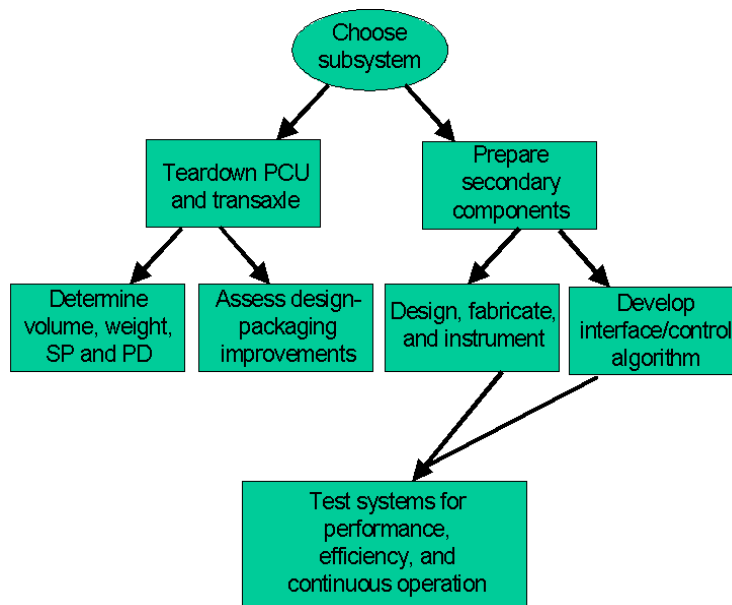
Fig. 1.1. Flow diagram of baseline benchmarking approach.

2. HYBRID ELECTRIC DRIVE SYSTEM DESIGN AND PACKAGING

The hybrid Camry includes significant advancements in HEV technology since the electric drive system features higher peak power and more extensive continuous operation capabilities, yet the size and weight of the system has decreased when compared to that of the Prius. This is primarily due to the care taken in packaging the inverter/converter system and the design of a higher-speed, higher voltage permanent magnet synchronous motor (PMSM). The Camry HEV subsystem design and packaging will be assessed and summarized in this section.

Table 2.1 presents an overview of several general HEV design features and published specifications and indicates similarities and differences between the Camry and Prius vehicles. The primary drive PMSM is referred to as MG2 and the generator is referred to as MG1. Although both PMSMs can function as a motor or a generator, MG2 is commonly referred to as "motor" and MG1 is commonly referred to as "generator." Both MG1 and MG2 are powered by separate three-phase inverters which share the same direct current (dc)-link. The battery voltage is boosted by a bi-directional boost converter which feeds the dc-link. This configuration facilitates the use of multiple power flow modes wherein the ICE, MG1, and/or MG2 may supply energy to the battery pack, the battery pack may supply MG1/MG2 alone, or the ICE and battery pack can simultaneously power the vehicle.

Table 2.1. Comparison of hybrid Camry and the Prius design features and published specifications

Design Feature	Hybrid Camry	2004 Prius
Motor peak power rating	105 kW @ 4500 rpm (disputed to be 70kW)	50 kW @ 1200–1540 rpm
Motor peak torque rating	270 Newton meter (Nm) (667 after speed reduction gear)	400 Nm
Top rotational speed	14,000 rpm (5,670 rpm after speed reduction)	6,000 rpm
Separate generator used?	Yes (although the motor also serves as a generator during regenerative braking)	Same as Camry
Generator specifications	Not published	33 kW
Source of power to MG2	Battery and/or ICE via generator	Same as Camry
PMSM rotor design	Interior permanent magnets (PMs) with "V" configuration at each pole with a reinforcement web in the laminations (middle of the V) to enable high-speed operation	Interior PMs with "V" configuration at each pole (no reinforcement)
Motor winding configuration	Parallel	Series
Number of rotor poles	8	Same as Camry
Boost converter output voltage	250–650 Vdc output	200–500 Vdc output
Boost converter power rating	30 kW	20 kW
PMSM cooling	Oil circulation with water/glycol heat exchanger	Same as Camry
Inverter/converter cooling	Water/glycol loop	Same as Camry
Hybrid transaxle	Planetary gears used for speed reduction and power split	A single planetary gear used for power split
Fan-cooled high-voltage (HV) Ni-MH battery	244.8 V, 6.5 Ah, 30 kW	201.6 V, 6.5 Ah, 20 kW

Design and packaging assessments are presented in Subsections 2.1 and 2.2 beginning with the power control unit (PCU) and concluding with the transaxle. Studies on the PCU include subjects such as general design and packaging, power electronic devices, and multifaceted capacitor assessments. Assessment topics associated with the transaxle are general design and packaging, PMSM design, and magnet hysteresis measurements. These assessments provide useful feedback regarding technological developments and other characteristics needed to determine packaging complexity and fabrication costs.

2.1 PCU

The general locations of the Camry inverters and the bi-directional boost converter assembly are shown in Fig. 2.1. The figure makes evident the fact that the motor and generator inverters, dc-link capacitor, and half of the cold plate comprise about 65% of the total volume. The buck/boost converter and half the cold plate comprise the remaining 35%. The size and proportions of the PCU are similar to that of a conventional 12 Vdc car battery.
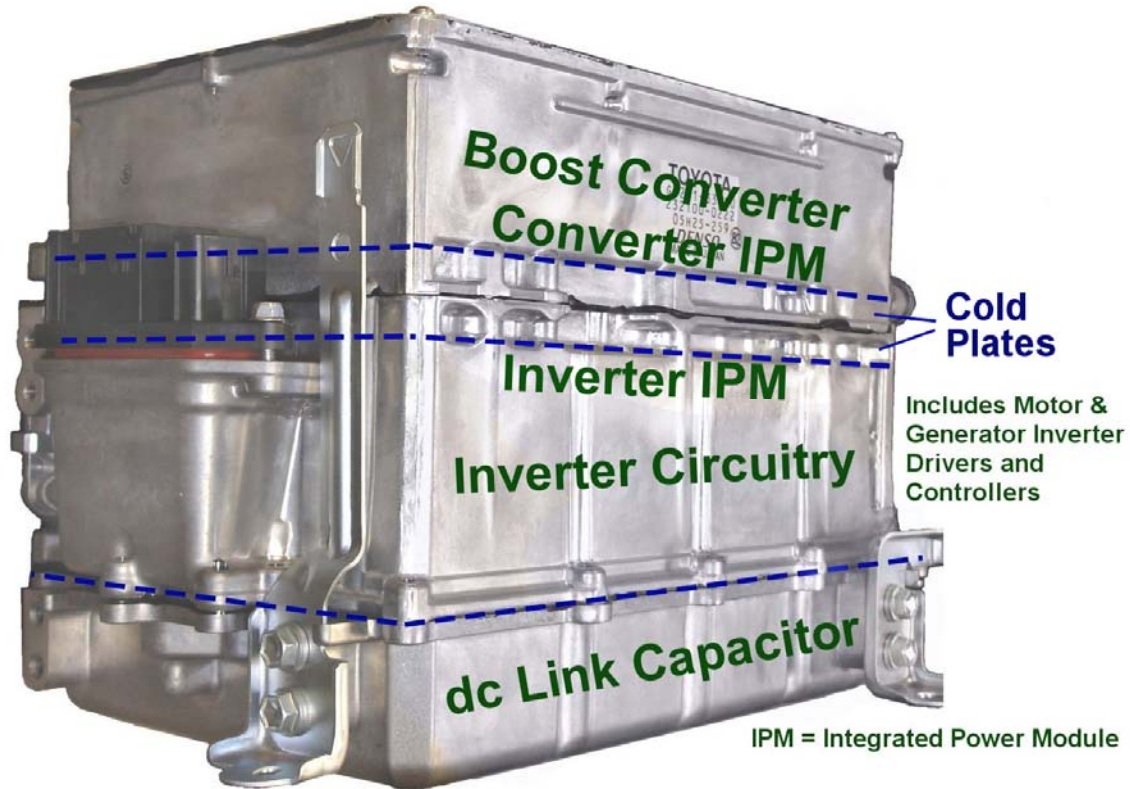
Fig. 2.1. Subsystems of the Camry inverter and converter assembly.

Because the Ni-MH battery is rated at 30 kW, it is assumed that the boost converter will not operate at power levels exceeding 30 kW. Similarly, it is assumed that the motor inverter has a peak power rating that matches the measured power rating of the motor.

The overall circuit diagram of the PCU is shown in Fig. 2.2. A 250 Vdc battery supplies power to the PCU, which is connected to the low voltage (LV) side of the boost converter. A 500 V, 378μF capacitor is connected across the input with a 212 μH inductor between the battery and the boost converter power electronics module. A small 53.8 kΩ resistor, 750 V, 0.9 μF filter capacitor, and 750 V, 2098μF smoothing capacitor is located on the HV side of the boost converter. This HV bus serves as the dc link for both the motor and generator inverter. Table 2.2 provides specification comparisons between the components found in the Prius and Camry PCU. The boosted voltage ranges from 250–650 Vdc depending on driving conditions such as desired acceleration and required regenerative braking and is controlled accordingly by commands from the MG electronic control unit (ECU) and the THS ECU. Detailed capacitor test results are provided in Section 2.1.3.
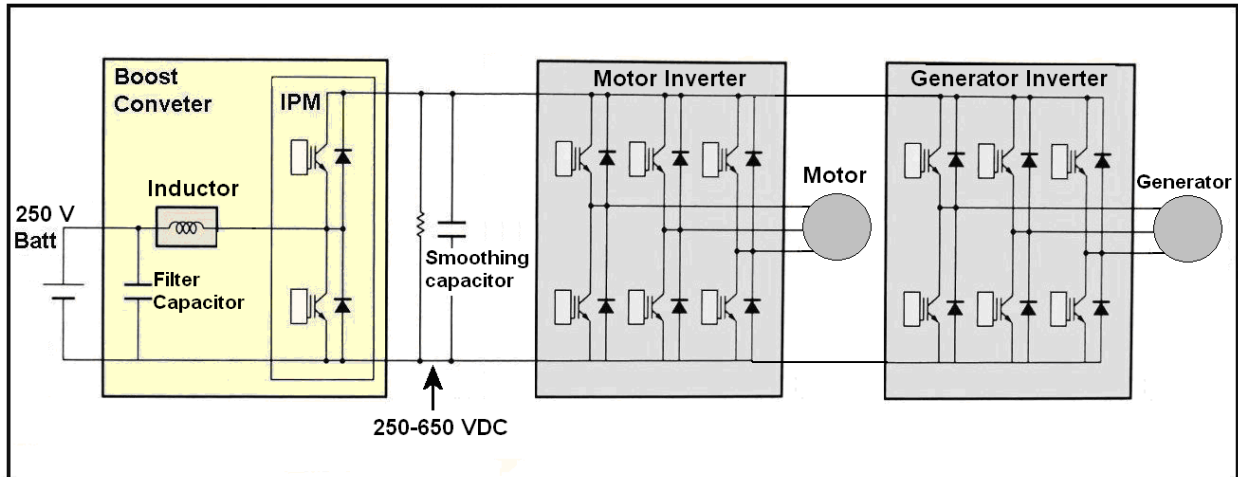
Fig. 2.2. Circuit diagram of PCU.

Table 2.2. Comparison of hybrid Camry and the Prius PCU component specifications

Design Feature	Hybrid Camry	2004 Prius
Boost converter power rating	30 kW	20 kW
Battery voltage	244.8 V	201.6 V
Filter capacitor (LV side)	500 Vdc, 378 µF	600 Vdc, 282 µF
Inductor	212 µH at 1 kHz	373 µH at 1 kHz
Small resistor (HV side)	53.8 kΩ	64.3 kΩ
Small capacitor (HV side)	750 Vdc, 0.9 µF	750 Vdc, 0.1 µF
Smoothing capacitor	750 Vdc, 2098 µF	600 Vdc, 1,130 µF

Figures 2.3 and 2.4 show the converter and inverter compartments, respectively, prior to disassembly. Figure 2.5 shows the general assembly and packaging of the major subcomponents of the Camry inverter and converter. Not shown for the inverter is the dc-link capacitor and its casing which serves as a cover to the inverter assembly. Because the inverter/converter assembly was designed to be integrated into an existing vehicle (the non-hybrid Camry), there was a need to package the unit in a minimal volume, which is evident in the figures provided in this section. The Camry MG ECU is located within the PCU just above the inverter driver board. Communication between the Camry MG ECU and other ECUs is accomplished though controller area network (CAN) digital data transmission. The Prius MG ECU is located outside of the PCU with analog control signals being transmitted over a conductor length of several feet. Together, the MG ECU and THS ECU monitor vehicle conditions and control the PCU components to orchestrate proper system operation.

In the inverter compartment, the controller board includes power regulation electronics, two identical MG microprocessors, a boost-converter microprocessor, two Tamagawa AU2802 integrated circuits (IC) for MG speed/position detection, hardware for CAN communication, MG current measurement, safety interlock devices, and temperature feedback. The driver board includes regulated isolation power supplies, isolated driver electronics, and hardware to prevent faults and overlapping as well as voltage, current, and temperature sensing circuitry for each insulated-gate bipolar transistor (IGBT). More information regarding the power electronics modules for the inverters and converter is provided in Section 2.1.2.
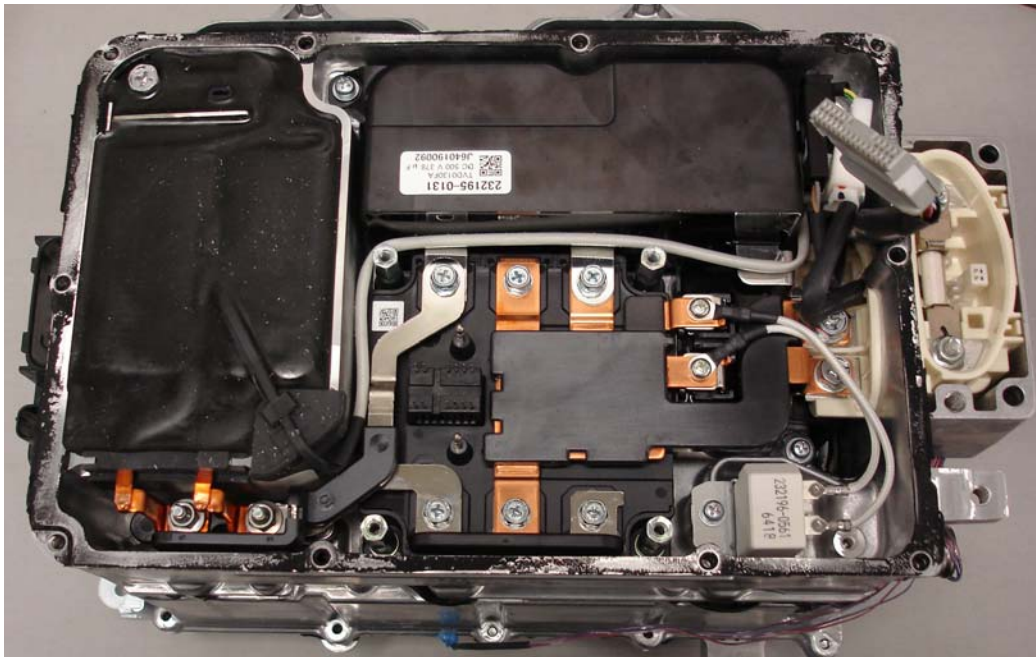
Fig. 2.3. Boost converter compartment with lid and intelligent power module (IPM) driver board removed.
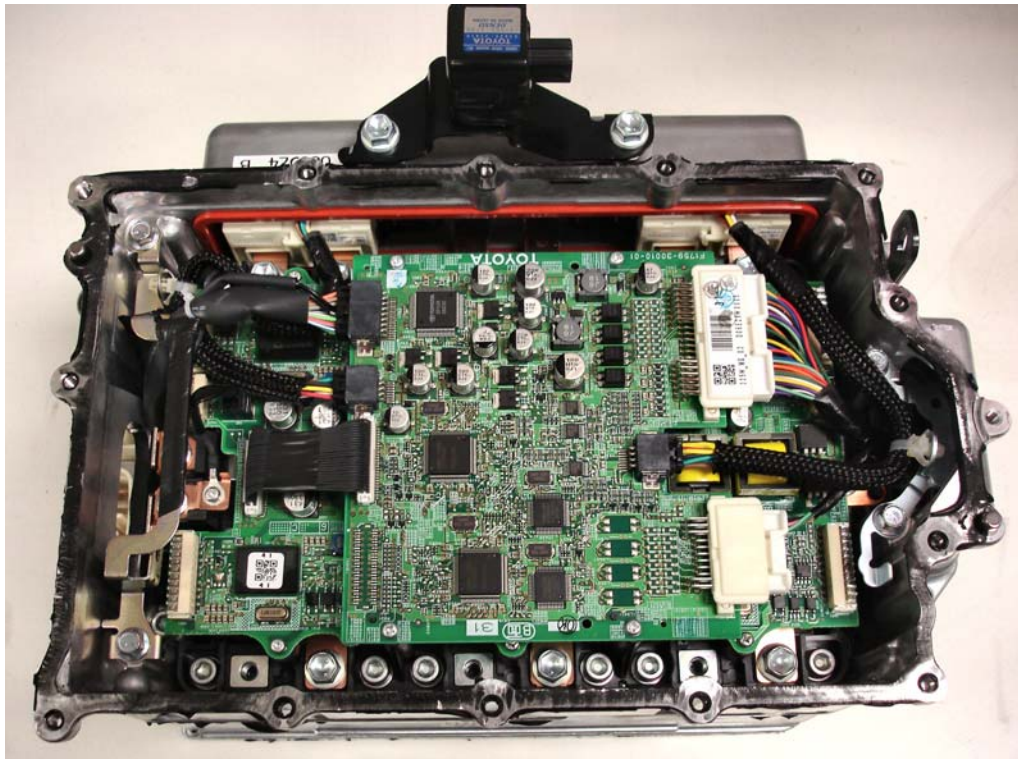
Fig. 2.4. Inverter compartment (upside down) with dc-link capacitor and casing removed.
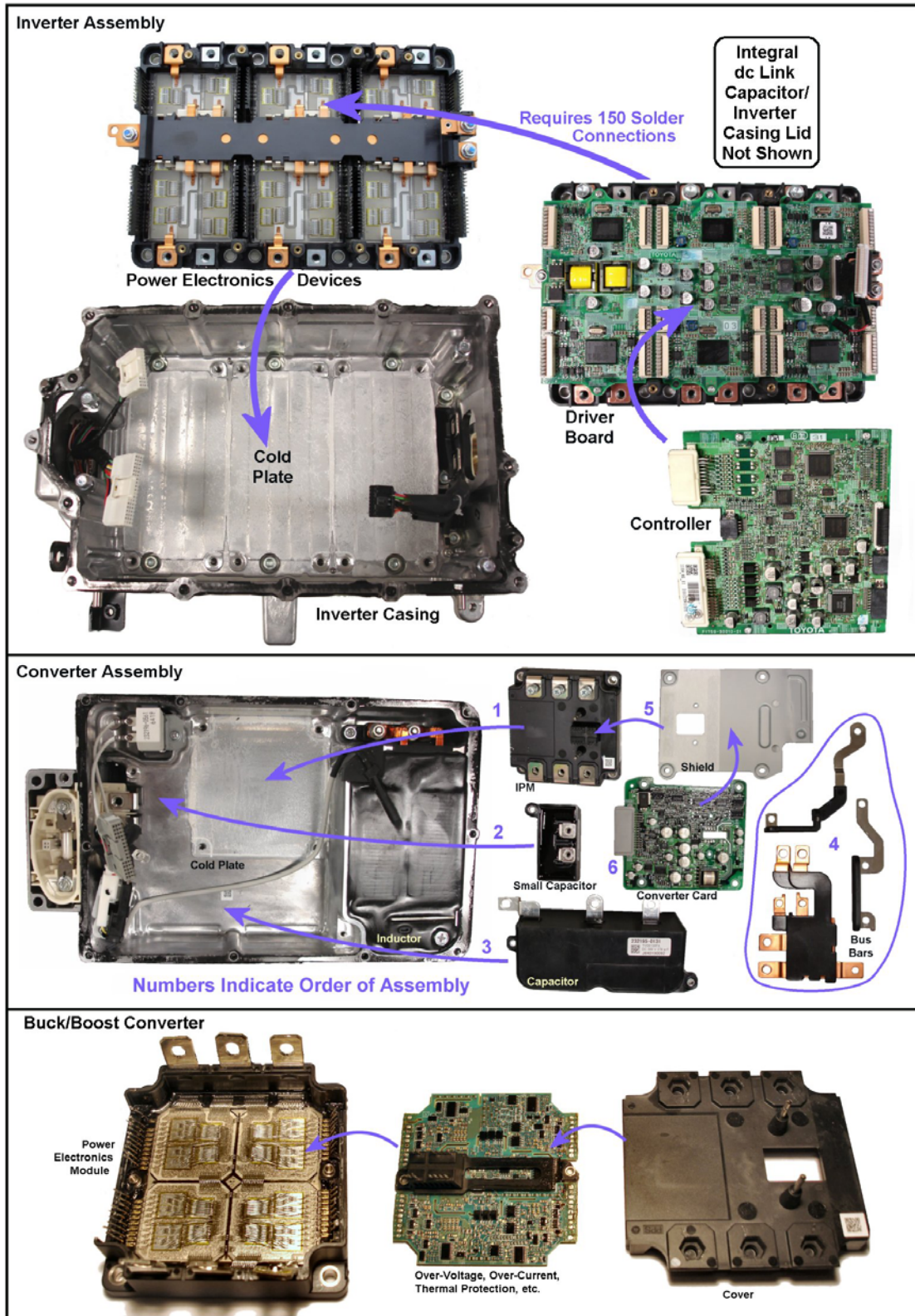
Fig. 2.5. General assembly and packaging of the Camry inverter and converter.

The converter compartment contains the IPM, IPM driver, power supply board, LV filter capacitor, large inductor, bus bars, and an electromagnetic interference (EMI) shield for the circuit board. Additionally, a small filter capacitor and resistor are located in the upper portion of the PCU and are connected to the HV dc link. Connectors are also included for the inductor thermistor and safety interlock device feedback signals.

The Prius has an inverter which supplies power to the air conditioning (A/C) compressor, and it is located in the bottom section of the PCU, whereas the Camry A/C inverter is not housed within the PCU. A dc-dc converter which converts the high battery voltage of about 200V to an accessory voltage level of about 14V is also located in the bottom section of the Prius PCU, whereas this component is located in the battery module of the Camry.

Figure 2.6 shows the cooling plate coolant paths for the converter (top view) and inverter (bottom view) and an enlargement of the converter coolant path configuration. The inverter photo was flipped to make comparisons easier. The holes for the inlet and outlet coolant fittings are shown in the upper and lower left-hand corners of the cold plates. The fins increase the surface area and heat transfer, and the ripples are fabricated in the fin casting to create turbulence, which also increases heat transfer. Asymmetric features in the channel walls and/or no-fin areas promote mixing. In general, the design features are likely the result of detailed heat transfer/coolant flow modeling.
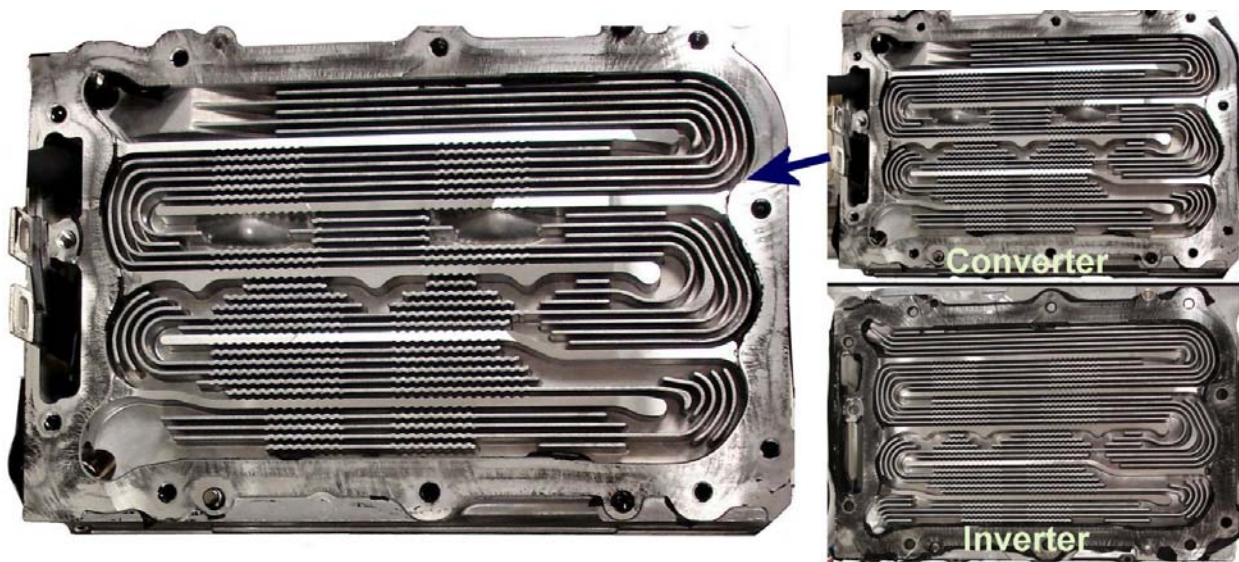
Fig. 2.6. Coolant flow paths in mating converter and inverter cold plates.

Table 2.3 provides physical measurements of the hybrid Camry inverter and boost converter. The inverter/converter casing was unbolted and separated in order to obtain precise mass measurements that are reflected in the total mass shown for each subsystem. The table also gives estimates for the mass and volume of the motor inverter by itself (i.e., excluding the generator inverter).

For certain components, the dimensions and volumes are approximate since the geometries are sometimes irregular. The entire aluminum casing unbolts and separates midway through the thickness of the cold plate and the volumes are divided up between the inverter and converter accordingly.

The mass of the large, potted inductor used in the buck/boost converter, although an integral part of the converter casing, is estimated to be 3.0 kg. This estimate was derived by subtracting the estimated mass of the converter aluminum (2.0 kg) from the total measured mass of the two (5.02 kg).

Table 2.3. Mass and volume measurements for the hybrid Camry inverter and converter

Item	Mass (kg)	Volume (L)	Dimensions (cm)
Inverter/converter as received from OEM.	17.86 (17.42 without mounting brackets)	11.7	Summation of inverter and converter sections (below)
Inverters (MG1 and MG2)			
DC-link capacitor mold in an aluminum case.	3.57	2.6	$18.5 \times 27 \times 5.3$
Side housing assembly containing the three-phase bus connectors and current transformers (CTs).	1.2	0.98	$\sim 4.5 \times 23 \times 9.5$
Inverter electronics and main casing to mid-point of cooling plate.	5	4.3	$18.5 \times 27 \times 10.5$
Connector and housing at end of casing.	(incl. above)	0.31	$10.2 \times 3.8 \times \sim 8$
Complete inverters	**9.8**	**8.19**	Combine the above
Inverter for motor only			
DC-link capacitor mold in an aluminum case.	3.57	2.6	$18.5 \times 27 \times 5.3$
Side housing assembly containing the three-phase bus connectors and CTs.	0.69	0.56	$\sim 4.5 \times 12 \times 9.5$
Inverter electronics and main casing to mid-point of cooling plate.	~3.3	~2.8	$11.1 \times 27 \times 10.5$
Complete motor inverter	**~7.5**	**~6**	Combine the above
Converter			
Boost converter inductor.	~3.5	1.14	$8.8 \times 17.5 \times 7.4$
Converter filter capacitor.	0.57	0.84	$6.3 \times 18.1 \times 7.4$
Electronics compartment and casing.	$\sim 0.9 + 1.7$	1.51	$11.3 \times 18.1 \times 7.4$
Complete converter	**~6.6**	**3.5**	$17.5 \times 26.9 \times 7.4$

Based on the results shown in Table 2.3, Table 2.4 provides the peak power density and peak specific power of both the motor inverter and the bi-directional boost converter. Comparisons to corresponding estimates for the Prius are also shown. The Camry specifications in Table 2.4 are very impressive as the power density of the motor inverter and bi-directional boost converter has more than doubled when compared to that of the Prius. The Camry motor inverter specific power is also significantly larger, yet the boost converter specific power is only slightly higher as the mass increase closely followed the rated power increase.

Table 2.4. Specific power and power density estimates for inverter/converter

Parameter	Camry	Prius
Motor inverter peak specific power (without converter), kW/kg.	70/~7.5 = **~9.3**	50/8.8 = **5.7**
Motor inverter peak power density (without converter), kW/L.	70/~6 = **~11.7**	50/8.7 = **5.7**
Bi-directional boost converter specific power, kW/kg.	30/~6.6 = **~4.5**	20/4.8 = **4.2**
Bi-directional boost converter power density, kW/L.	30/3.5 = **8.6**	20/5.1 = **3.9**[1]

[1] This low converter power density is largely the result of the non-optimal packaging of the converter filter capacitor in the Prius inverter/converter housing.

It is interesting to note that the converter mass increased by 38% and the volume decreased by 31% in going from the 2004 Prius to the 2007 Camry PCU design. A mass increase is likely unavoidable given that the power increased from ~20 kW to ~30 kW. Regarding the decrease of volume, the Camry converter has a small amount of associated null space as is evident in Fig. 2.7 while the Prius converter design (Fig. 2.8) integrates a tall inductor next to a short IPM resulting in wasted space above the IPM and additional wasted space exists around both components. Not shown in Fig. 2.8 is the volume of the converter portion of the monolithic capacitor module and surrounding space. Although the *potential* exists for easily reducing the volume of the Prius converter, the volume calculation is based on the actual dimensions of the casing. However, the component specifications are provided separately to allow for various approaches of calculating specific power and power density. See Appendix A for details on the measurement of the Prius PCU and motor inverter mass and volumetric assessment details.

Fig. 2.7. Converter assembly with subsections shown consistent with volume measurements.
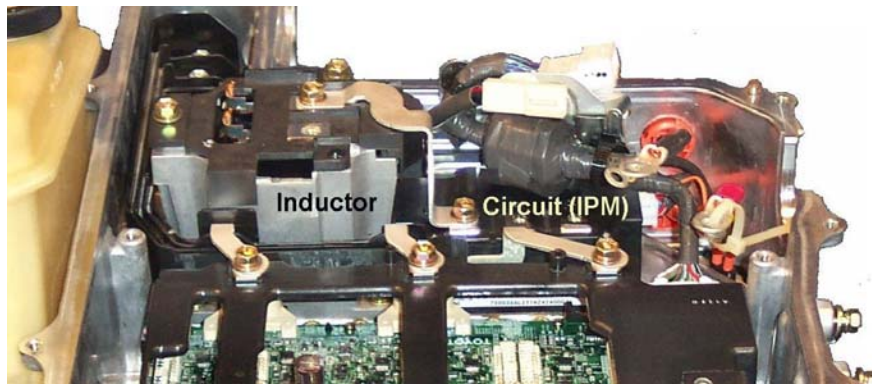
Fig. 2.8. Non-optimized packaging used in the 2004 Prius converter.

All capacitors located within the Camry PCU are shown in Fig. 2.9 for a comparison of sizes. It is important to note that that the Prius capacitor module contains both capacitors which are connected to the HV and LV side of the bi-directional boost converter as well as a small filter capacitor, whereas the Camry capacitors are housed in separate modules. Figure 2.10 shows the Camry dc-link capacitor and a negative image of an x-ray of the capacitor. The x-ray shows that there are two rows of 12 discrete sub-modules inside the entire capacitor module, with each capacitor having a capacitance of 87 µF. The equivalent Prius capacitor has 8–142 µF capacitors in parallel to provide a total capacitance of 1,130 µF. Figure 2.11 shows the 378 µF Camry filter capacitor and an x-ray of the capacitor which is across the battery input of the PCU. As suggested by the x-ray image, the 378 µF capacitance is attained with two 189 µF capacitors in parallel. Similarly, the small 0.9 µF capacitor is made up of two 0.45 µF capacitors,

as shown in Fig. 2.12. Various characteristics of these capacitors were measured and are presented in Section 2.1.3.

Fig. 2.9. Comparison of all capacitors located within Camry PCU.

dc Link Capacitor: 2098 ufd @ 700 v

X-ray of Capacitor Module: 24 submodules (~87 uF each)
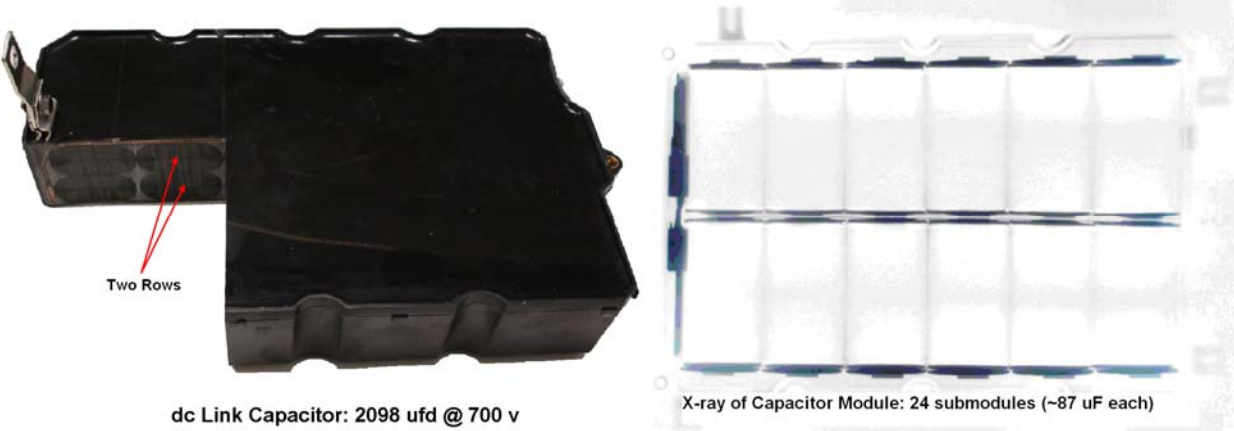
Fig. 2.10. Cutaway of dc-link capacitor removed from shell (left) and x-ray of module (right).

Fig. 2.11. Battery level capacitor (upper) and x-ray of module (lower).

Fig. 2.12. Small dc-link capacitor: overhead view (left) and x-ray of module – side view (lower).

Figure 2.13 shows a view of the inverter/converter assembly upside down with the three-phase motor and generator bus connector assembly unbolted and detached. It can be seen that CTs are used on two of the three bus connectors. The red rubber seal inserts into the inverter housing in order to facilitate a sealed union. In general, the inverter and converter housings are very well sealed and are water tight to prevent contamination and corrosion from environmental effects.
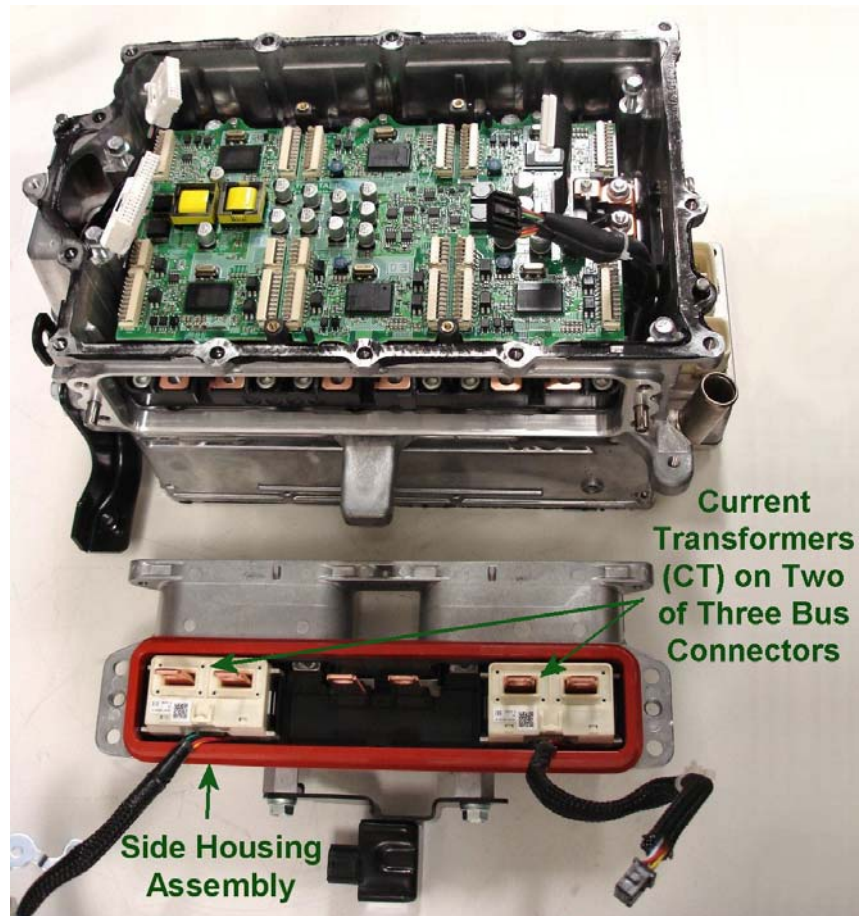
Fig. 2.13. Side housing removed from inverter section of PCU (shown upside down).

2.1.1 Power Electronics Devices

The general packaging features of the Camry inverter and converter power electronic devices were assessed and compared to the Prius designs. Figure 2.14 shows a comparison between the Camry and the Prius IPMs which were photographed while sitting adjacent to each other. All power electronic devices shown are immersed in a high-temperature, protective silicone gel. Although the power capability of the IPM increases from the Prius to the Camry, the size of the IPM noticeably decreases. The general layout of the IPM design is similar, wherein the shared dc bus, indicated by the red line, runs between the motor and generator inverters. However, a closer inspection yields several differences between the two. Bus bars are used to interconnect the dc link and phase outputs to the power electronics devices of the Prius IPM, yet the Camry IPM does not use a conventional bus bar architecture to accomplish this task. Instead, a more interweaved layout is used which enhances the area utilization of the IPM. The Camry IPM layout allows for the space below the dc-bus bars to be used as extra surface area for power electronics devices, as shown in Fig. 2.15. It can also be noticed that there is enough space for the Camry generator inverter to contain twice the number of IGBTs than what is currently present. Toyota has made an effort to standardize the size of the PCU and this space is likely utilized in HEVs with larger power trains, such as the Toyota Highlander HEV or the Lexus GS450h. The maximum power supplied to the motor inverter must be less than (due to losses) the sum of the battery power and the generator power. It is likely that the full capability of the motor inverter is not fully utilized in the vehicle, as the generator inverter can supply only 1/3 of the power capability to the motor inverter and any additional power must be supplied by the battery which has a power rating of 30 kW, and the combined peak power is approximately 70 kW.

13
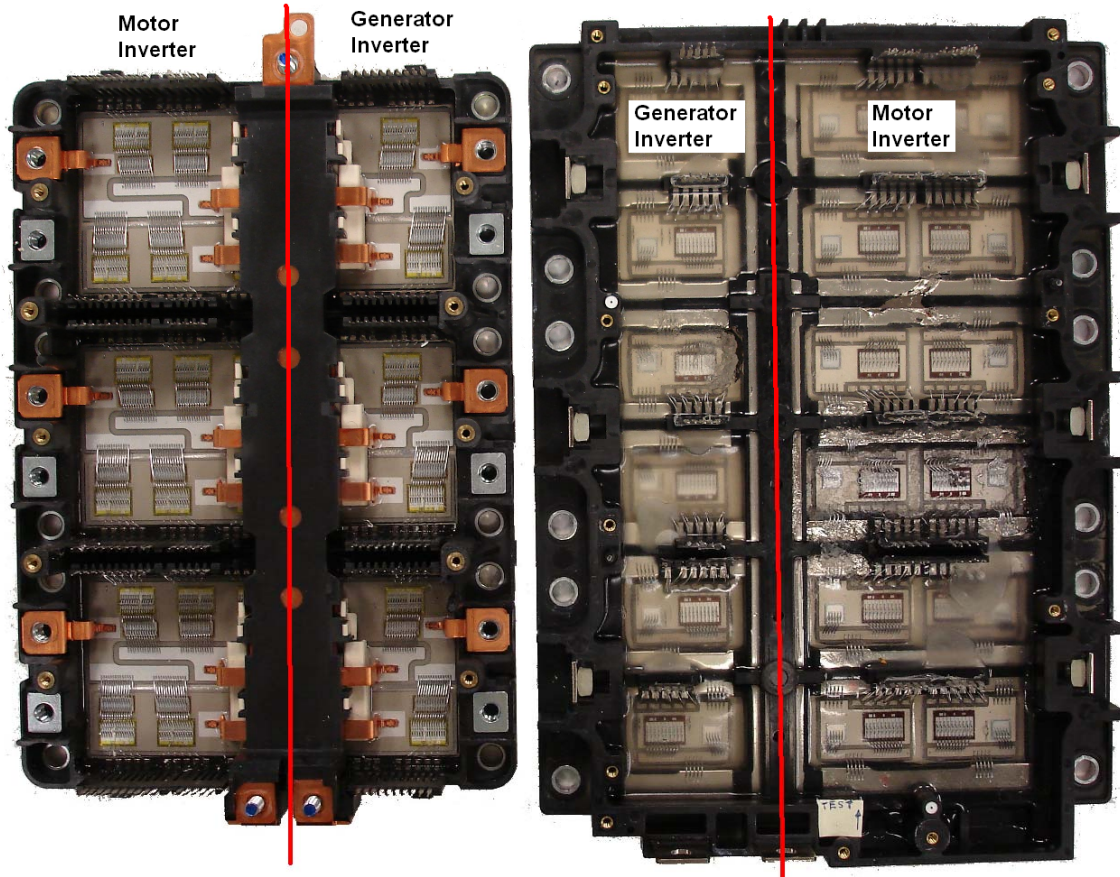
Fig. 2.14. Comparison of Camry inverter IPM (left) and Prius inverter IPM (right).
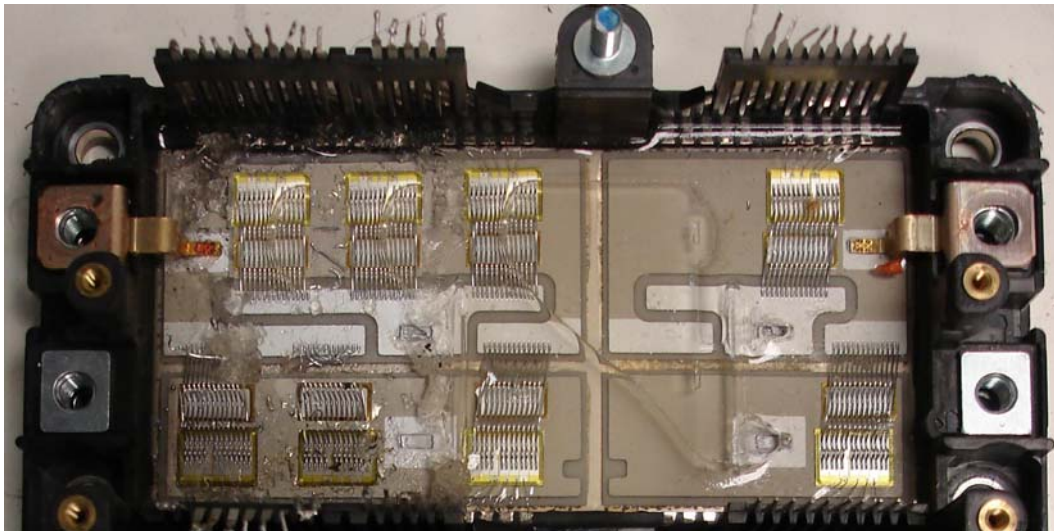
Fig. 2.15. Camry IPM with dc-bus bars removed.

Figure 2.16 provides a more detailed representation of the design discrepancies as well as a dimensional comparison of the IGBTs and diodes of the Camry and Prius inverter power electronics. Since the emitters and collectors of the Camry IPM are not connected to bus bars as they are in the Prius, additional room is available for situating the diodes in an orientation which is more efficient in terms of surface area

utilization. In the Prius inverter image shown in Fig. 2.16, the IGBT emitter and diode anode are tied to a common metal plate, which is connected to a bus bar that is partially visible on the left edge of the image. The IGBT collector and diode cathode are connected to a bar which is just beyond the right edge of the image. Conversely, the Camry dc link and three-phase outputs connect directly to the emitter-anode common plate and the collector-cathode surface, thereby eliminating the use of a bus bar infrastructure.
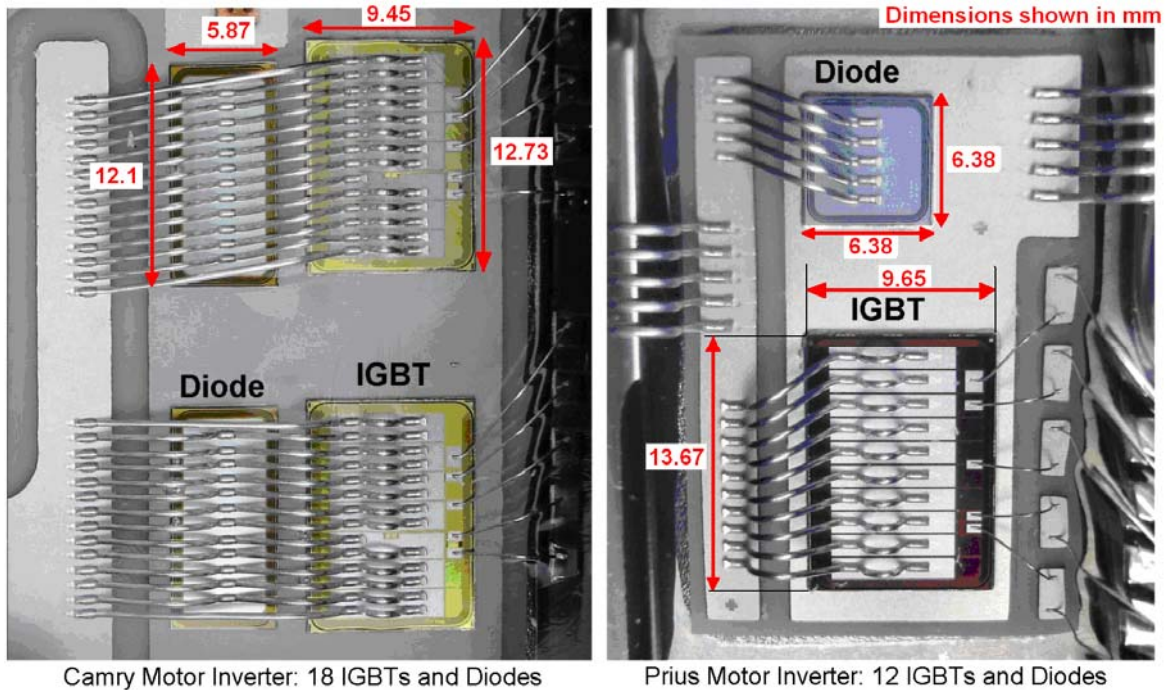
Fig. 2.16. Dimensions (in mm) of Camry inverter IPM (left) and Prius inverter IPM (right).

As indicated by the labeled dimensions, the Camry inverter IGBT size has decreased from the Prius inverter IGBT size in both length and width, whereas the size of the diode increased significantly. Although the Camry IGBT chip size has decreased when compared to that of the Prius IGBT, the power capability has increased slightly. This is primarily due to the use of a trench gate structure as opposed to the planar gate structure used in the Prius. The planar gate structure includes areas in the drift region below the emitter "n+" and "p" regions which do not pass as much current as the drift region areas below the gate. This inefficiency is due to the shape of the inversion layer which is formed when using a planar gate structure. An IGBT with a trench gate structure forms a more uniform inversion layer during on-state operation, and therefore higher current densities are created in the drift region. Additionally, the voltage rating of the Camry IGBT devices has increased, facilitating higher power capability and higher power density of the generator, motor, and the respective inverters.

A detailed comparison of the Camry and Prius IGBTs is shown in Fig. 2.17. The Camry IGBT contains two wire bonds for each emitter strip, whereas the Prius only has one wire bond for each emitter strip. Both IGBTs include leads for semiconductor junction temperature measurement feedback, gate voltage control, current measurement, and emitter voltage feedback. These signals are used to control the device and prevent fault conditions from occurring. Cross-sectional views of the IGBTs are provided in Fig. 2.18. Small metallic nodes are visible on the Camry IGBT, yet there is no evidence of these nodes on the Prius IGBT. These nodes are likely associated with the trench gate structure, but are not directly associated with the trench pitch as the metal nodes are separated by about 20 μm, which is much larger than typical trench pitches.
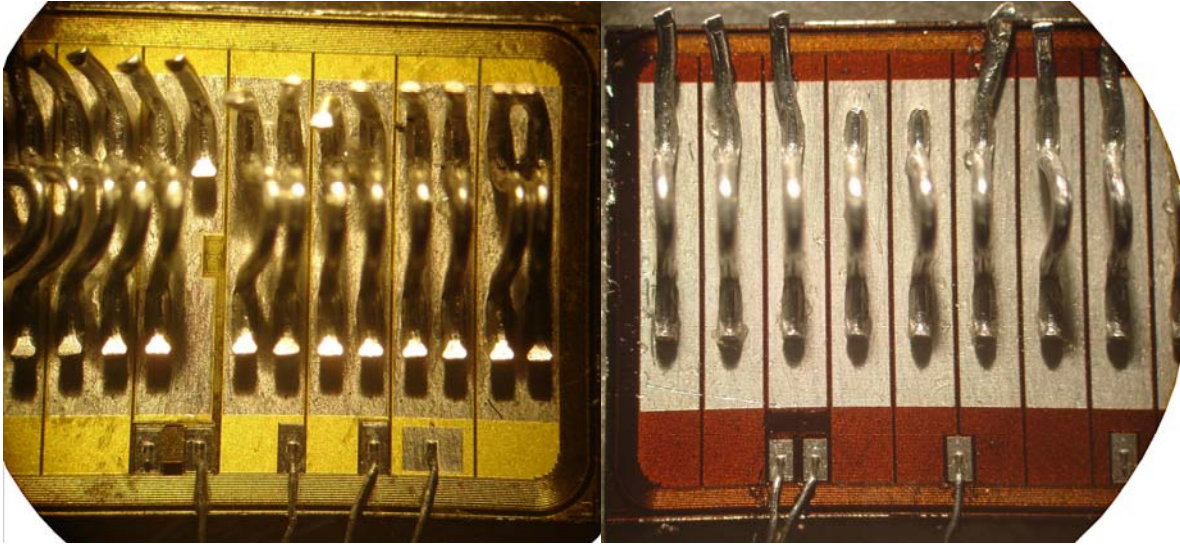
Fig. 2.17. Close-up view of Camry inverter IGBT (left) and Prius inverter IGBT (right).
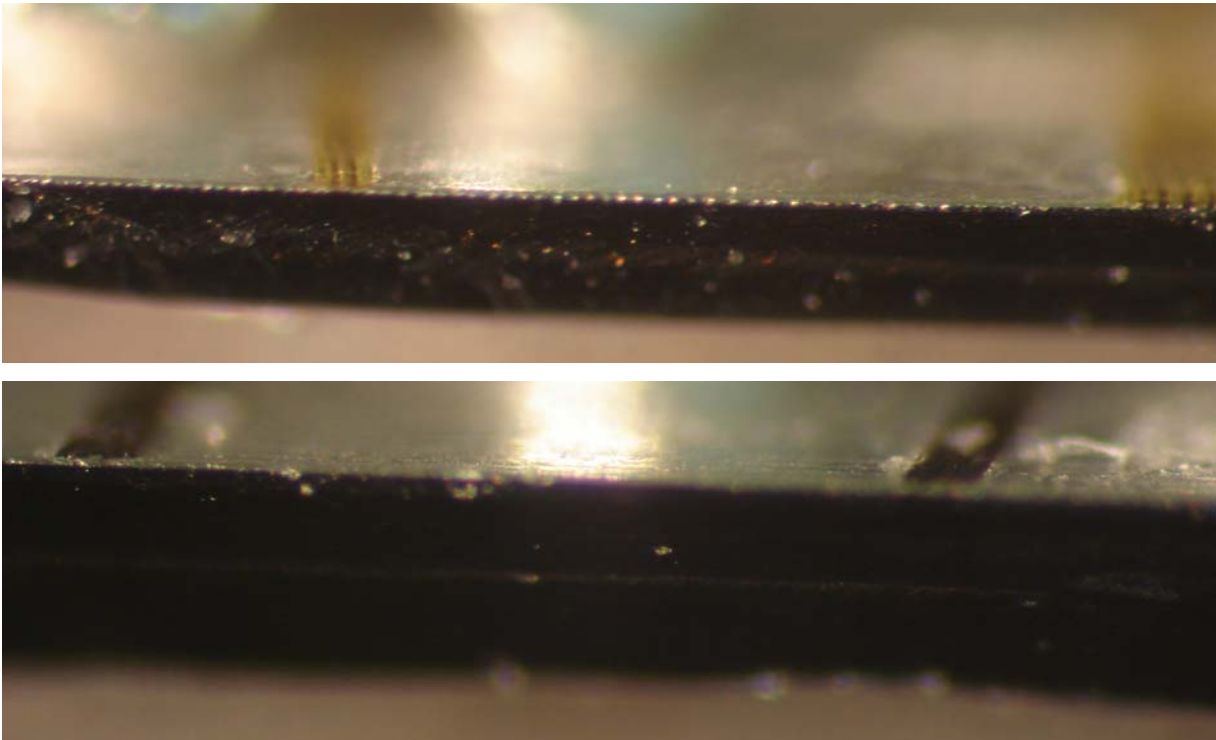
Fig. 2.18. Cross-sectional view of Camry IGBT (upper) and Prius IGBT (lower).

Diodes from the Camry and Prius inverters are shown in Fig. 2.19. The shape of the Camry inverter diode is elongated providing well-suited orientation with the adjacent IGBT. Several traces are located around the perimeter of the Camry and Prius diodes and IGBTs, which is possibly a preventative measure against catastrophic arcing.

Fig. 2.19. Close-up view of Camry inverter diode (left) and Prius inverter diode (right).

The Camry and Prius boost converter IPMs are shown in Fig. 2.20. Although the power rating of the boost converter has increased by 50% from the Prius, the area of the Camry boost converter IPM footprint is only slightly larger than that of the Prius. Similar to the discrepancies between the inverters, smaller bus architecture is used in the Camry boost converter IPM. There is a considerably larger amount of null space within the Prius boost converter module. The Camry boost converter has four IGBTs and diodes in parallel for the upper portion of the IPM and four IGBTs and diodes in parallel for the lower portion of the IPM. The four upper IGBTs and four lower diodes are primarily used during regenerative braking and recharging situations. The four lower IGBTs and four upper diodes are primarily used to boost the battery voltage. The Prius boost converter IPM is similar in functionality, but has only two IGBTs and two diodes in parallel for the upper and lower portions. The Prius boost converter IPM also only has three terminals versus six on the Camry IPM, four of which are used to conduct power. The upper-left terminal does not connect to the IPM, but serves as a support for the negative dc-link bus bar and capacitor connection. The lower-left terminal serves as a support for the positive dc-link bus bar (which connects to the inductor) and capacitor connection, and through a small wire it is connected to a pin which interfaces with the IPM driver-board.
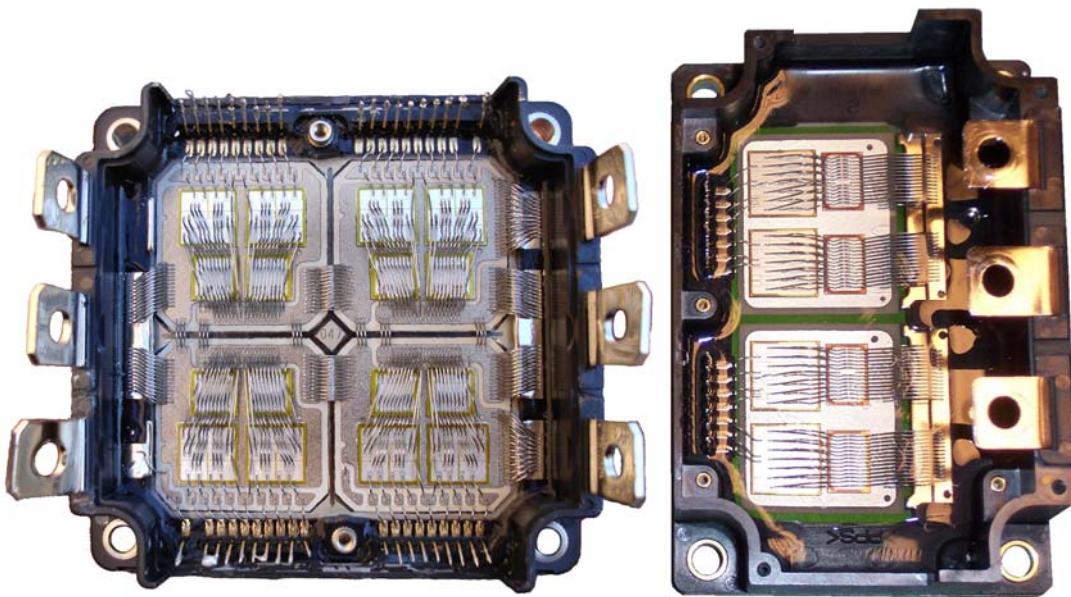
Fig. 2.20. Comparison of Camry converter IPM (left) and Prius converter IPM (right).

Figure 2.21 provides a close-up comparison of the power electronics devices of the Camry and Prius boost converter IPMs. The fabrication process for the Camry boost converter IPM is more intricate due to the increased number of devices that need to be interconnected, thereby increasing wire bond count and driver and sensor feedback signals.
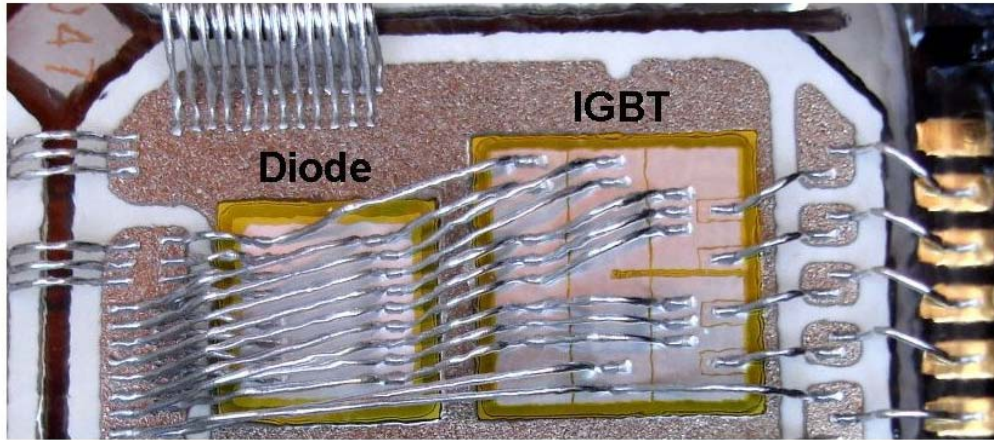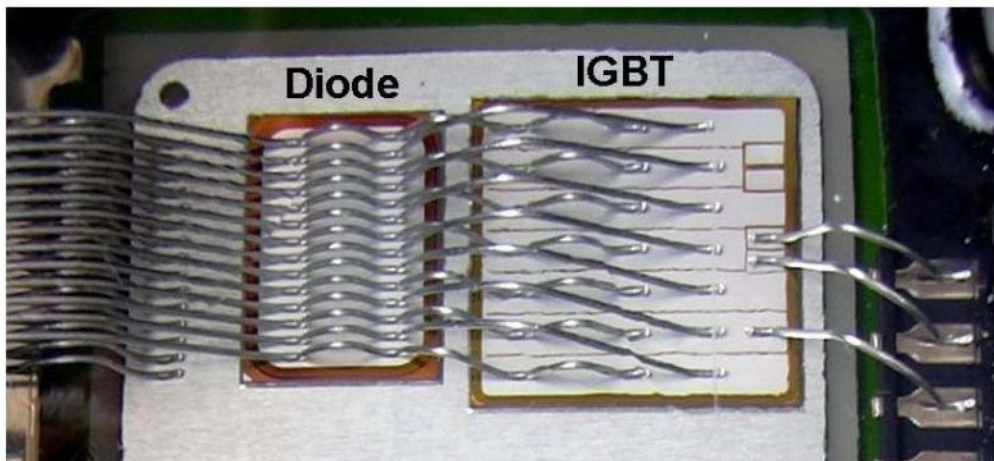
Fig. 2.21. Close-up comparison of Camry converter IPM (upper) and Prius converter IPM (lower).

Table 2.5 summarizes the device count, wire-to-silicon (Si) bond count on the emitter surface, and amount of Si used in the Camry and Prius motor inverters and boost converters. The ratios of heat spreader area to total power electronic device Si area for the Camry motor inverter and boost converter are 10.1 and 4.3, respectively. The smaller ratio suggests a great success in size reduction (i.e., a small heat sink relative to the amount of Si). For comparison, the corresponding ratios for the Prius are 21.7 and 6.8. Again, these improvements are the result of the challenges of implementing the hybrid system into an already existing vehicle, whereas the Prius was strictly designed to be an HEV where volumetric constraints were not as restrictive.

Table 2.5. Summary of power electronic device packaging

Parameter	Motor Inverter		Buck/Boost Converter	
	IGBTs	**Diodes**	**IGBTs**	**Diodes**
Camry				
Number of devices	18	18	8	8
Emitter wire bond count per device.	27	12	18	17
Area of total Si die per device, mm^2.	120.3	71	177	104
Summation of Si area, mm^2.	2165	1278	1400	830
Heat spreader area/Si area.	34800/3443 = 10.1		9530/2230 = 4.3	
Prius (for comparison)				
Number of devices.	12	12	4	4
Emitter wire bond count per device.	20	5	21	28
Area of total Si die per device, mm^2.	131.9	40.7	228	119
Summation of Si area, mm^2.	1583	488	910	475
Heat spreader area/Si area.	45100/2071 = 21.7		9400/1385 = 6.8	

2.1.2 Capacitor Test Results

As capacitor technologies mature, it is important to ascertain the capabilities and limitations of these new technologies by subjecting them to standardized tests to evaluate their characteristics. Test results will assist in benchmarking not only the capabilities and limitations of these technologies, but also to provide a baseline for comparison. All the capacitors studied are of the metallized plastic film type and were manufactured by Matsushita under the Panasonic brand name, except for the large Camry dc-link capacitor which was manufactured by Nichicon. As noted in Section 2.1, the capacitor modules are made up of several sub-capacitors. Tests were conducted upon the entire modules as well as the individual capacitors which were destructively removed from the entire module.

Capacitor tests were conducted both statically and dynamically. The former is a capacitor parameter assessment and the latter is a thermal characteristic assessment. The static test mode does not entail an externally applied dc-bias voltage and ripple current, but uses only signals supplied by an LCR meter. The capacitor parameters that are measured in the static mode are: (1) equivalent series resistance (ESR), (2) dissipation factor (DF), and (3) capacitance value. The capacitor is placed in an environmental chamber and the temperature is cycled through temperatures ranging from -40º to 140 ºC using steps of 20ºC. These three parameters are measured at each temperature step.

The ESR is the real component of the equivalent impedance of the capacitor and corresponds directly with total energy loss which is dissipated as heat during operation. The DF is the ratio of the ESR over the capacitive reactance, which simplifies to ωRC and will be represented as the percentage of real power associated with a particular reactive power component. Both of these parameters were measured during static tests and the results were plotted over a wide frequency and temperature range.

In dynamic tests, a dc-bias voltage and ripple current is applied to the capacitor and the temperature of the capacitor is monitored. When a capacitor is used on a dc bus, the maximum ripple current capability is an important specification. The dynamic test determines the amount of heat generated by the capacitor as a function of ripple current at various ambient temperatures.

2.1.2.1   Static capacitor test results of the 2098 µF dc-link smoothing capacitor module

The data acquisition system (DAQ) consists of a Dell Precision 380 Workstation running LABView 8.5. In the static mode, the instruments used to log data are an Espec environmental chamber and an Agilent 4284 LCR meter. At the beginning of the static thermal cycling tests, after all temperature steps and test frequencies have been entered, the program turns on the environmental chamber and commands a target temperature to the chamber. After the target temperature has been reached and a pre-programmed delay time has been met, the program sends a command to the LCR meter to output the first test frequency and then begins to monitor the ESR from the capacitor under test. When that value is stable, the ESR is recorded and the next parameter is measured and recorded. After the values for ESR, DF, and capacitance are recorded at the first test frequency, the command is given to the LCR meter to output the next test frequency and the monitoring and recording process is repeated. After all data are recorded at all test frequencies, the next temperature step is commanded to the environmental chamber and the process is repeated.

The Camry capacitor module was tested in the static mode from -40 to 140°C over a frequency range of 100 Hz to 30 kHz. ESR, DF, and capacitance was measured and recorded. An interesting fact is observed in Fig. 2.22 as the capacitance approaches infinity beyond 16 kHz. The module can be represented as an RLC circuit with very small resistance and inductance. At high frequencies, even a small parasitic inductance component has a significant influence upon the entire equivalent reactance of the module. There is a certain resonant frequency where the capacitive (negative reactance) effect and inductive (positive reactance) effect are equal, and therefore the total reactance is zero and the imaginary admittance or susceptance is infinite. Thus, the equivalent capacitance approaches infinity as the frequency approaches resonant frequency. Just beyond the resonant frequency, the equivalent reactance is inductive and increases from zero as frequency increases. Figure 2.23 shows that the Prius capacitor module also has a similar effect near 15 kHz. As discussed shortly hereafter in Section 2.1.2.4, additional tests were conducted to investigate this matter further.
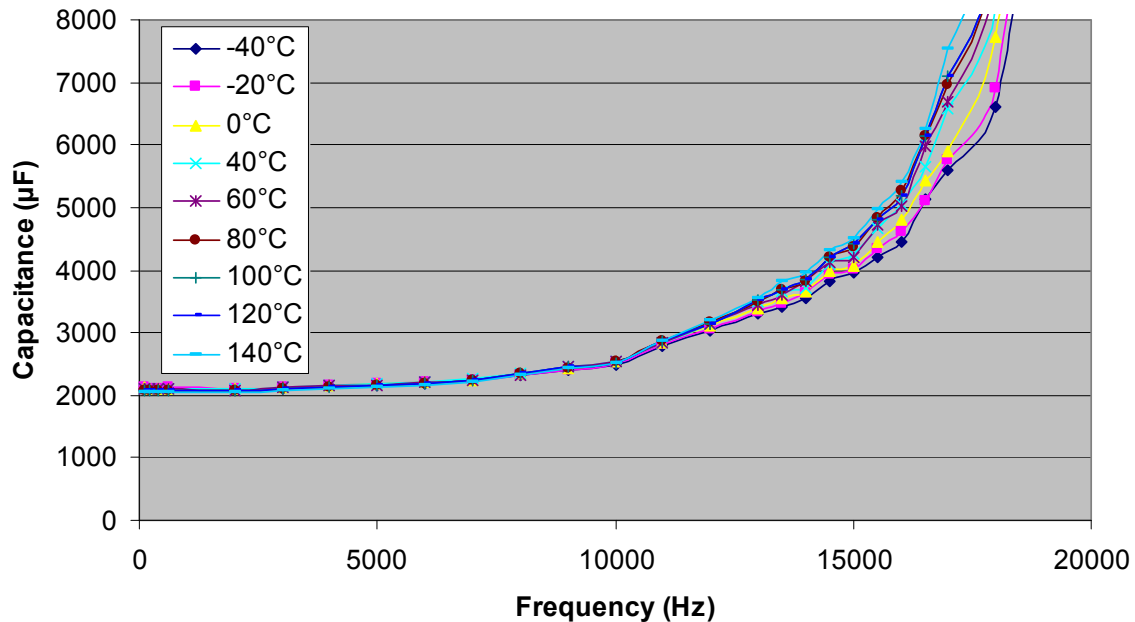
Fig. 2.22. Camry capacitor module equivalent capacitance vs. frequency.
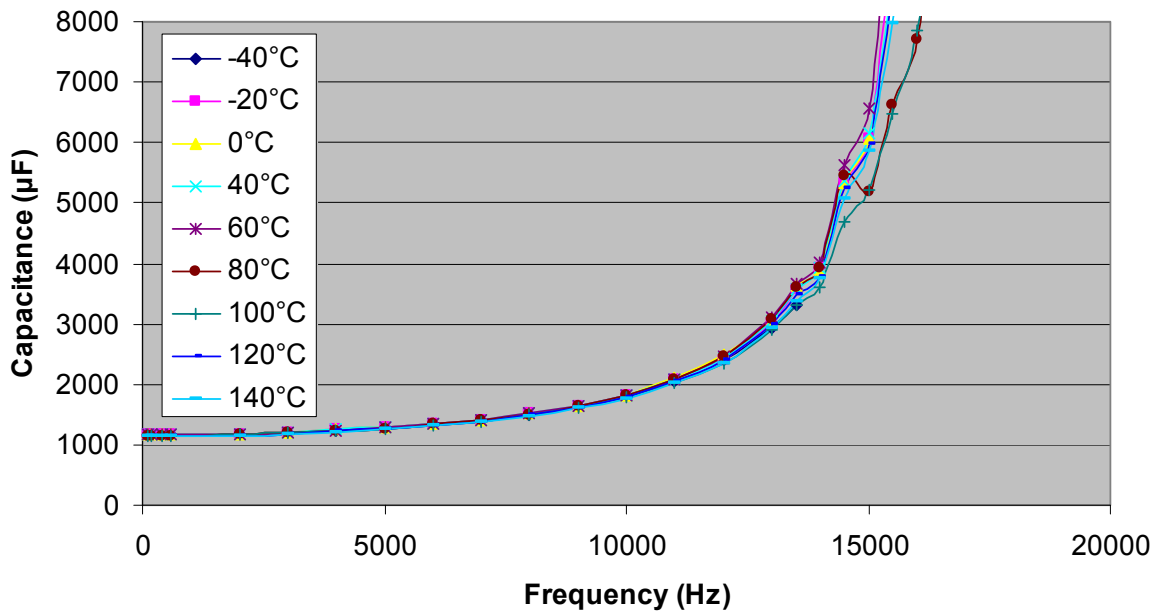
Fig. 2.23. Prius capacitor module equivalent capacitance vs. frequency.

As shown in Fig. 2.24, the response of the entire Camry module capacitance was very minimal over the full temperature range. The largest change in capacitance over the temperature range is observed at 15 kHz, which is also the frequency at which the highest capacitance was measured. For low frequencies, capacitance tended to increase with increasing temperature until peaking at a particular temperature and then the capacitance decreased slightly as temperature increased above this temperature. This peak capacitance temperature increased with increasing frequency. The Prius capacitor module showed similar effect and slight variation of capacitance with temperature.
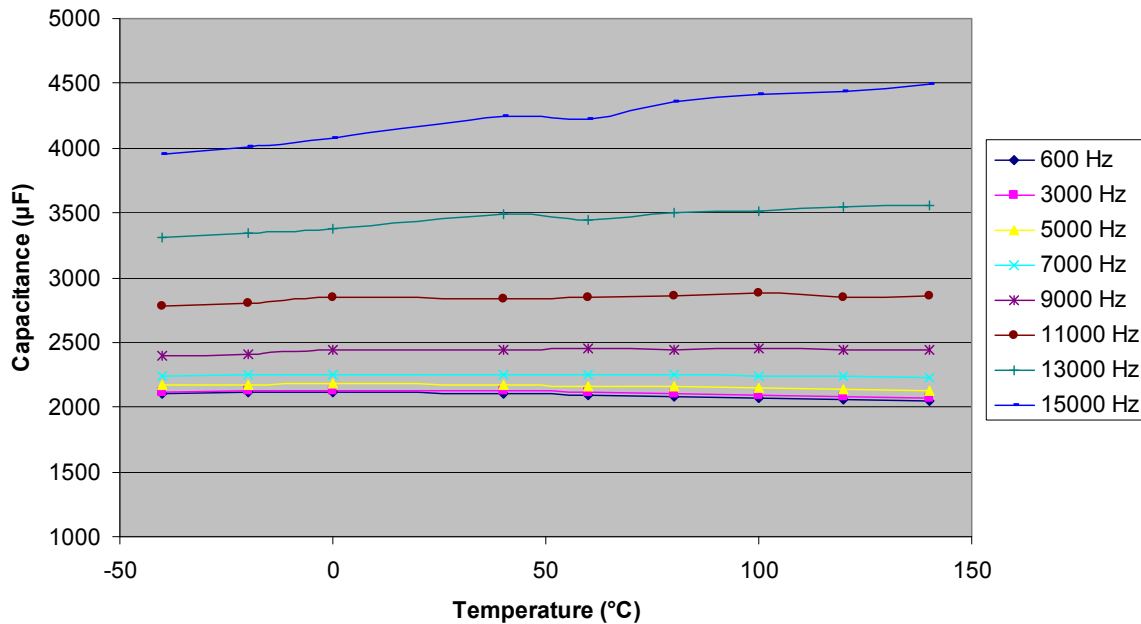
Fig. 2.24. Camry capacitor module equivalent capacitance variation with ambient temperature.

21

Figures 2.25 and 2.26 show the ESR response to frequency for the Camry and the Prius module, respectively. Although the curve characteristics indicate that the influence of frequency upon the ESR of both modules is reasonably different, the ESR measurement is similar, particularly at low frequencies. Measurements indicate that ESR values generally increased with increasing temperature for both modules at all frequencies.
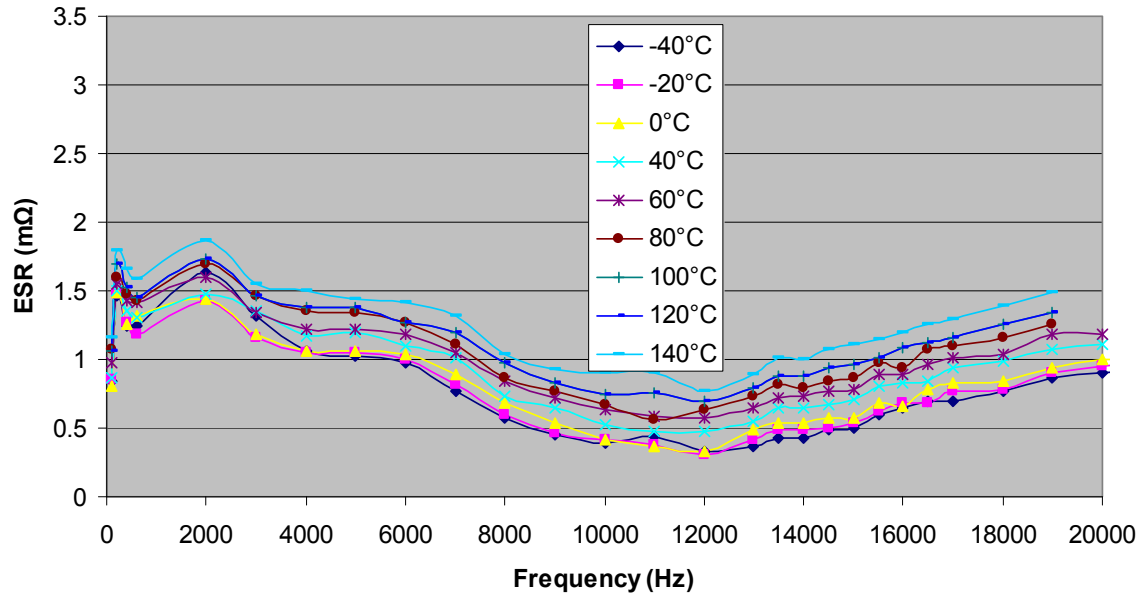
Fig. 2.25. Camry capacitor module ESR vs. frequency.
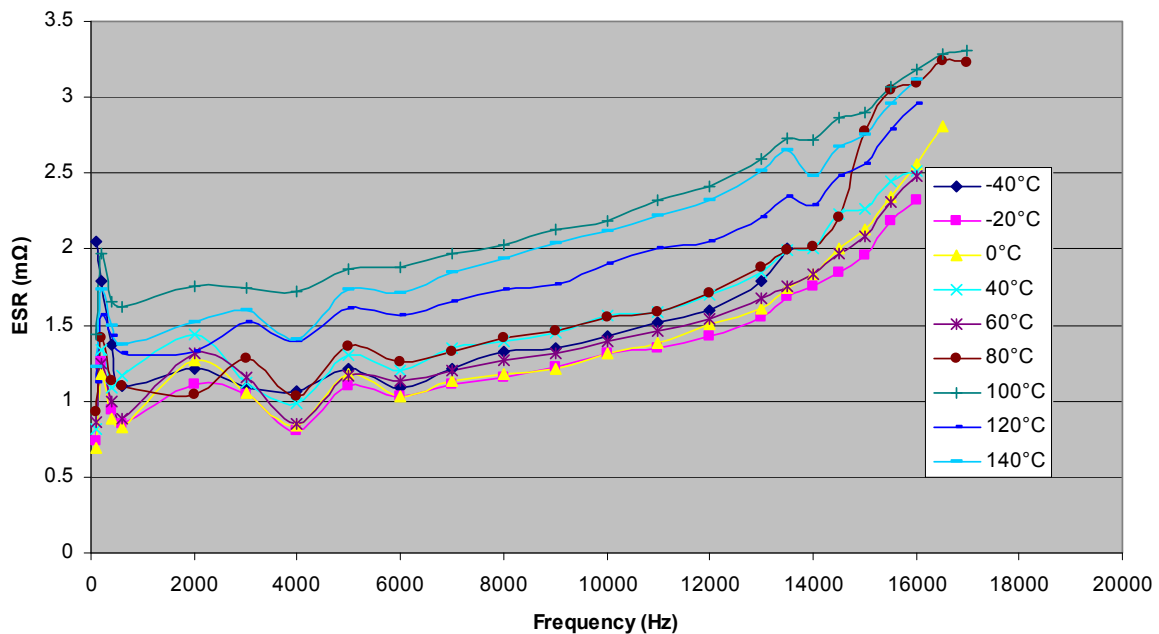
Fig. 2.26. Prius capacitor module ESR vs. frequency.

To obtain a clearer perspective of the impact of temperature upon ESR, Figs. 2.27 and 2.28 shows ESR plotted versus temperature for each frequency for the Camry and the Prius capacitor module, respectively.

22
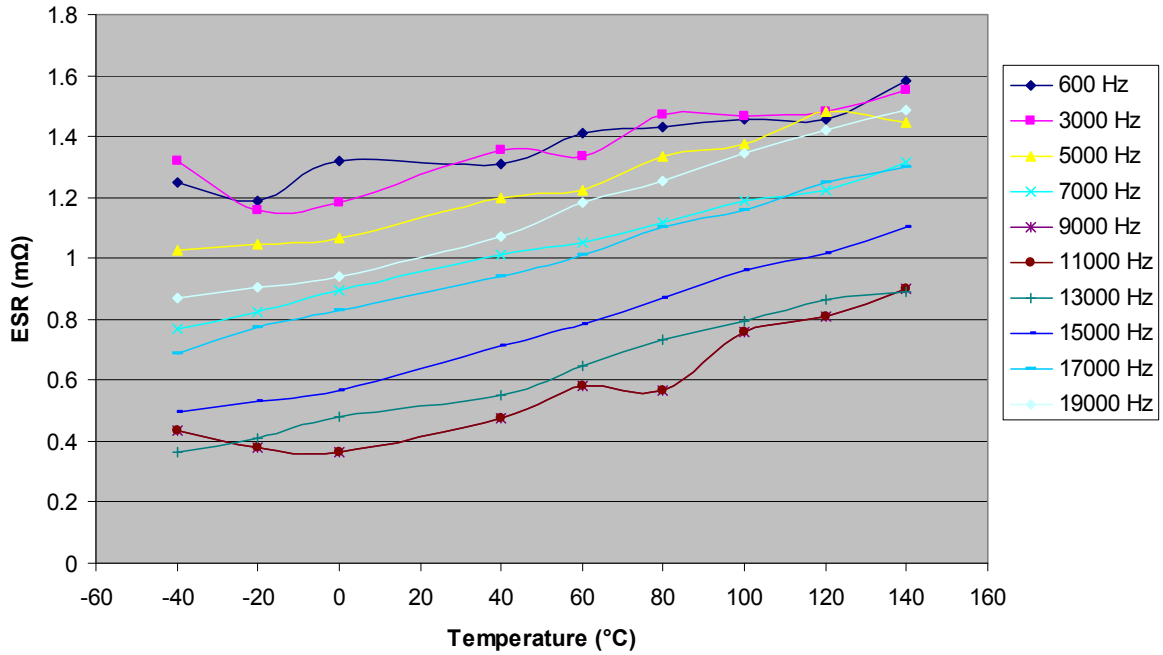
Fig. 2.27. Camry capacitor module ESR vs. temperature.
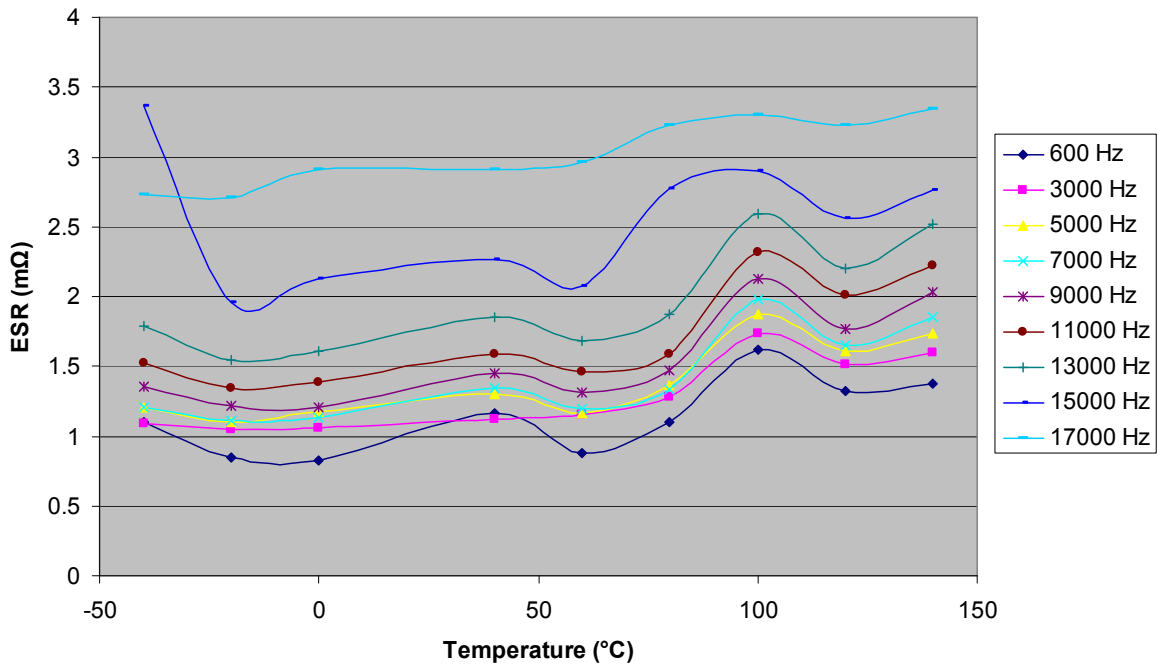
Fig. 2.28. Prius capacitor module ESR vs. temperature.

Again, the ESR of both modules generally increases with increasing temperature. Strangely, the ESR of the Prius module has a substantial lobe at 100°C for all frequencies as well as a high ESR measurement at -40°C and 15 kHz.

The variations of DF with frequency for the Camry and Prius capacitor module are shown in Figs. 2.29 and 2.30, respectively. These graphs are similar to the capacitance versus frequency graphs in Figs. 2.22

and 2.23. Since DF is the product of ESR, capacitance, and frequency, both graphs include curves which approach infinity near the resonant frequency. The behavior of the Camry capacitor module DF as a function of frequency is somewhat peculiar as the frequency increases beyond 6 kHz and then resumes typical behavior beyond about 12 kHz.
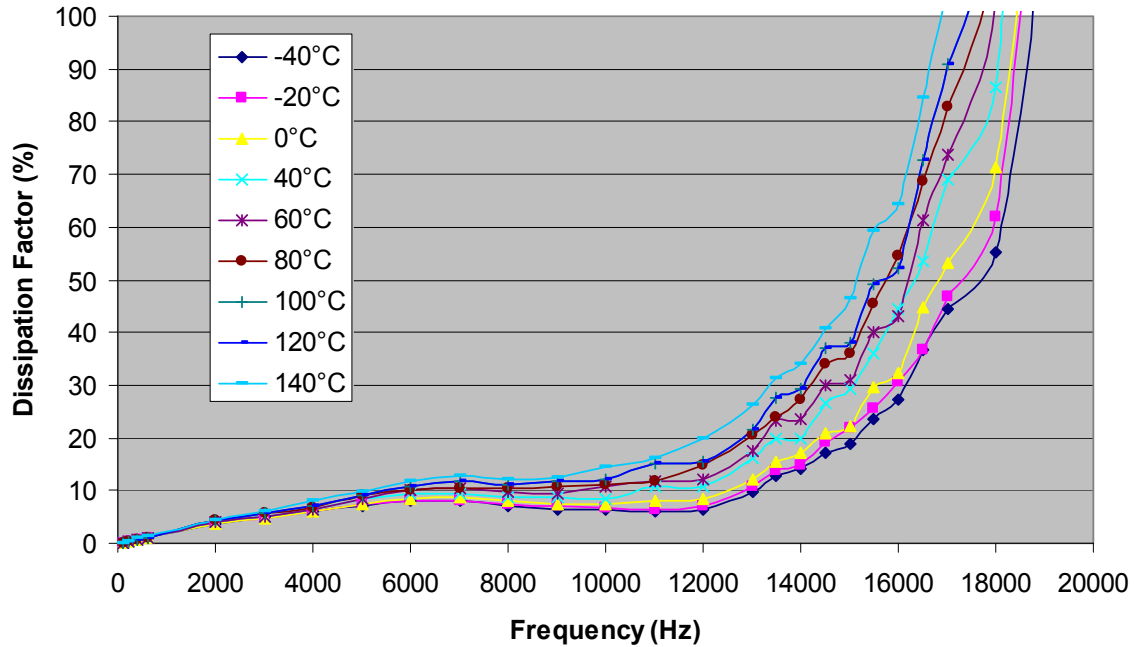
Fig. 2.29. Camry capacitor module DF frequency response.
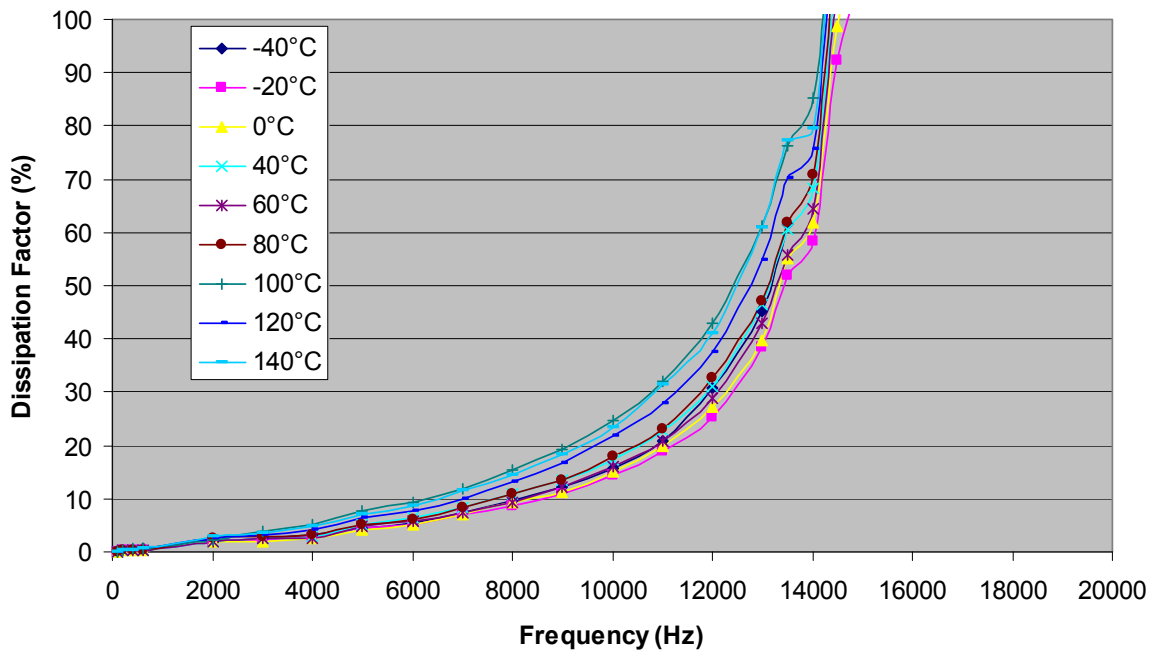
Fig. 2.30. Prius capacitor module DF frequency response.

The impact of temperature on the DF of the Camry and Prius capacitor modules for each test frequency is observed in Figs. 2.31 and 2.32, respectively. Similar to the impact of temperature upon capacitance, the DF generally increases with increasing temperature. Additionally, temperature has a greater impact on DF at higher frequencies. Since the ESR naturally increases with increasing temperature, the amount of real power dissipated at a particular amount of reactive power increases as temperature increases.
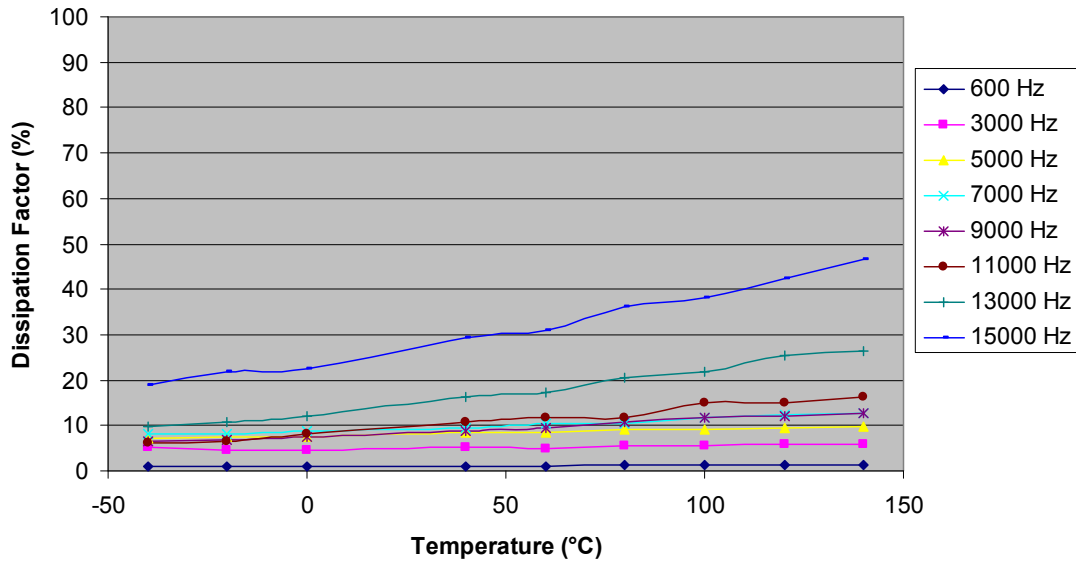
Fig. 2.31. Camry capacitor module DF temperature response.
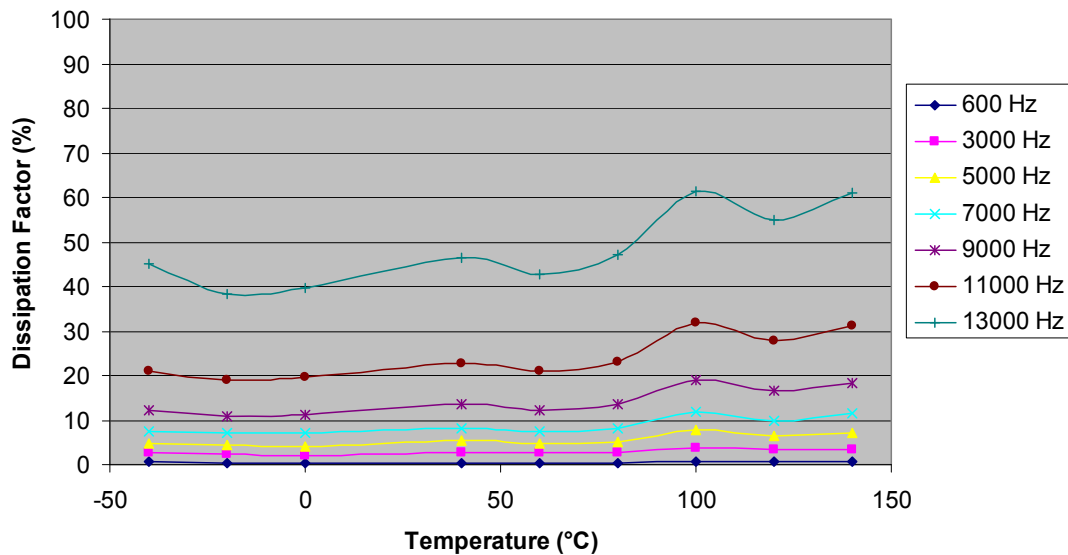
Fig. 2.32. Prius capacitor module DF temperature response.

2.1.2.2 Dynamic capacitor test results from large dc-link capacitor module

The Camry capacitor module was tested with a dc bias of 100 V and a maximum ripple current of 250 A. Figure 2.33 shows the circuit used to apply a ripple current with a dc bias to the capacitor module under

test. A capacitor was placed across the output of the dc power supply to decrease the potential of damaging the dc power supply with the high ripple currents generated during testing.
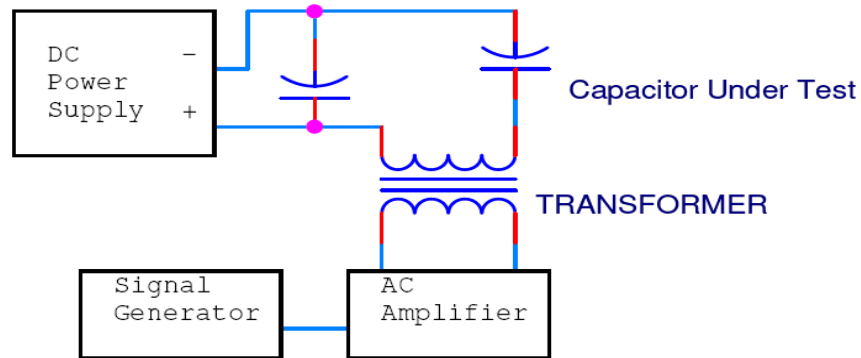
Fig. 2.33. Ripple current test schematic.

Thermocouples (TCs) were applied to the module in the center of both sides as shown in Fig. 2.34. Ripple current was applied in 50 A steps starting at 100 A and stopping at 250 A [root mean square (rms)]. The temperature was allowed to stabilize for 30 minutes before data was recorded. The two TC temperatures were averaged and plotted to determine the module's temperature response to high ripple current values. These data are shown in Fig. 2.35, which shows that the average temperature rise from 0–250 A was 11°C for the Camry capacitor module. The data for the 7.5 kHz test stopped at 190 A due to the limitations of the alternating current (ac) amplifiers. Nonetheless, the test results indicate that the Camry is capable of withstanding high ripple currents without reaching excessive temperatures. Results from dynamic tests upon the Prius module at 4 kHz are provided in Fig. 2.36, and indicate that the steady state temperature of the Prius module with a 200 A ripple current is about 52°C, whereas the steady state temperature of the Camry module with a 200 A ripple current at 5 kHz is only 28°C.
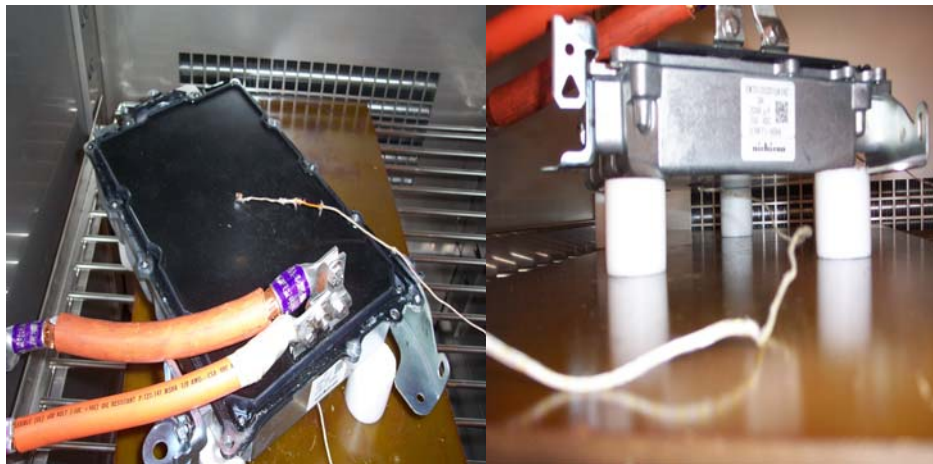
Fig. 2.34. TCs on the Camry capacitor module.
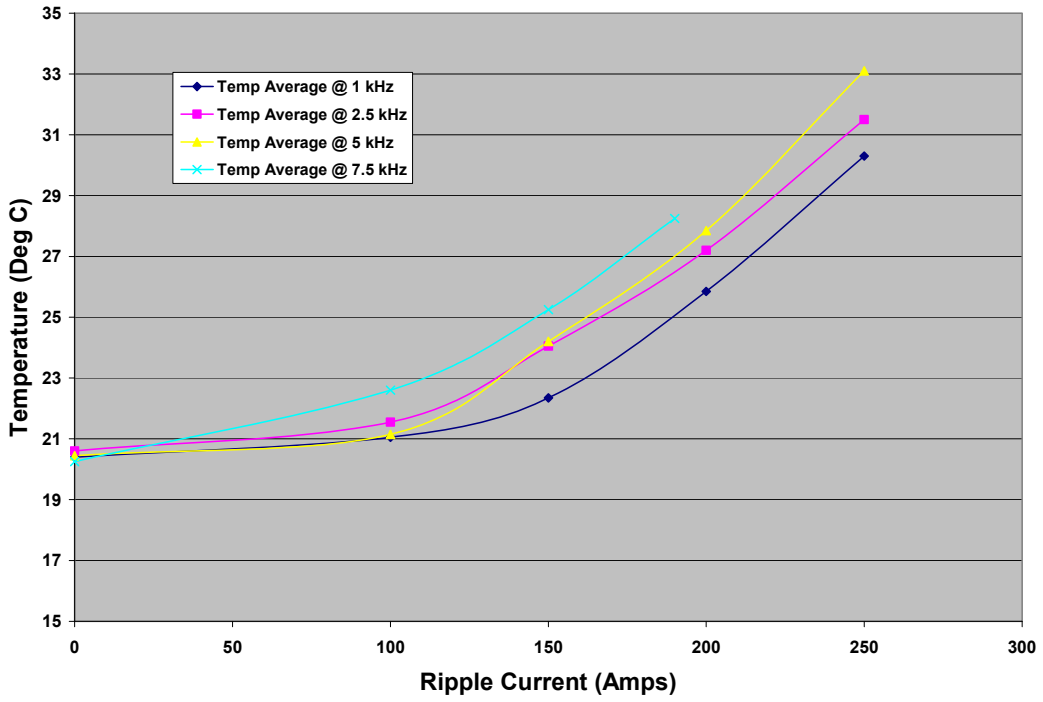
Fig. 2.35. Camry capacitor module steady-state temperature response vs. ripple current.
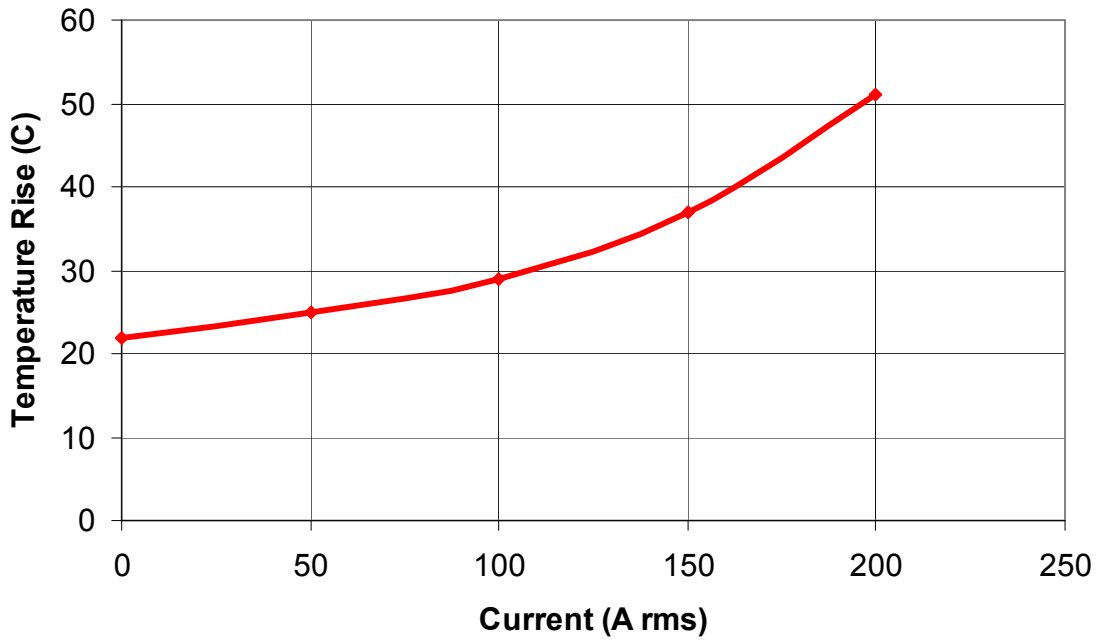
Fig. 2.36. Prius capacitor module steady-state temperature response vs. ripple current at 4 kHz.

2.1.2.3 Static capacitor test results of single sub-cell capacitor of smoothing capacitor module

The Prius and Camry capacitor modules are composed of 8 and 24 sub-cells, respectively. A sub-cell was removed from the Camry module and tested under the same test conditions that the entire module was subjected to. Since the module architecture greatly influences the overall function of the module and the difference of the number of sub-cells is significant, the most informative comparison is between the entire modules and not the sub-cells. Therefore, a comparison is not made between the Camry and Prius sub-cells; yet the Prius sub-cell capacitor test results are provided in Appendix B. Additional Camry sub-cell capacitor test results are also provided in Appendix B.

The large Camry capacitor module contains 24 86 µF sub-cell in parallel to form a total capacitance of 2098 µF; whereas the large Prius capacitor module contains (8) 141 µF sub-cell to form a total capacitance of 1,130 µF. The capacitance, ESR, and DF were measured over temperatures ranging from -40–140ºC and frequencies from 1–35 kHz and the results are shown in Figs. 2.37, 2.38, and 2.39, respectively. The capacitance increases only slightly until subjected to frequencies above 15 kHz. Figure 2.38 indicates that the ESR increases quickly with frequency at low frequencies and peaks at 5 kHz and slowly decreases with increasing frequency. Note again that the most common switching frequency of the motor and generator inverters is 5 kHz. When compared to the test results from the Prius capacitor sub-cell provided in Appendix B, the capacitance of the Camry capacitor sub-cell increases much more slowly with frequency. The ESR of the Prius capacitor sub-cell is slightly lower than that of the Camry capacitor sub-cell. The DF is much lower for the Camry capacitor sub-cell. Again, these comparisons are not straightforward as the architectural discrepancies significantly impact the overall characteristics. Nonetheless, a broad comparison of the characteristics is informative.
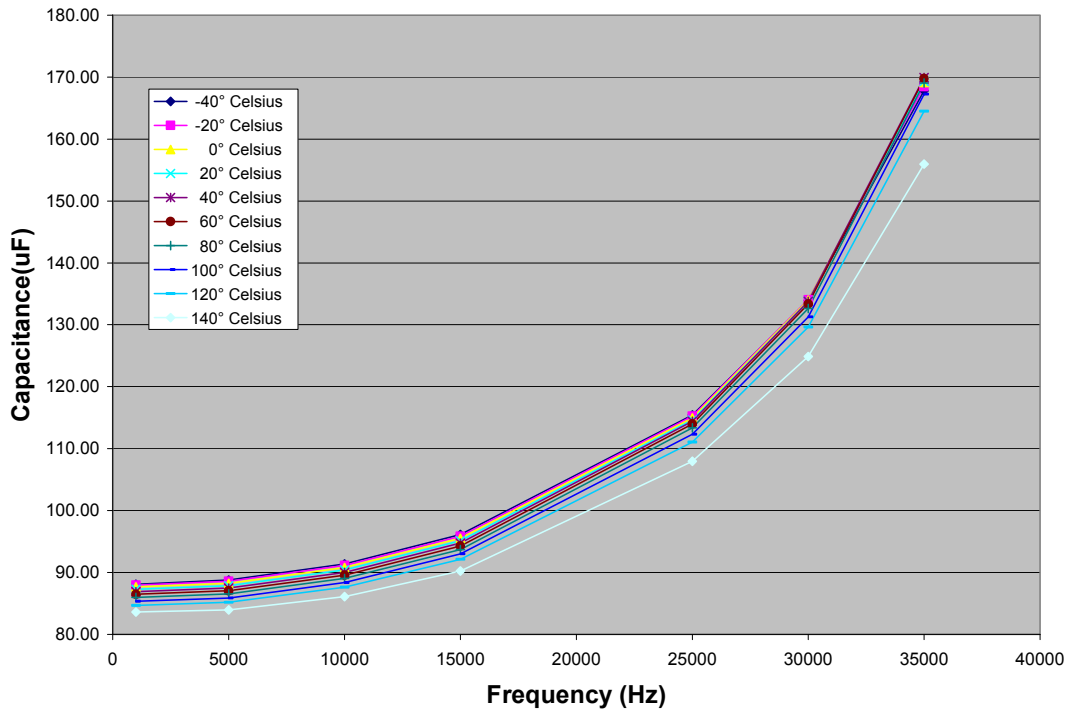
Fig. 2.37. Camry single 86 µF capacitor, capacitance vs. frequency.
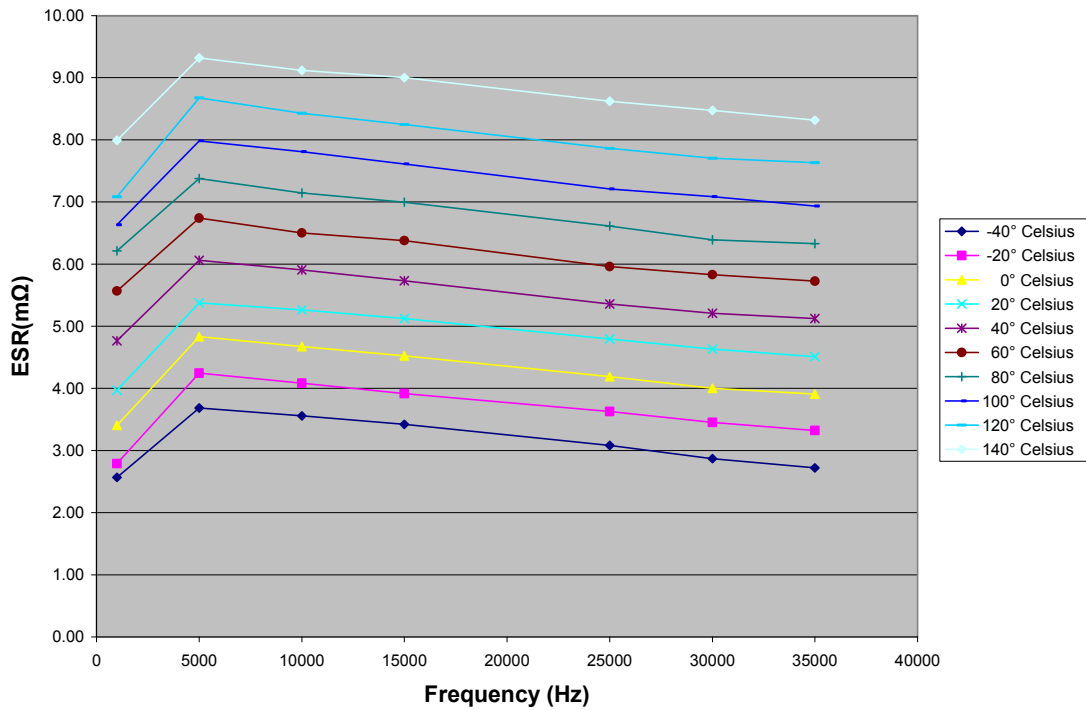
Fig. 2.38. Camry single 86 μF capacitor, ESR vs. frequency.
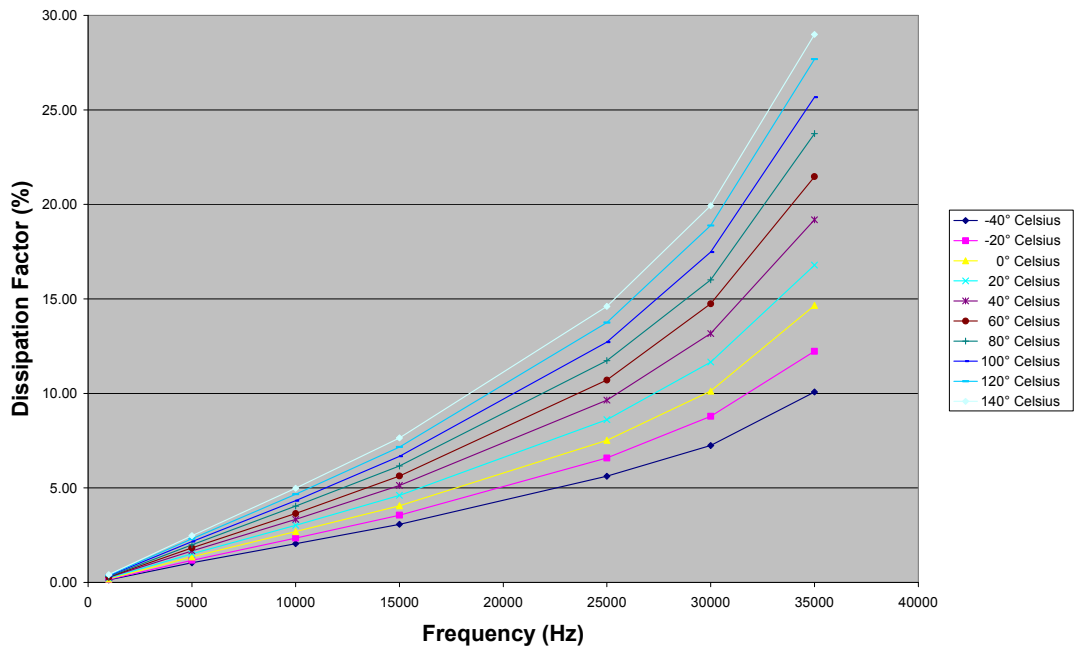
Fig. 2.39. Camry single 86 μF capacitor, DF vs. frequency.

Figures 2.40, 2.41, 2.42, and 2.43 provide the combined capacitance, ESR, and DF responses versus temperature for frequencies of 1 kHz, 5 kHz, 15 kHz, and 35 kHz, respectively. In comparing these figures, it is apparent that the high temperatures have a significant effect on the capacitance, ESR, and DF, particularly at high frequencies. Even at relatively low frequencies, the DF varies significantly with

temperature and frequency. Figures showing the results obtained while testing the Camry capacitor sub-cell at additional frequencies are provided in Appendix B. Furthermore, similar test results from the Prius capacitor sub-cell are provided in Appendix B.
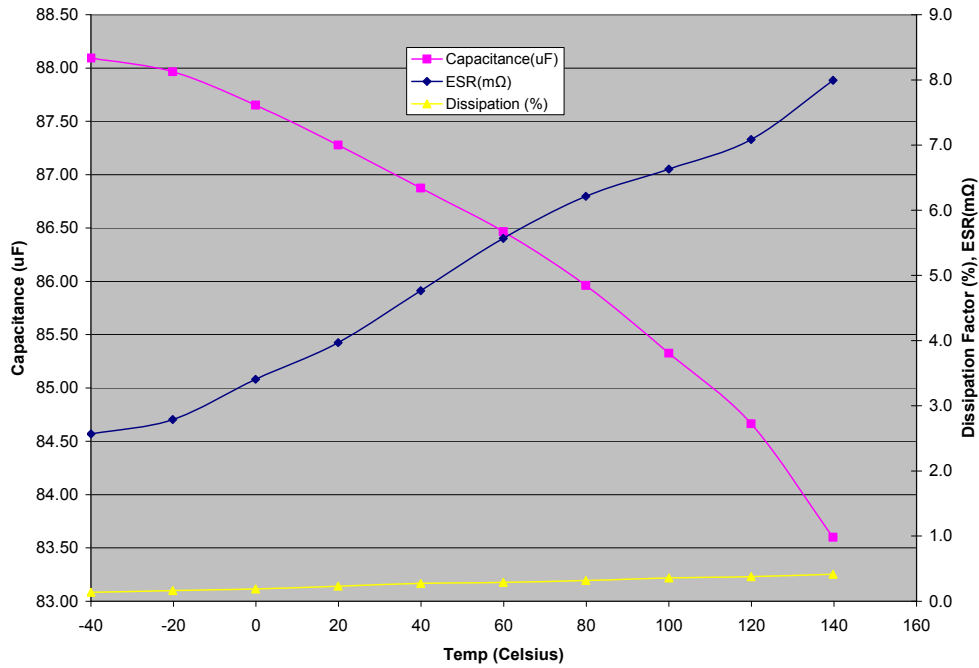
Fig. 2.40. Camry single 86 µF capacitor, capacitance, ESR, and DF vs. temperature at 1 kHz.
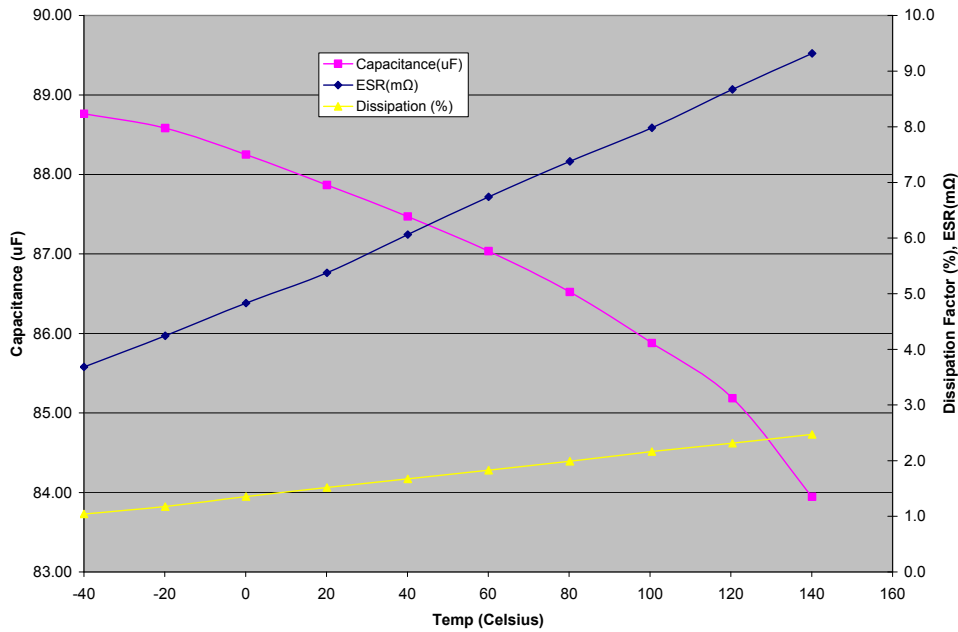
Fig. 2.41. Camry single 86 µF capacitor, capacitance, ESR, and DF vs. temperature at 5 kHz.
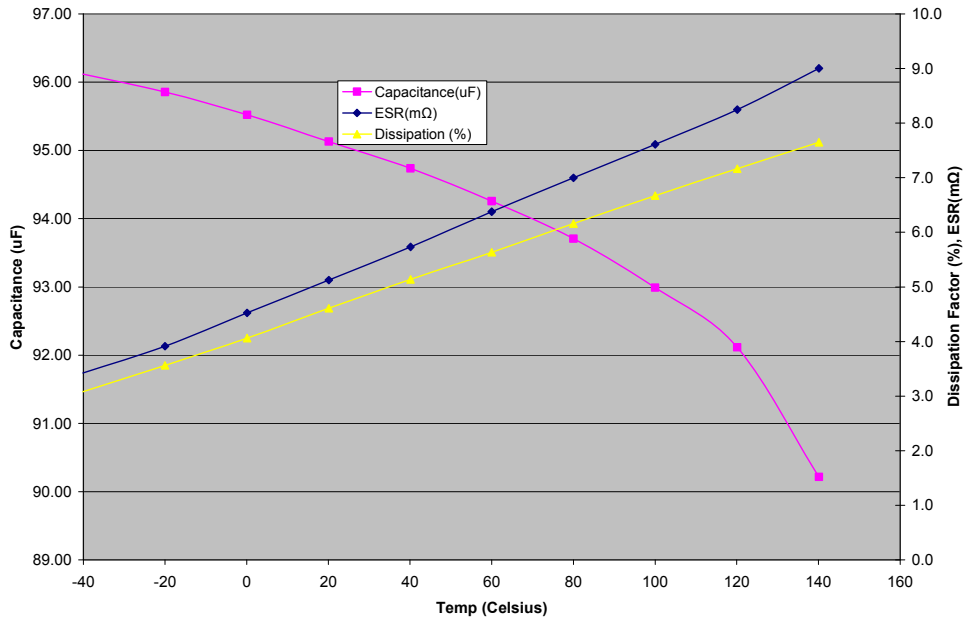
Fig. 2.42. Camry single 86 µF capacitor, capacitance, ESR, and DF vs. temperature at 15 kHz.
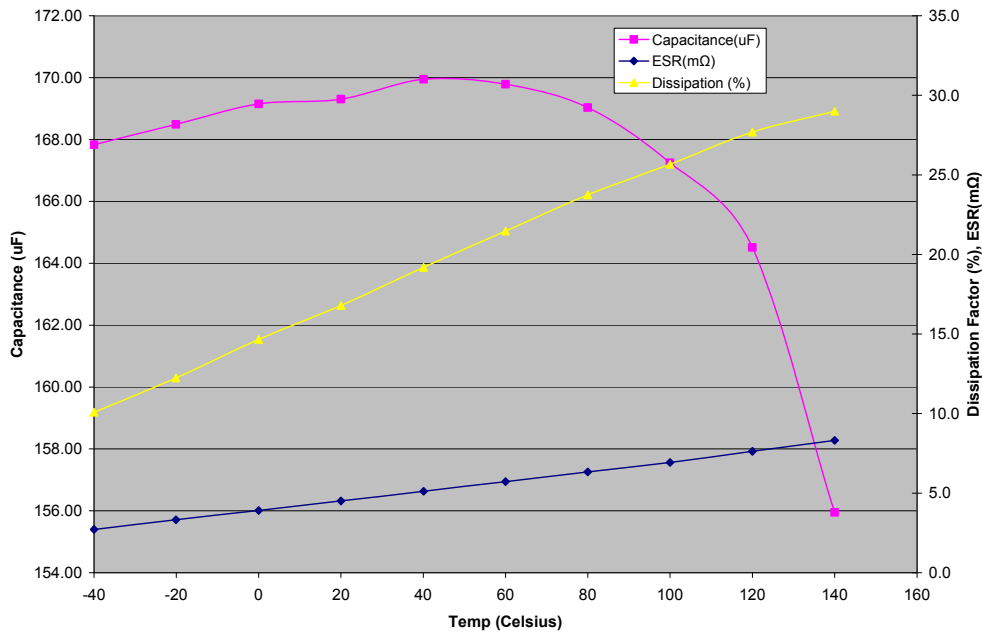
Fig. 2.43. Camry single 86 µF capacitor, capacitance, ESR, and DF vs. temperature at 35 kHz.

Figures 2.44 and 2.45 provide the combined capacitance, ESR, and DF responses versus frequency for temperatures of 20ºC and 140ºC, respectively. Although a quick comparison of the figures does not clearly reveal significant influences of temperature variation, notice the difference of scale between the figures. While the scale for capacitance remains the same, the scale for DF and ESR changes from 0–18 to 0–35 in Figs. 2.44 and 2.45, respectively. Thus, as indicated in the comparison of the previous figures, ESR and DF are significantly influenced by temperature variation. Since the unit is located within close proximity of the high operation temperatures of the ICE in addition to heat generated by components

31

within the PCU (including the capacitor itself), the capacitor module is often subject to high temperatures. Similar figures for the Camry and Prius capacitor sub-cells are provided in Appendix B.
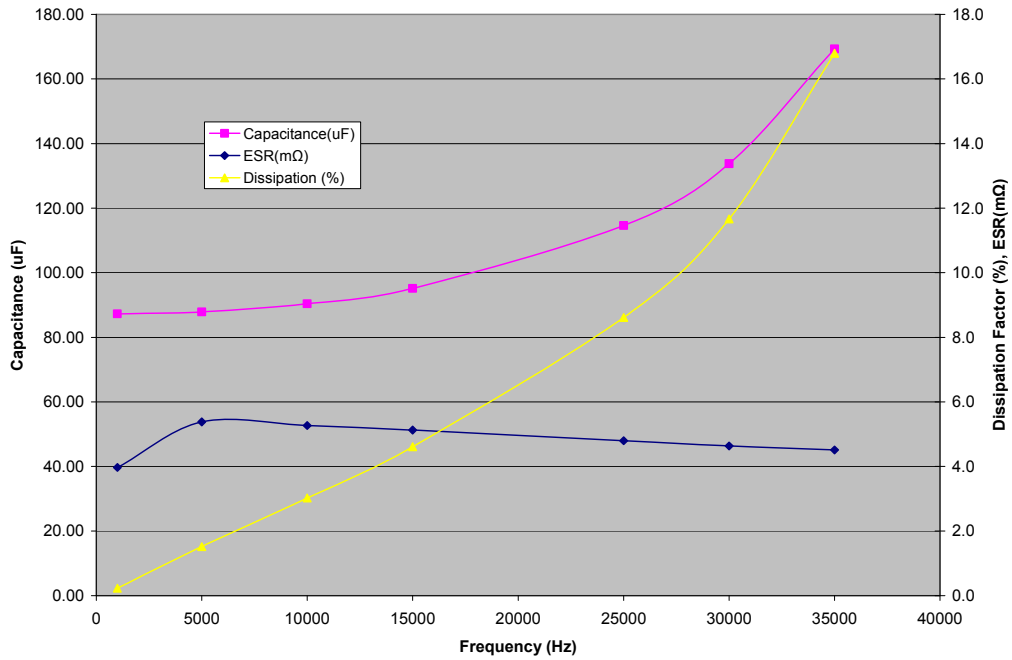
Fig. 2.44. Camry single 86 µF capacitor, capacitance, ESR, and DF vs. frequency at 20°C.
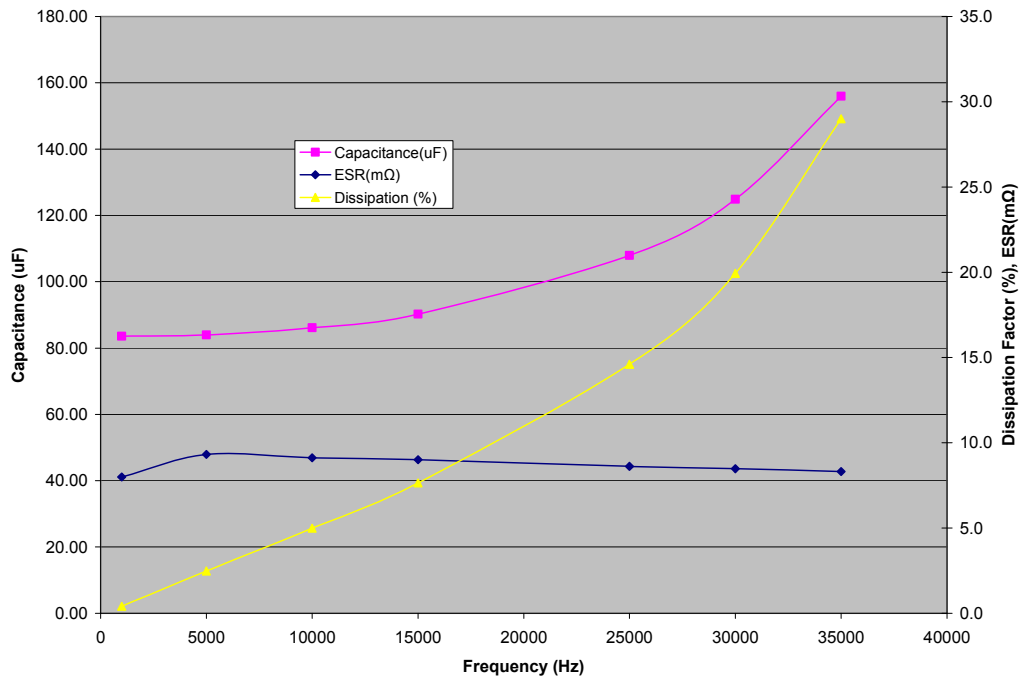
Fig. 2.45. Camry single 86 µF capacitor, capacitance, ESR, and DF vs. frequency at 140°C.

2.1.2.4   Inspection into positive reactance measurement of large dc-link capacitor module

Further inspections into the influence of frequency upon characteristics of the Camry and Prius capacitor modules were conducted using the dynamic test setup described above. A Yokogawa PZ4000 power analyzer was used to monitor the current and voltage waveforms in order to determine the respective rms values and phase differences between the two. No dc bias was applied during these tests, and all currents and voltages discussed hereon are sinusoidal in nature and the corresponding signal levels are given in terms of rms values.

The primary intent of these tests was to evaluate the voltage and current phase angle for various ripple current frequencies, as well as obtain general information regarding the voltage response of the capacitor module to a particular ripple current amplitude for various ripple current frequencies. Figures 2.46, 2.47, and 2.48 show the phase angles between the current and voltage of the Camry and Prius capacitor modules at various frequencies. These tests were conducted with about 25 A of current applied to the modules at frequencies from 5–20 kHz and all signals were measured with a Yokogawa PZ4000 wattmeter. These figures are screenshots of the Yokogawa PZ4000 measurements and they include Uac1, the rms of the ripple voltage (with no dc component), and Iac1, the rms of the ripple current, as well as the frequency, which is shown in the upper left corner of the display. The phase angle between the current and voltage was also measured, but the value is not shown in these figures. A leading phase angle is obtained when the current leads the voltage, which is typical for a capacitive reactance. A lagging phase angle is associated with an inductive reactance, in which the current lags the voltage.
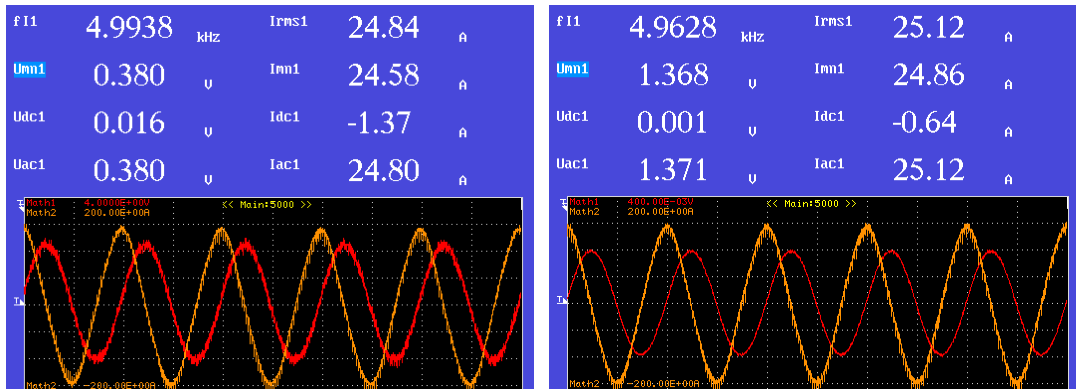
Fig. 2.46. Waveforms of the Camry (left) and Prius (right) capacitor module at 5 kHz.
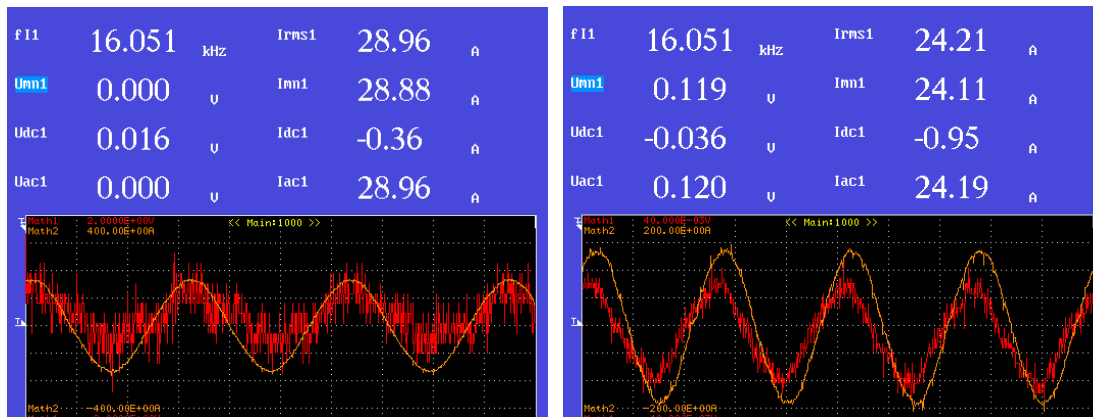
Fig. 2.47. Camry (left) and Prius (right) capacitor module waveforms at 16 kHz.

33
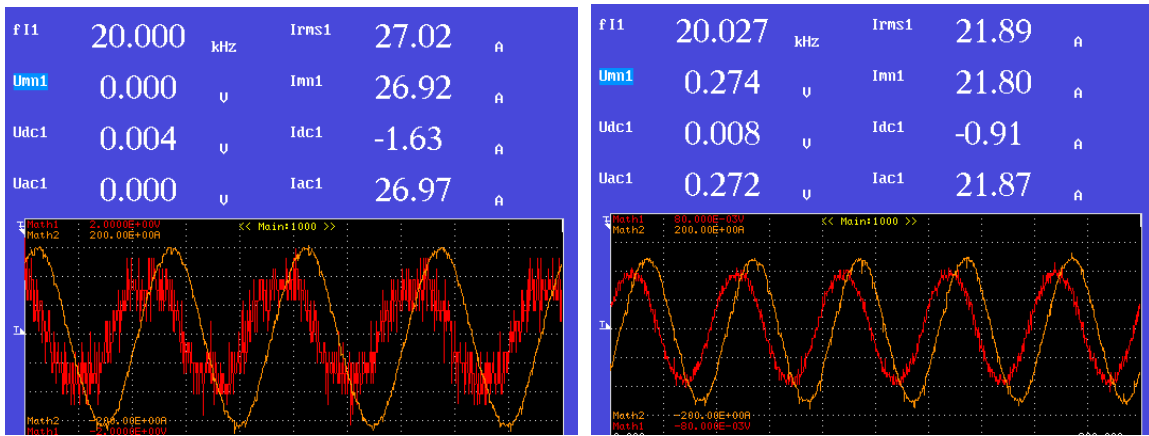
Fig. 2.48. Waveforms of the Camry (left) and Prius (right) capacitor module at 20 kHz.

Figure 2.46 shows the phase angles between the current and voltage at 5 kHz for the Camry and Prius capacitor module with the current waveform being the orange trace and having the highest amplitude. For both modules, the current is leading the voltage by an angle which is close to 90° indicating a typical capacitive response at 5 kHz. The voltage ripple of the Prius module at 25 A is higher than that of the Camry module as the capacitance of the Camry is higher than that of the Prius at this frequency.

Figure 2.47 shows screenshots obtained during a similar test with a frequency of 16 kHz for the Camry and Prius capacitor modules. The voltage waveforms contain significant noise levels as the amplitude is very low for these frequencies. The phase angle between the voltage and current of the Camry module at 16 kHz is nearly zero, and the current is lagging the voltage of the Prius module at 16 kHz indicating that the reactance is positive and the module behaves like an inductor at this frequency.

In Fig. 2.48, the frequency of the ripple current applied to both modules is 20 kHz. The phase difference between the current and voltage is large enough to easily concur that the current is lagging the voltage significantly.

A second series of tests were conducted with the Camry and Prius capacitor modules. The overall test procedures were similar to those just discussed, yet the amplitude of the signal generator (shown in Fig. 2.33) waveform was kept constant. Conditions were similar but not identical between the tests on the Camry and Prius capacitor modules and a comparison of the test results provides only general information regarding the frequencies at which the resonance and phase angle changes occur.

Figures 2.49 and 2.50 compare the responses of the Camry and Prius capacitor modules to various frequencies. In Fig. 2.49, as the applied frequency on the Camry module increases from 1 kHz, the current increases and peaks at a frequency of about 2 kHz. A similar characteristic is noticed for the Prius module and the current peaks between 2 and 3 kHz. As indicated by both figures, the current leads the voltage for low frequencies indicating a dominant capacitive effect until a frequency of about 16 kHz for the Camry and 15 kHz for the Prius. Leading phase measurements are indicated by the yellow traces, which end just prior to these resonance frequencies where the capacitive and inductive effects are equal and the corresponding reactance is zero. As the frequency increases beyond the resonant frequency, the module behaves as an inductive load as the parasitic inductance has a greater effect on the reactance than the capacitance does, even though the parasitic inductance is very low. These characteristics re-affirm that the large dc-link capacitor is used for smoothing of low machine level ripple frequencies associated with the operation the motor and generator, as opposed to being used primarily for attenuation of switching transients.
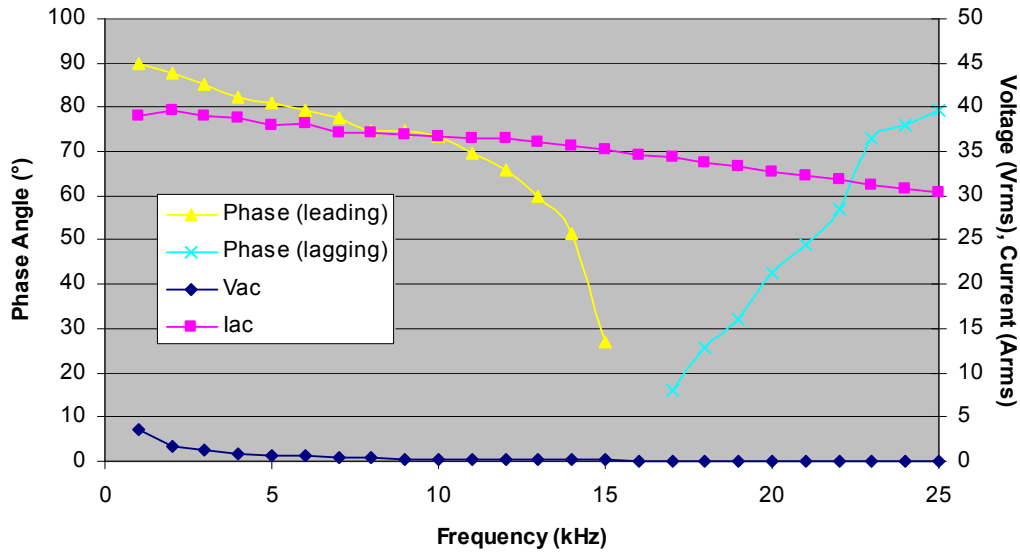
Fig. 2.49. Camry capacitor module voltage and current response to frequency.
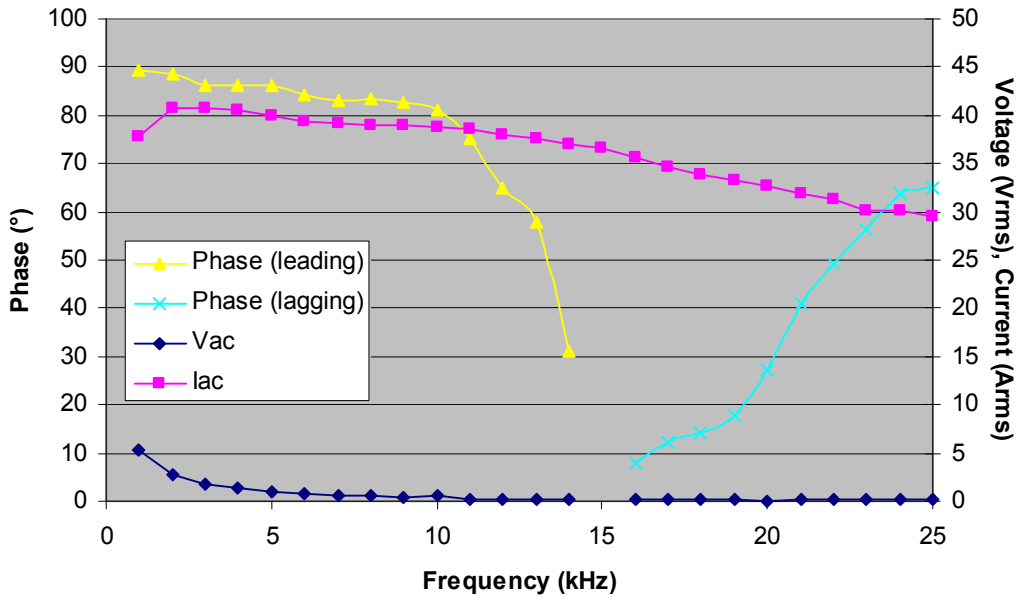
Fig. 2.50. Prius capacitor module voltage and current response to frequency.

2.1.2.5 Static capacitor test results of battery level filter capacitor evaluations

Figures 2.51 and 2.52 compare the capacitor test results of the 500 V, 378 μF capacitor of the Camry and the 600V, 282 μF capacitor of the Prius, respectively. Each capacitor resides between the battery and the boost converter and is located within the PCU. Significant differences are noticed between the characteristics of the two capacitors, particular when comparing the influence of frequency upon capacitance and DF. The equivalent capacitance of the Prius begins to approach infinity near about 22 kHz, whereas the equivalent capacitance of the Camry capacitor only increased slightly as the maximum test frequency of 30 kHz was reached. Since DF is a product of ESR, capacitance, and frequency, the DF curves have characteristics similar to those of the capacitance curves.
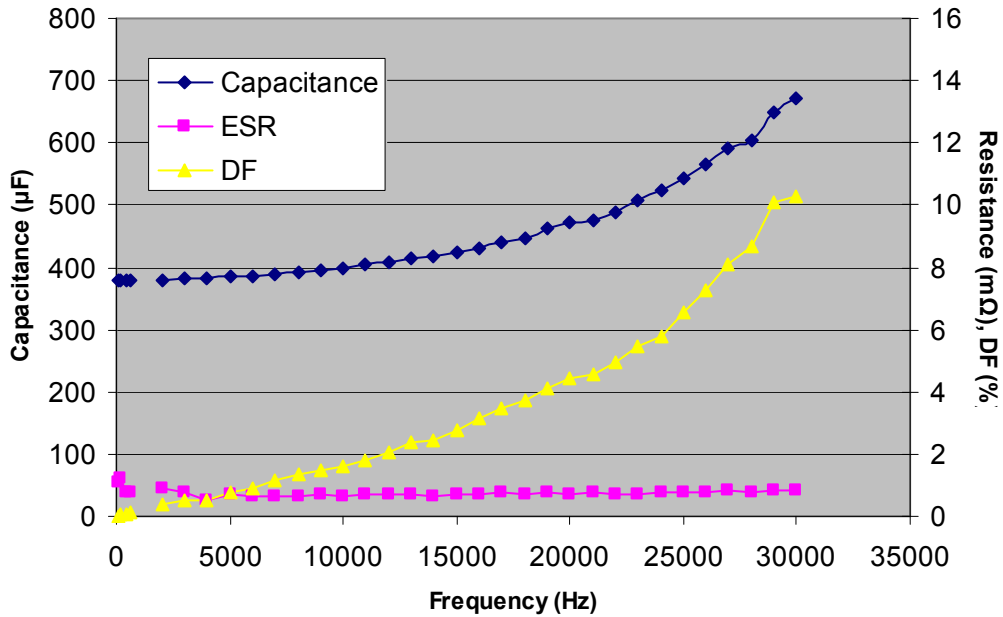
Fig. 2.51. Camry battery level 378 µF capacitor, capacitance, ESR, and DF vs. frequency.
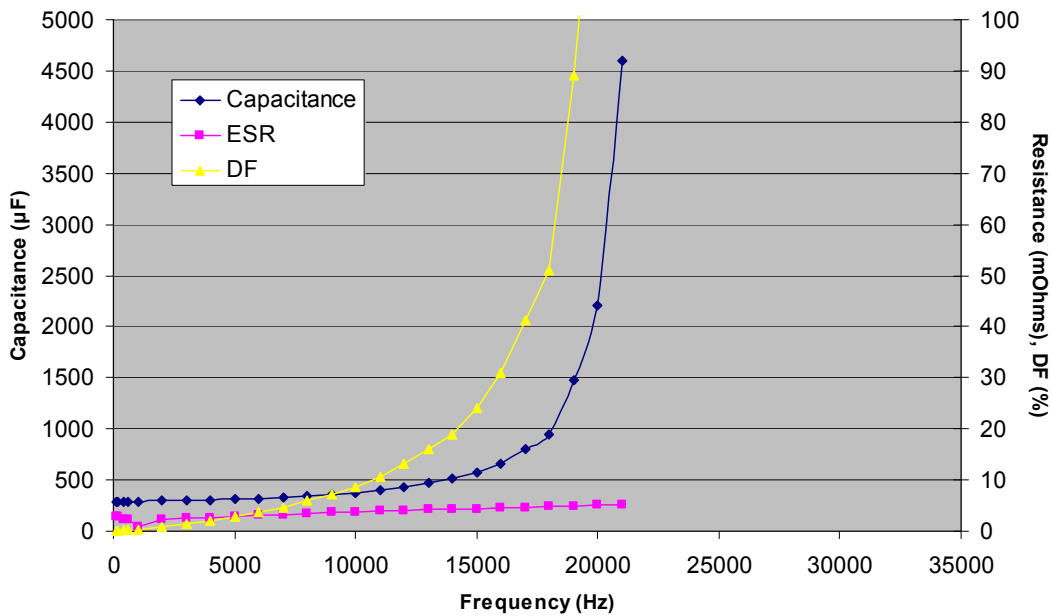
Fig. 2.52. Prius battery level 282 µF capacitor, capacitance, ESR, and DF vs. frequency.

2.1.2.6 Static capacitor test results of small dc-link capacitor evaluations

Figures 2.53 and 2.54 compare the capacitor test results of the dc-link 750 V, 0.9 µF capacitor of the Camry and the 750V, 0.1 µF capacitor of the Prius, respectively. Although the equivalent capacitance of the small Camry capacitor appears to decrease significantly, a closer look at the capacitance axis limits indicates that frequency has a small effect on the equivalent capacitance of the small Camry and Prius capacitors. Unlike the ESR of the other capacitors, the ESR of both small capacitors is much higher for

low frequencies and decreases quickly with increasing frequency. All data points were taken at room temperature. The DF is relatively low even at high frequencies. These characteristics indicate the high frequency filtering capabilities of the small capacitors.
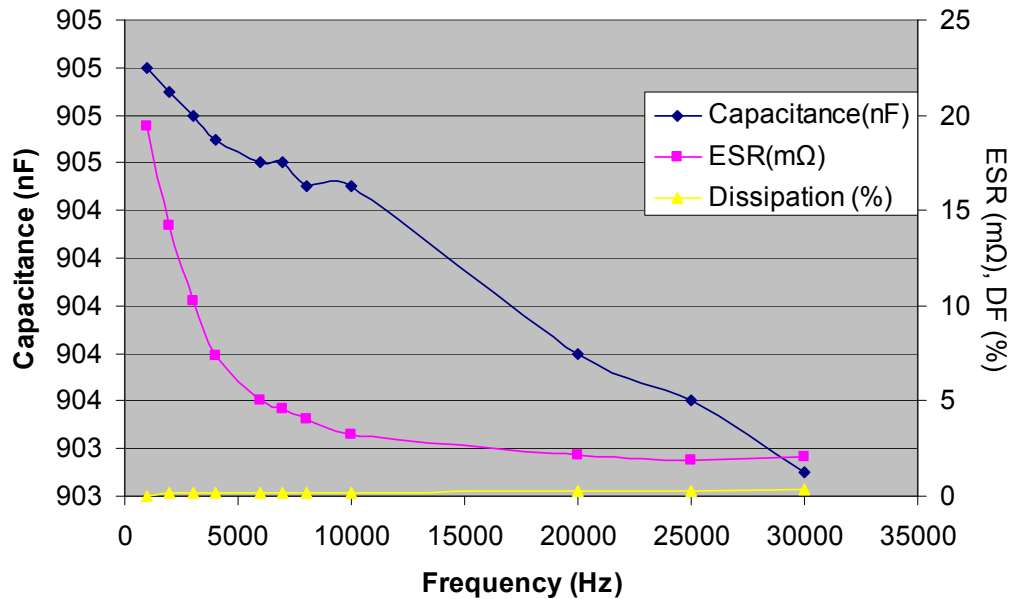
Fig. 2.53. Camry dc-link 0.9 µF capacitor, capacitance, ESR, and DF vs. frequency.
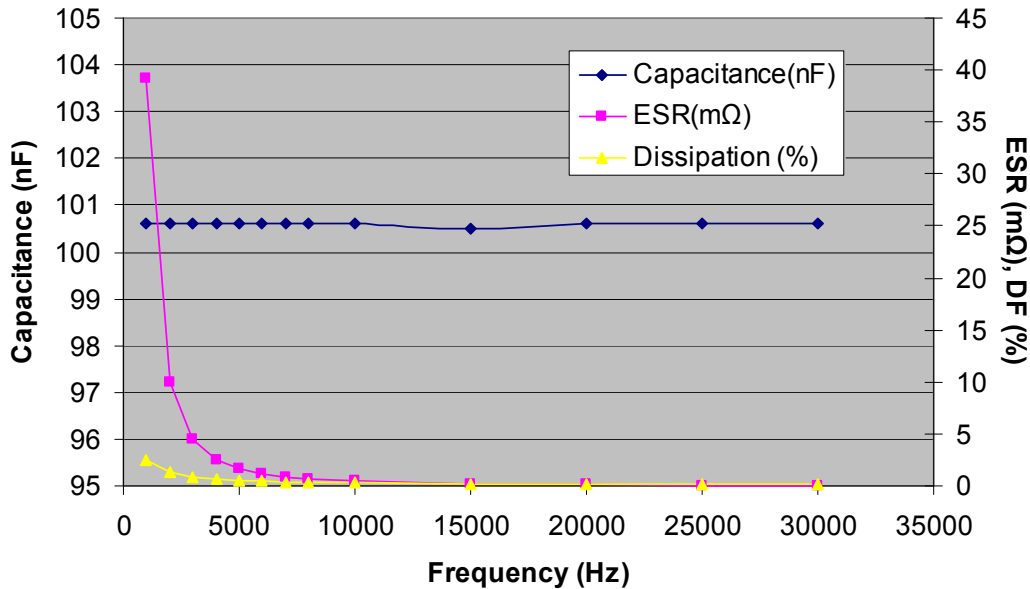
Fig. 2.54. Prius dc-link 0.1 µF capacitor, capacitance, ESR, and DF vs. frequency.

2.2 TRANSAXLE

The 2007 hybrid Camry transaxle assembly is comprised of motor, generator, and gear box subassemblies. The mass of the entire unit is 108 kg, which is shown in Fig. 2.55. An ICE mounts to the transaxle and a mechanical interface is established with spline shaft, which is slightly visible in the figure.

The electric motor and generator outputs are not directly accessible yet through a combination of various gear configurations, the total motive force output of the hybrid system is supplied to the drive shafts by the differential gear outputs which are indicated in the figure. The generator is located adjacent to the ICE input (referred to as front end) and the motor is located in the rear portion of the transaxle, as shown in Fig. 2.56. The gear section of the transaxle is located between the generator and motor sections, as shown in Fig. 2.57.
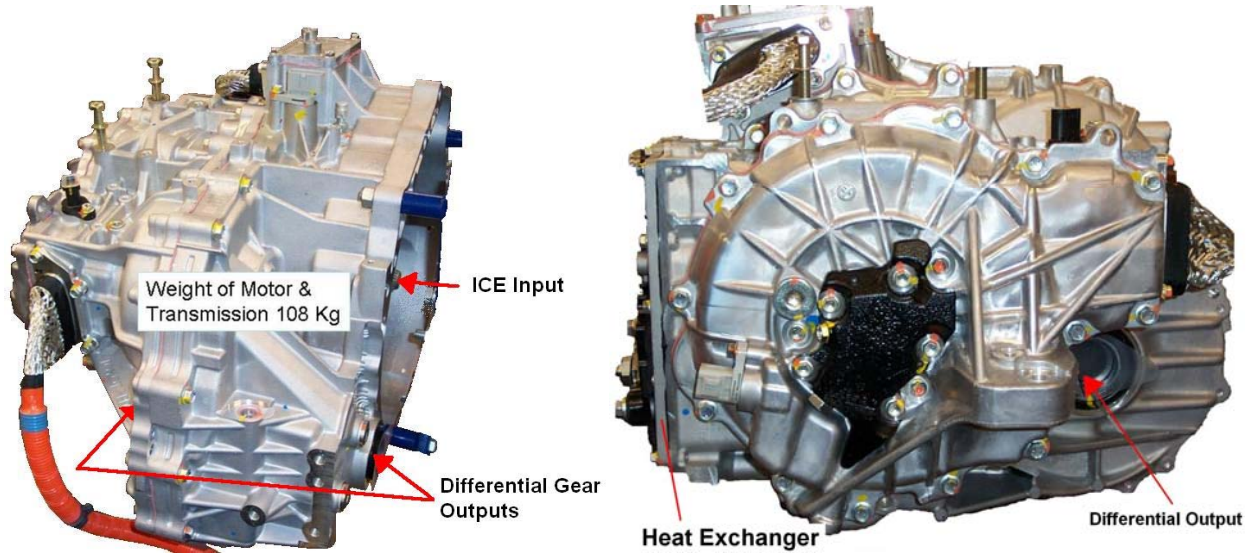
Fig. 2.55. Hybrid Camry transaxle isometric view (left) and rear view (right).
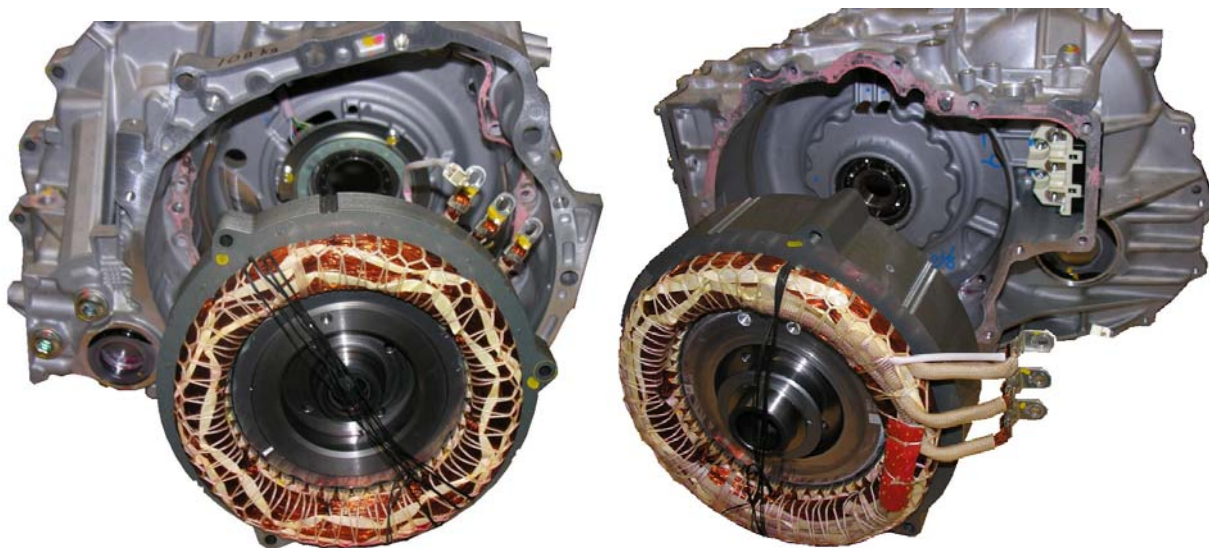
Fig. 2.56. Camry generator front view with ICE spline removed (left) and motor rear view (right).
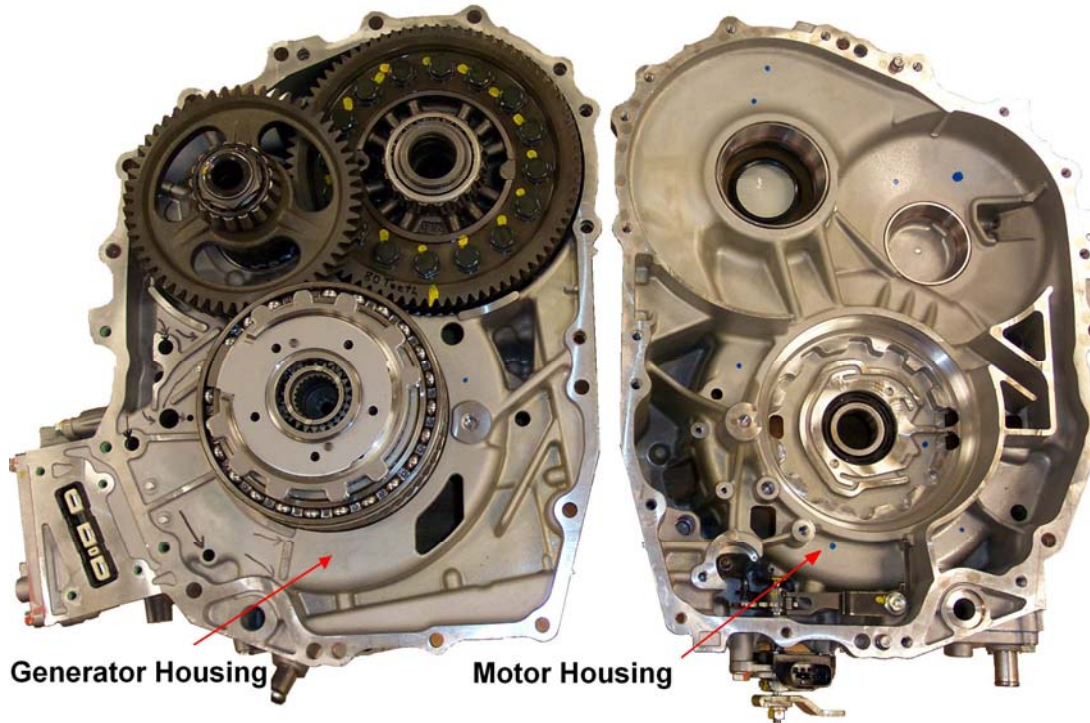
Fig. 2.57. Camry transaxle gear section open sandwich view.

2.2.1 Thermal Management and Lubrication System

The thermal management and lubrication system of the transaxle utilizes a mechanically driven trochoid oil pump as well as oil slinging movement by the drive gears to circulate oil throughout the transaxle. As shown in Fig. 2.58, the trochoid shaft is driven by the planetary carrier, which is connected directly to and rotates at the same speed as the ICE. The black plate was removed from the rear of the trochoid system to provide a view of the interior of the trochoid pump. An oil pickup is located near the bottom of the motor section which serves as an input to the trochoid pump. The central component of the trochoid pump resembles a gear and is machined such that the oil collects in the gaps of the pump teeth and forces the oil through the trochoid shaft shortly thereafter. The motor rotor shaft is hollow and the trochoid pump shaft extends through the hollow shaft of the motor rotor. A portion of the oil is dispensed to the motor bearing which is located next to the toothed central component of the trochoid pump. Small holes are located along the side of the trochoid pump shaft to supply oil to another motor bearing on the opposite end of the motor rotor. The tip of the trochoid pump shaft supplies oil to the power split and speed reduction gear through the same interface in which the shaft is driven. The 2004 Prius contains a similar trochoid pump mechanism.

Note that oil is not circulated by the trochoid pump if the ICE is not active. Therefore, if the vehicle is operating in electric mode only, then the system fully depends on the oil slinging action of the gear train for oil circulation. A general diagram of the oil flow paths is provided in Fig. 2.59. Oil that has settled in the bottom portion of the gear section is picked up by the differential gear teeth and is then slung to the driver gear, to reservoirs in the upper portion of the gear section, and to the power split planetary gear unit. The oil reservoirs are flooded if the differential gear is rotating above 900 rpm. A large reservoir is adjacent to a heat exchanger in order to transfer heat to the cooling system. Weep holes and oil ports distribute oil to the motor and generator stator as well as several bearings throughout the system. Note that the circulation due to gear slinging is dependent upon vehicle speed.

39
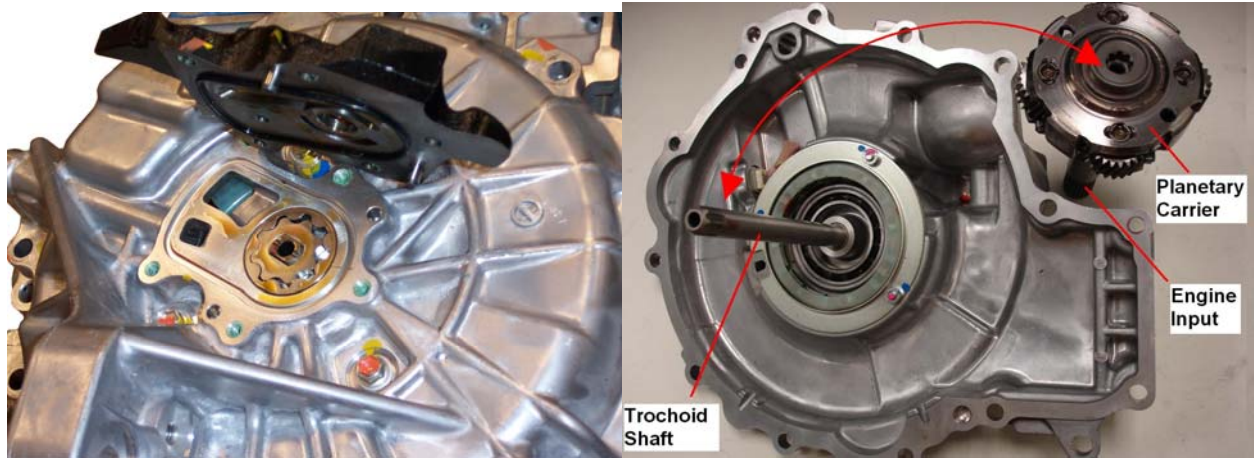
Fig. 2.58. Trochoid oil pump view from outside rear (left) and from inside motor section (right).
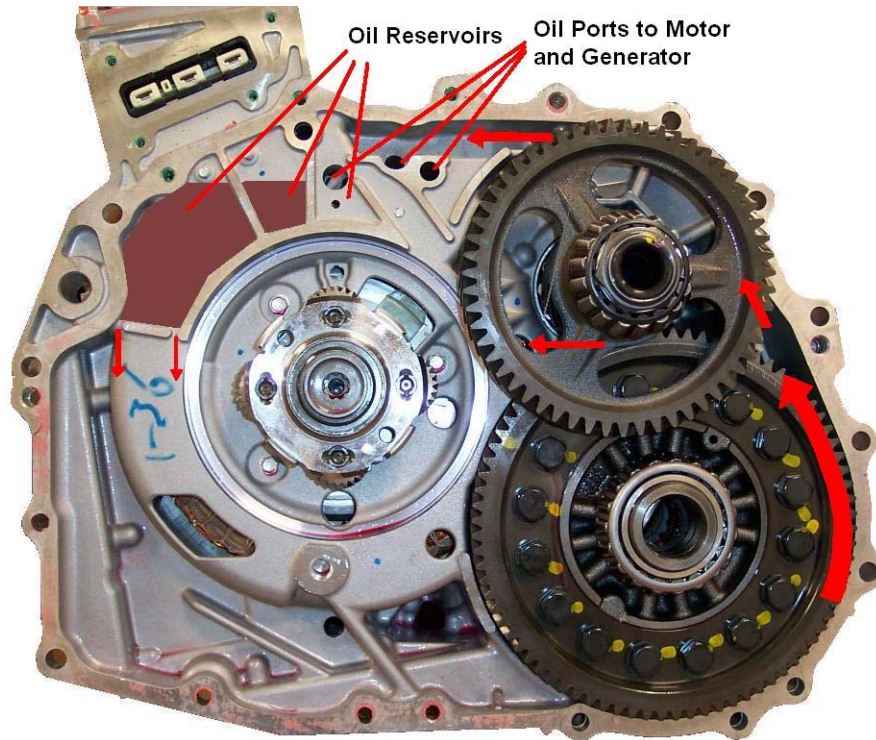
Fig. 2.59. Oil slinging paths formed by gear train.

A heat exchanger is located on the one side of the motor periphery and the generator also has a small heat exchanger which is part of a series coolant loop with the motor heat exchanger as well as the PCU heat exchanger. According to specifications in the Camry repair manual, the coolant loop consists of a standard 50% ethlyene glycol and 50% water mixture which flows at 10 L per minute and has an average operation temperature of 65ºC. Vehicle tests at Argonne National Laboratory (ANL) indicate the average coolant temperature may be considerably lower depending on operation conditions. The coolant capacity is listed as 2.9 L. A separate radiator is dedicated to the THS coolant loop which is isolated from the ICE coolant loop that operates at much higher temperatures.

2.2.2 Transaxle Gear Train

The Camry transaxle has three primary gear systems which are designed to carry out power split, speed reduction, and drive functions. A general comparison of the 2004 Prius gear train and the 2007 Camry gear train is provided in Fig. 2.60. The number of teeth on each gear is noted in black text on a white background. There are several noticeable differences between the two designs. The Prius transaxle design has a chain coupling between the power split planetary ring and the counter drive gear, whereas the planetary ring and counter drive gears mesh directly within the Camry transaxle. Additionally, the Camry transaxle has only three separate axes about which gear systems rotate, compared to four axes in the Prius transaxle. The number of teeth on the planetary gear components does not differ between the two designs. The total gear ratio from the Camry power split planetary ring to the differential output is $(80/23) \times (55/54) = 3.542$, where the equivalent gear ratio for the Prius is $(75/26) \times (44/30) \times (35/36) = 4.113$.
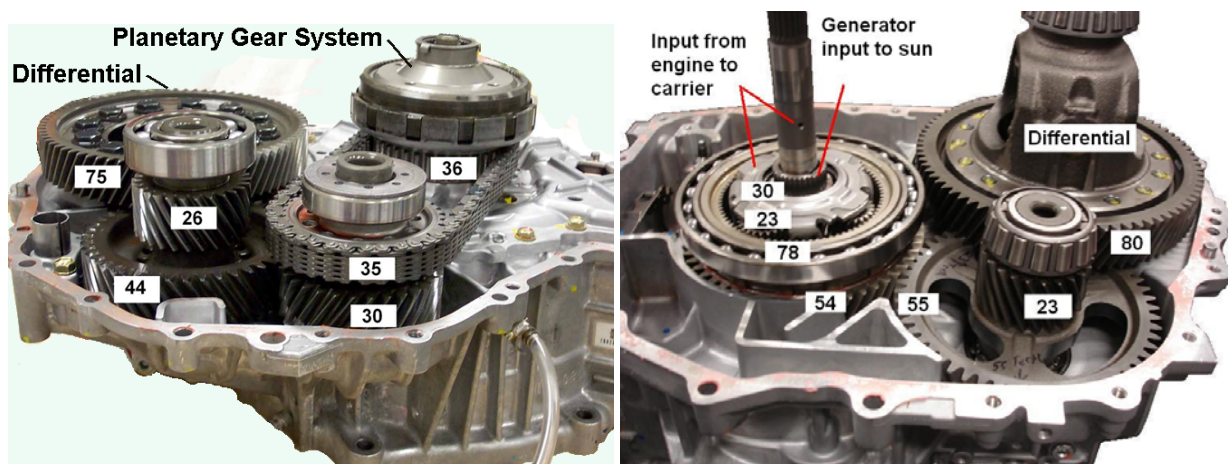
Fig. 2.60. 2004 Prius gear train (left) and 2007 Camry gear train (right).

Another significant difference between the designs is that the Camry has a speed reduction gear, which is comprised of a planetary gear unit. The speed reduction planetary gear assembly is shown along with the power split planetary gear unit in Fig. 2.61. The planetary gear units share the ring gear in which the electric motor, MG2, is connected to the ring gear through the speed reduction gears. The number of teeth is shown for each gear and the planetary carrier is fixed to the chassis. Thus, the gear ratio between the electric motor shaft is $(57/18) \times (18/23) = 2.478$, where the MG2 spins 2.478 times faster than the ring gear and therefore the torque output of MG2 is effectively multiplied by 2.478 prior to reaching the ring gear. Gear teeth on the outer periphery of the ring gear, collectively referred to as the counter drive gear, mesh with the counter driven gear which supplies motive force to the drive shafts though the final and differential gear units. Consequently, the speed of MG2 is directly proportional to the speed of the vehicle. The generator rotor shaft is hollow and connects to the sun gear of power split planetary and the input shaft from the ICE is fed through the hollow generator shaft and connects to the planetary carrier. A locking gear mechanism is adjacent to the counter drive gear which is engaged when the vehicle gear selector is placed in park. A summary of the number of gear teeth for each gear is provided in Table 2.6. Since the Prius drive gear train is moderately different from the Camry drive train, a comparison is not easily made between each component of the drive train, but is more meaningful if the overall gear ratio is compared, as provided previously.
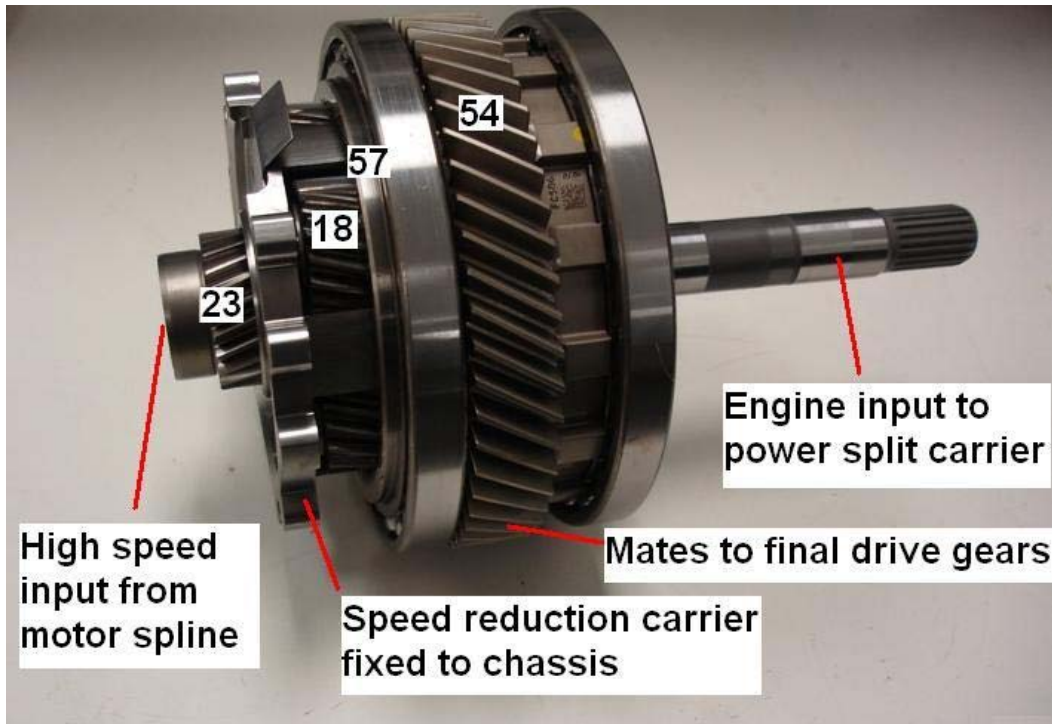
Fig. 2.61. Camry speed reduction planetary and power split planetary.

Table 2.6. Camry transaxle gear information

Power Split Planetary Gear Unit	The No. of Ring Gear Teeth		78
	The No. of Pinion Gear Teeth		23
	The No. of Sun Gear Teeth		30
Motor Speed Reduction Planetary Gear Unit	The No. of Ring Gear Teeth		57
	The No. of Pinion Gear Teeth		18
	The No. of Sun Gear Teeth		23
Counter Gears	The No. of Drive Gear Teeth		54
	The No. of Driven Gear Teeth		55
Final Gears	The No. of Drive Gear Teeth		23
	The No. of Driven Gear Teeth		80
Total Deceleration Ratio			3.542

2.2.3 Motor Mass and Volumetric Assessments

When comparing the Camry and Prius electric drive characteristics, the mass and volume of the primary electric drive motor, MG2, was decreased although the peak and continuous power capabilities of the motor increased. This was primarily accomplished by increasing the rated speed of the motor from about

6,000–14,000 rpm. To clarify the benefit of increasing the speed rating, the torque and power rating of the Prius motor is given in Fig. 2.62. These are shown to present the general speed, torque, and power relationship of any motor as power is equal to torque times speed. Therefore, a much lower torque is required to produce a certain power level at a higher speed than for a lower speed. For example, a torque of 382 Nm is required to produce 40 kW at 1000 rpm, whereas only 38.2 Nm is required to produce 40 kW at 10,000 rpm. Additionally, torque is proportional to current and, roughly speaking, the amount of current required to produce a consistent power level decreases with increasing speed. While this is not entirely an accurate statement as there are many factors to consider when making such a comparison, the concept generally holds true.
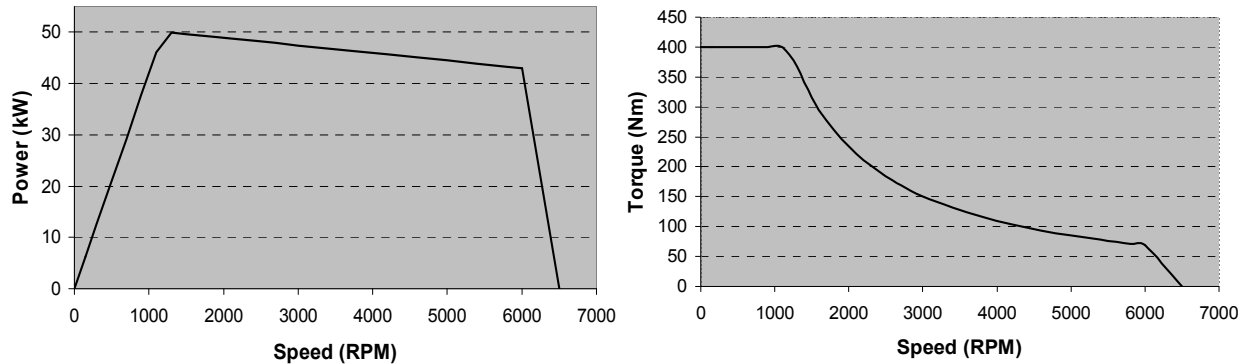
Fig. 2.62. Speed, torque, and power relationship.

There are a few negative aspects of moving to higher motor speed ratings however. Typically, the low speed torque rating of the motor is compromised when the speed rating is increased. Therefore, the lowest speed at which rated power can be developed, namely base speed, increases. Again, these relationships depend upon various motor design parameters such as rotor diameter, lamination stack length, magnet strength, and winding configuration, yet these relationships are typically pertinent. As rotor speed ratings increase, additional mechanical design aspects must be considered. Improved support must be provided by the rotor laminations to retain the PMs which are subjected to forces which are directly proportion to the square of the rotor speed. Additionally, bearings must be designed to withstand the high speeds of the rotor shaft. Depending on the characteristics of the PMs, rotor, and stator, core losses and induced back-emf voltages typically increase with increasing rotor speed. The high speed reduction gear used in the Camry design is required to convert the high speed of the motor to properly match the remaining transaxle design. Although the torque rating of the Camry is only 270 Nm, the maximum torque is converted to about 670 Nm through the speed reduction gear.

Figures 2.63 and 2.64 provide various views of the Camry transaxle and the volume associated with the primary drive motor. Certain key dimensions are shown, but several others are needed to determine volume since the motor terminal box, and especially the heat exchanger shown in Fig. 2.64 have complex geometries. Since the motor casing also houses some of the gear box, the motor casing had to be well defined to arrive at the mass and volume, excluding areas unrelated to the motor. For example, in Figs. 2.63(a) and 2.63(b), the surface chosen for the end of the motor housing is indicated.
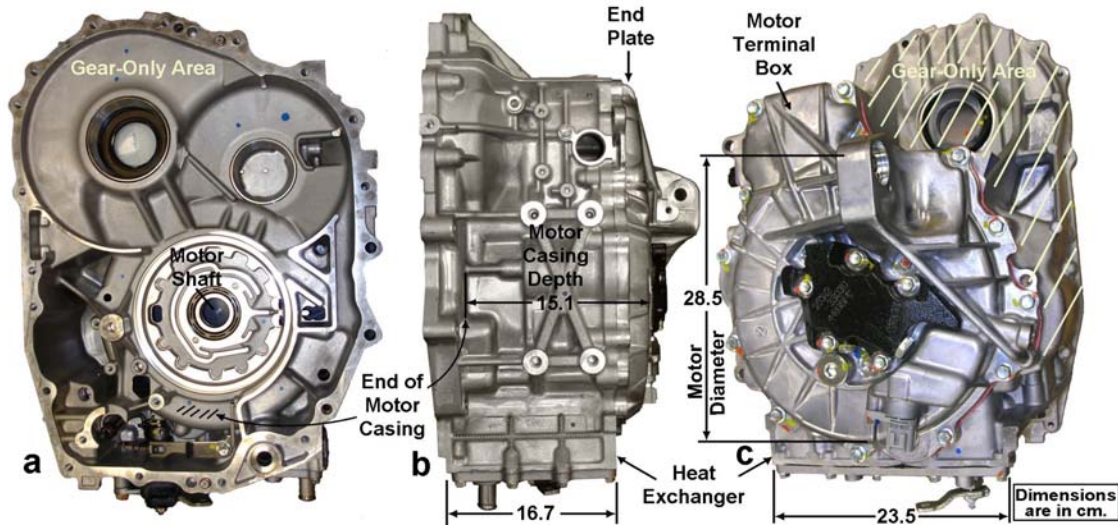
Fig. 2.63. Camry motor assembly after separation from generator assembly.
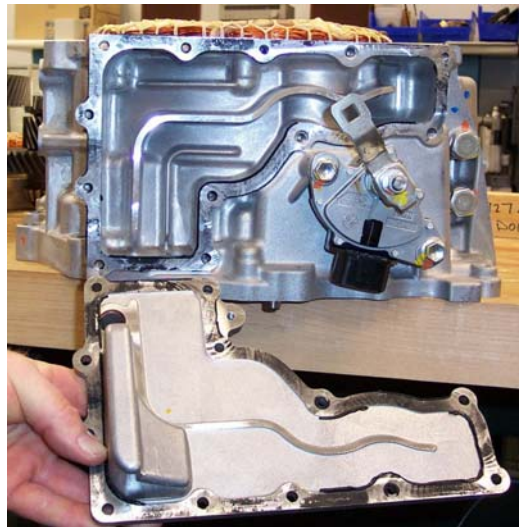
Fig. 2.64. Coolant channel at bottom of motor casing.

The results of the packaging assessment were used to generate estimates of peak specific power and peak power density as summarized and compared to the Prius specs in Table 2.7. Because of advantages gained by increasing the maximum speed from 6,000–14,000 rpm, Toyota was able to optimize the Camry design such that motor volume and mass were both lower than for the Prius in spite of a higher published peak power rating. It is appropriate to include the mass and volume of the Camry speed reduction planetary gear in this comparison with the Prius and doing so mitigates the perceived improvement upon the Prius design.

Table 2.7. Specific power and power density estimates for the PMSM

Parameter	Camry	Prius
Motor peak specific power (without converter), kW/kg	70/~41.7 = **~1.68**	50/45.0 = **1.11**
Motor peak power density, kW/L	70/~14.8 = **~4.73**	50/15.4 = **3.25**

44

Figure 2.65 shows the stator assembly that was removed from the Camry transaxle assembly. The entire Camry stator assembly mass is 18.0 kg, whereas the Prius stator assembly mass is 25.9 kg, with 5.7 kg and 6.8 kg of copper within each stator, respectively. The three-phase power input ("output" during regenerative braking) leads are clearly evident. A thermistor is embedded in the stator windings and the corresponding leads are routed adjacently to the motor leads. There are 18 wires bundled in each motor lead which splits in half to form a parallel winding configuration. The Camry stator windings have 9 strands of copper with 14 turns per pole and the Prius stator windings have 13 stands of copper with 9 turns per pole in parallel and series configurations, respectively. Notice that the product of the number of strands and the number of turns has a comparable result between the Camry and the Prius.
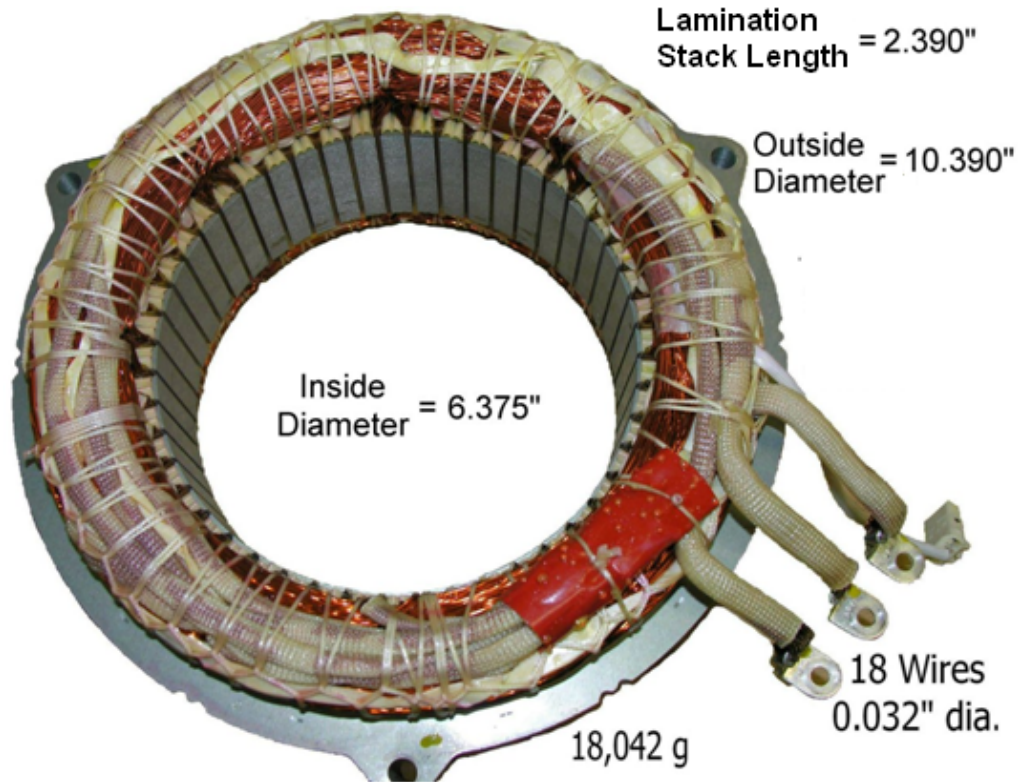
Fig. 2.65. Camry motor stator.

A comparison of the Camry and Prius laminations is provided in Fig. 2.66. In Fig. 2.66(a), a Camry motor stator lamination is placed on top of a Prius motor stator lamination, showing that the outer diameter (OD) of the Camry lamination is slightly smaller than that of the Prius. Through both Figs. 2.66(a) and 2.66(b) it is shown that the Camry motor stator slots are somewhat shorter, yet they are wider than the slots on the Prius motor stator laminations. The Camry generator stator laminations are identical to the Camry motor stator laminations. The motor lamination stack thickness has reduced from 3.29" on the Prius to 2.39" on the Camry. The Camry generator lamination stack thickness is 1.41". The inner diameters (IDs) of the Camry motor, Camry generator, and Prius motor stator laminations are equal. The stack lengths and outer diameters of the rotors have corresponding similarities.

a

b

Camry stator winding slots are shorter, yet wider than Prius
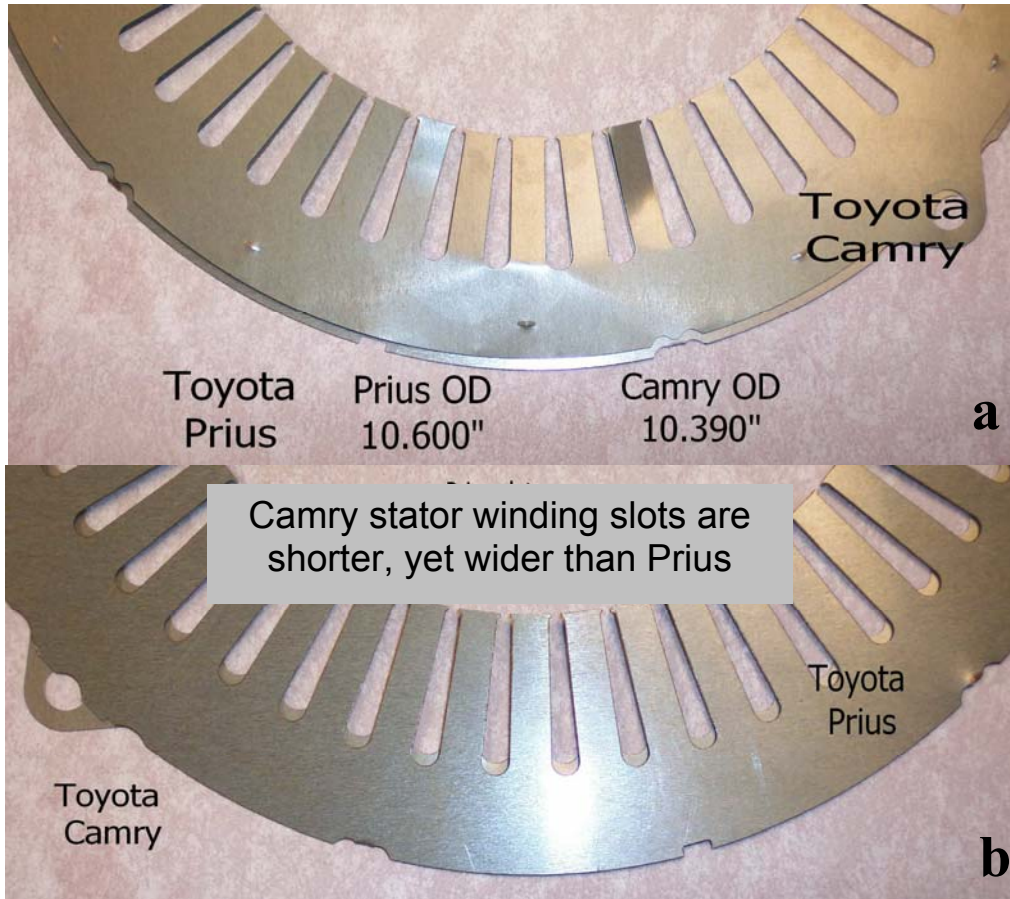
Fig. 2.66. Camry and Prius motor stator laminations.

Figure 2.67 shows details of the Camry rotor assembly and the "V" orientation of the neodymium iron boron (NdFeB) interior PM. Looking at the pair of magnets in the foreground, it is possible to see the narrow support bar that passes between them. This support bar, missing from the Prius motor laminations, helps to enable the motor to operate at much higher rotational speeds.

Fig. 2.67. Camry rotor assembled (left) and partially disassembled (right).

In making various comparisons between the Camry and Prius motor components, the highlights shown in Table 2.8 were generated. The table summarizes the general motor design, rotor and stator dimensions/mass, and the wiring and slot details of the stator. Because the rotor and stator lamination geometries are difficult to fully describe in a table, Figs. 2.68 and 2.69 provide this information. The length of the magnets decreased along with the decrease in the stator and rotor lamination stack length. However, the thickness and width of the Camry and Prius motor PMs are very similar. Details regarding the magnet characteristics are provided in Section 2.2.4. Various motor characteristics were experimentally measured and the results are presented in Section 3.

Table 2.8. 2007 Camry/2004 Prius motor design comparison highlights

Parameter	Camry	Prius	Comments
Lamination Dimensions			
Stator OD, mm	264	269	OD
Stator ID, mm	161.93	161.93	ID
Stator stack length, cm	6.07	8.4	
Rotor OD, mm	160.47	160.47	OD
Rotor lamination ID, mm	105	111	ID
Rotor stack length, cm	6.2	8.36	
Air gap, mm	0.73025	0.73025	
Lamination thickness, mm	0.31	0.33	
Mass of Assemblies			
Rotor mass, kg	9.03	10.2	Including rotor shaft.
Stator mass, kg	18.0	25.9	
Stator core mass, kg	12.38	19.05	Laminations only.
Stator Wiring			
Number of stator slots	48	48	
Stator turns per coil	14	9	
Parallel circuits per phase	2 legs	0	
Turns in series per phase	4 per leg	8	
Number of wires in parallel	9 per leg	13	
Wire size, American wire gauge (AWG)	20	19	
Phase resistance at 21°C, ohm	0.023	0.069	Average of phase-to-phase divided by two.
Total mass of stator copper, kg	5.6	6.8	
Slot depth, mm	30.9	33.5	
Slot opening, mm	1.88	1.93	
Casing			
Motor casing mass, kg	9.5	8.9	Camry has thicker walls, larger heat exchanger, speed reduction gear casing and bearings
Motor casing diameter, cm	30.2	29.9	
Motor casing axial length, cm	17.0	20.5	
Magnets (NdFeB)			
Magnet dimensions, mm	60.6×19.1×6.6	83.1×18.9×6.5	One magnet (1/2 of "V" or pole).
Magnet volume, cm^3	7.63	10.2	One magnet (1/2 of "V" or pole).
Magnet mass, grams	58	77	One magnet (1/2 of "V" or pole).
Total mass of magnets, kg	0.928	1.232	Entire magnet mass in rotor.
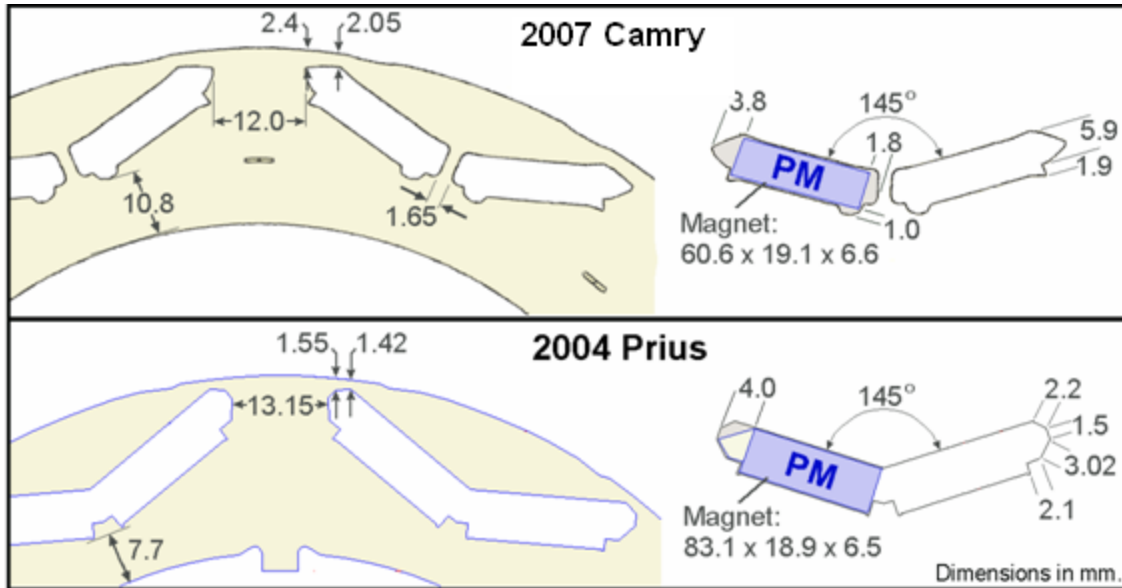
Fig. 2.68. Camry and Prius motor rotor lamination/PM design.
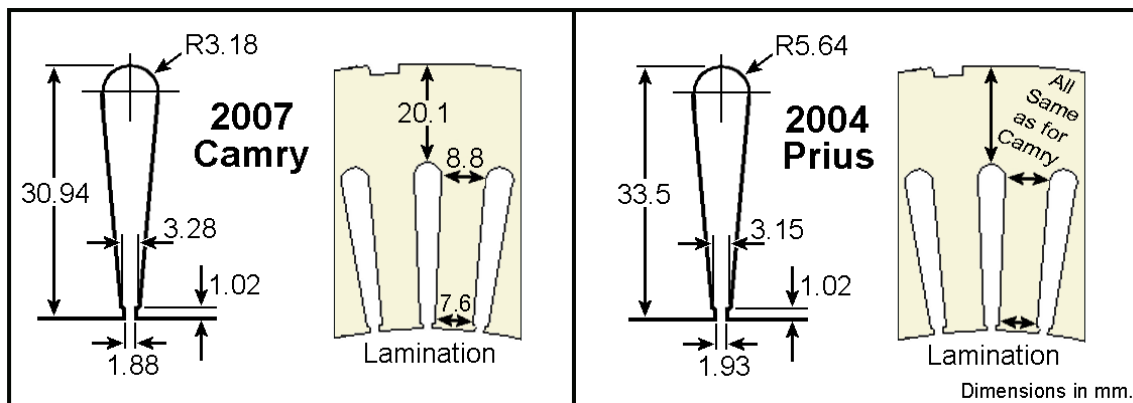
Fig. 2.69. Camry and Prius motor stator lamination/slot design.

Volume assessments of the Camry generator housing were conducted with the general approach and calculations shown in Fig. 2.70. The total volume of the Camry generator housing is about 11 L and the total mass is about 28 kg. The power rating of the Camry generator is approximately 40 kW compared to the 33 kW rating of the Prius generator. Comparisons of the Camry and Prius generator stators and rotors are provided in Figs. 2.71 and 2.72, respectively. It is evident that the generator has increased in both diameter and stack length by about 14% and 17.5%, respectively. The size of the Camry generator is more suited for continuous operation. A thermistor is embedded within the stator windings to provide temperature feedback and the MG ECU will discontinue operation of the generator upon reaching an over-temperature condition. A summary and comparison of the Camry and Prius generator specifications is provided in Table 2.9.
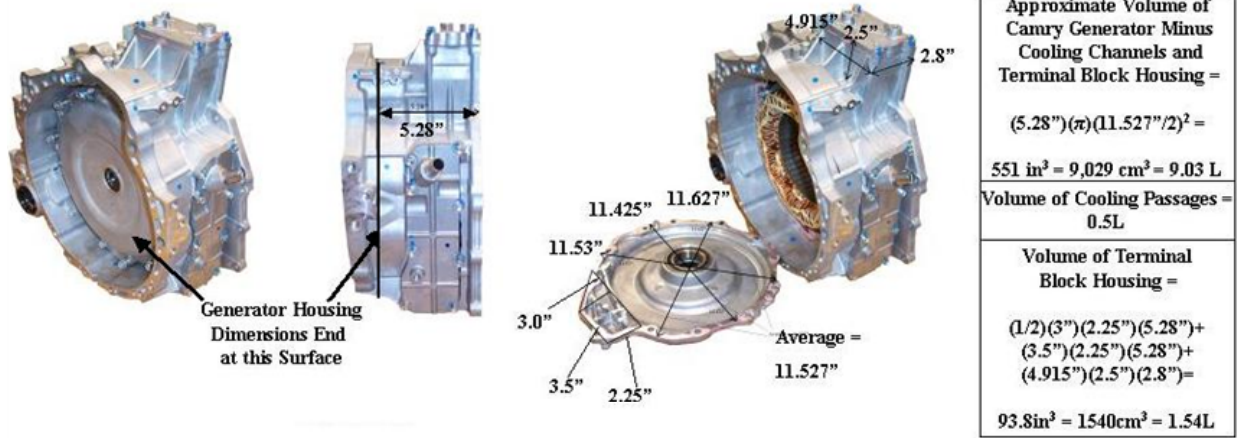
Fig. 2.70. Camry generator volume assessment.
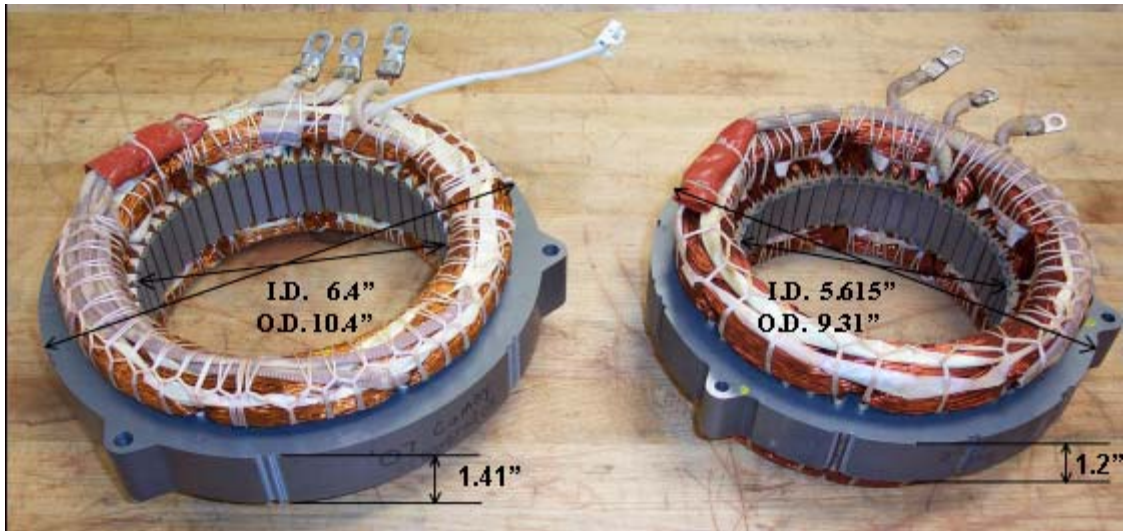
Fig. 2.71. Camry (left) and Prius (right) generator stator comparison.
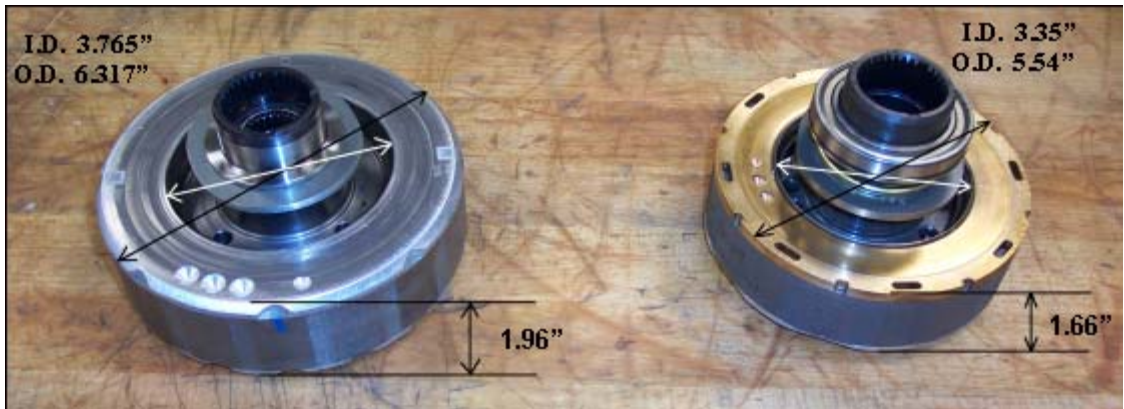
Fig. 2.72. Camry (left) and Prius (right) generator rotor comparison.

Table 2.9. 2007 Camry/2004 Prius generator design comparison highlights

Parameter	Camry	Prius	Comments
Lamination Dimensions			
Stator OD, mm	264.16	236.2	
Stator ID, mm	162.6	142.6	
Stator stack length, cm	3.58	3.05	
Rotor OD, mm	160.46	140.72	
Rotor lamination ID, mm	95.63	85.09	
Lamination thickness, mm	0.31	0.33	
Mass of Assemblies			
Rotor mass, kg	5.188	4.01	Including rotor shaft
Stator mass, kg	12.09	9.16	
Stator Wiring			
Number of stator slots	48	48	
Number of wires in parallel	18	12	
Wire size, AWG	20	20	

2.2.4 PM Characteristic Assessments

Hysteresis tests were conducted on the Camry motor PMs using the Walker Scientific AMH-40 hysteresisgraph (shown in Fig. 2.73), which is capable of producing 30,000 Oersteds of magnetic field strength. A hysteresis test provides information regarding the remanent flux density and coercivity of a magnet and these tests are often conducted over a wide range of temperatures. The remanent flux density, B_r, is the remaining flux density created by the magnet with no external field applied. Or simply stated the remanent flux density represents the strength of the magnet. The remanent flux density decreases to some extent with increasing temperature. The coercivity of a magnet is defined to be the intensity of the magnetic field required to reduce the magnetization of the magnet, and the coercivity of a magnet decreases with increasing temperature. Coercivity is an especially important characteristic of PMs that are used in HEV applications, which often involve high temperature and high field weakening operation conditions.

During hysteresis tests, the magnet is subjected to positive and negative magnetic fields while the impact of the externally applied magnetic field on the magnet is observed. A graph from hysteresis tests conducted on a magnet from the Camry motor rotor at 110°C is shown in Fig. 2.74. Two curves are shown on the graph with the burgundy trace being the normal, or total magnetic flux density, and the turquoise trace representing the intrinsic magnetic flux density. The intrinsic flux density is the flux density solely created by the magnet, which is obtained by subtracting the applied flux density from the total flux density. The remanent flux density is the value at which both curves intersect with the y-axis, which is at y = 11.86 kG in this case. The value of coercivity is found at the point where the intrinsic curve crosses the x-axis, which is x = 14.46 kOe in this case. A similar graph is provided in Fig. 2.75, with the hysteresis evaluation conducted at an ambient temperature of 198°C. Notice that the curves are much closer to the origin when compared to Fig. 2.74. As the temperature increased from 110–198°C, the remanent flux density and coercivity decreased from 11.86–10.29 kG and 14.46–5.757 kOe, respectively. The drastic decrease of the coercivity indicates that the magnet is much more susceptible to demagnetization at high temperatures.
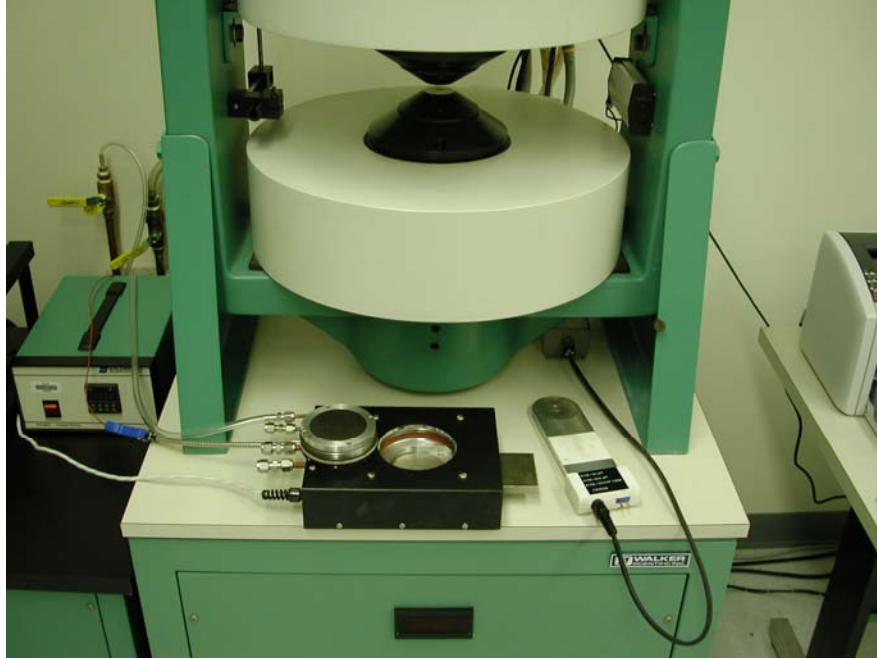
Fig. 2.73. Walker Scientific hysteresis graph.
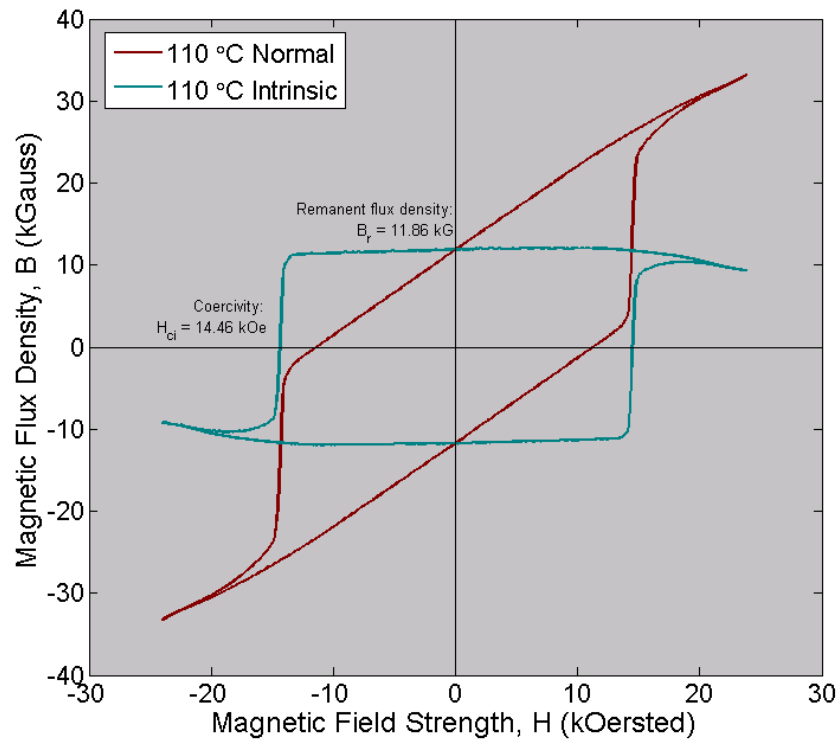
Fig. 2.74. Hysteresis graph for Camry motor magnet at 110ºC.
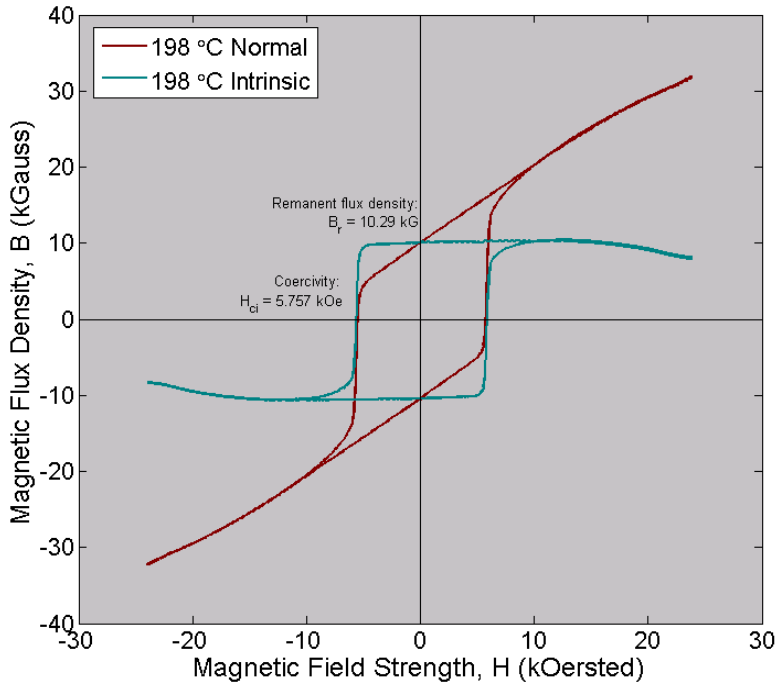
Fig. 2.75. Hysteresis graph for Camry motor magnet at 198ºC.

Intrinsic curves from hysteresis tests conducted with a Camry motor magnet at various temperatures have been combined onto one plot in Fig. 2.76. These curves further exemplify the diminishing nature of the remanent flux density and coercivity with increasing temperature. A similar graph containing the intrinsic curves obtained from the Prius motor magnet hysteresis tests is provided in Fig. 2.77. Although it is difficult to make a detailed comparison using these figures, a general comparison indicates that the coercivity of the Camry magnet is significantly lower than that of the Prius.
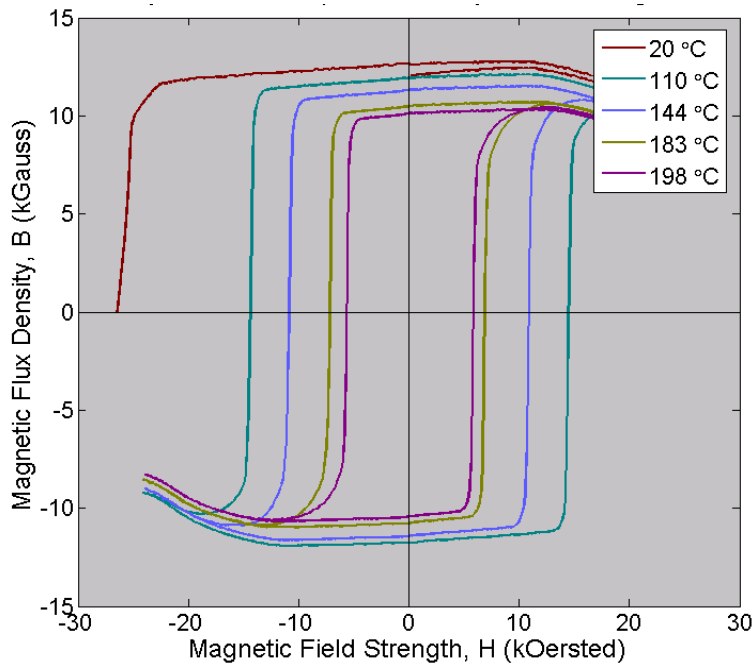
Fig. 2.76. Intrinsic hysteresis graphs for Camry motor magnet at various temperatures.

52
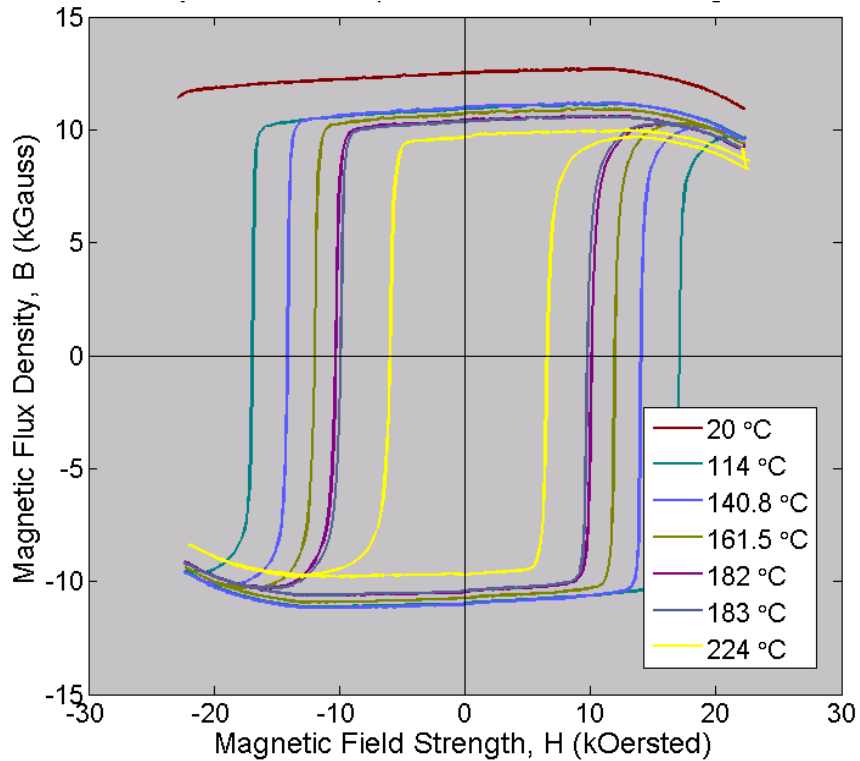
Fig. 2.77. Intrinsic hysteresis graphs for Prius motor magnet at various temperatures.

To provide a more straight forward comparison of the remanent flux density characteristics of the Camry and Prius motor magnets, the values were plotted versus temperature in Fig. 2.78. The strength of the Camry motor magnet is marginally higher than the strength of the Prius motor magnet, except for temperatures beyond about 215ºC. A similar plot is shown in Fig. 2.79 for the coercivity versus temperature relationship of the Camry and Prius motor magnets. The coercivity of the Camry motor magnet is about 70% of the coercivity of the Prius magnet, except for temperatures above about 200ºC where the coercivity values are a bit closer.

Although the Camry motor magnet is slightly stronger than the Prius magnet, the coercivity is much lower and, therefore, is much more susceptible to demagnetization when subjected to high temperatures and/or high strength magnetic fields which oppose the direction of the magnetic field of the magnet. It is common to apply opposing magnetic fields to the magnets when operating at high speeds, wherein high back-emf voltages are subdued to enable high speed operation within the voltage constraints. It is very likely that the cost of the Camry motor magnet is lower than the cost of the Prius magnet and although it has a lower coercivity, demagnetization can be avoided using preventative control techniques.

53
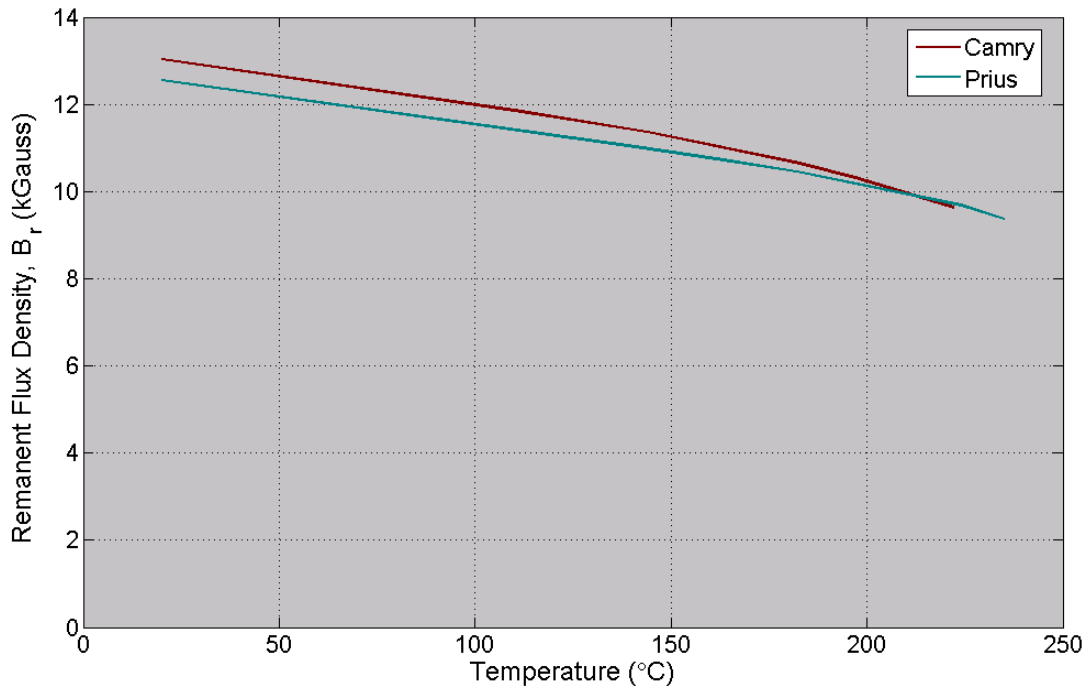
Fig. 2.78. Remanent flux density for Camry and Prius motor magnet.
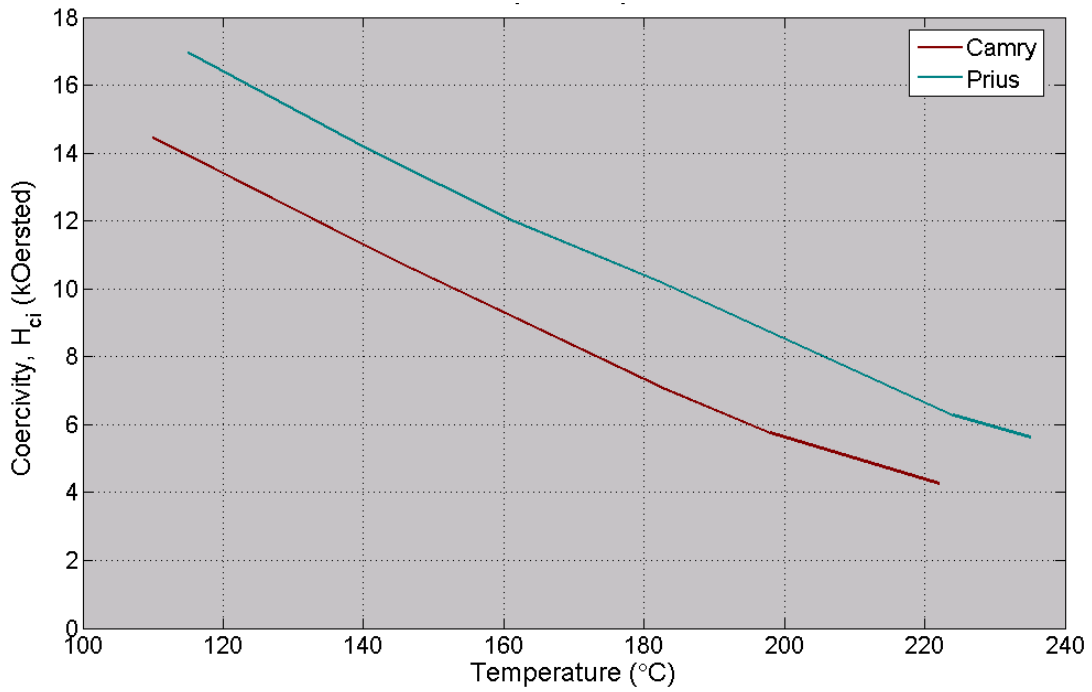
Fig. 2.79. Coercivity of Camry and Prius motor magnet.

3. BENCHMARKING TESTS OF CAMRY PMSM AND INVERTER

This section describes the hybrid Camry subassembly preparation and the back-emf, rotational loss, locked-rotor, performance/efficiency, and continuous load duration tests. With the exception of the back-emf, rotational loss, and locked-rotor tests which did not require inverter operation, each was performed using both the PMSM and inverter subsystems.

3.1 SUBSYSTEM PREPARATION FOR TESTING

As design and packaging assessments of the transaxle and PCU were being conducted, preparation for testing of the subsystems was commenced, including hardware design and fabrication, controller/interface development, and instrumentation for the DAQ. Two separate approaches were taken to adapt the Camry PMSM to separate dynamometer setups as each provided a benefit in terms of implementation time versus unmitigated testing capability. Although basic framework was available from previous benchmarking efforts, a large portion of the efforts devoted to controller/interface and DAQ development required innovation.

3.1.1 Hardware Preparation

The first test setup approach provided a quick resolution and means to initiate testing, yet it did not provide testability throughout the entire operation range of the PMSM. Therefore, while the initial tests were being conducted with the first test setup, a second approach was instituted. Additionally, the dynamometer test cell was upgraded to suit the high speed and power demands of the Camry PMSM.

Similar to the approach taken with the Prius transaxle hardware setup, the first approach involved welding the power split planetary gear as shown in Fig. 3.1. This causes the ICE input shaft, which is easily accessible, to rotate at the same speed as the ring gear of the power split planetary gear unit. For the Prius design, the ring gear rotates at the same speed of the primary drive motor, MG2. However, the MG2 of the Camry is connected to the ring gear through the speed reduction planetary gear unit. Thus, although the first approach provided a quick means to access the motive force of the motor, uncertainties were associated with the influence of speed reduction gear losses upon power and efficiency measurements. To obtain accurate motor efficiency measurements, it is crucial to accurately measure the mechanical power produced directly by the motor. Nonetheless, the setup provided a quick means of test initiation and valuable insights, such as controller development aspects. Additionally, the setup eliminated the immediate need for equipment with high speed testing capabilities, which was not installed until a later time during the project duration.

The second approach involved design and fabrication of a shaft and faceplate (shown in Fig. 3.2) which adapts to the Camry motor rotor, transaxle mounting pattern, and the high speed torque cell face mount and spline shaft. Design considerations were carefully surmised to ensure that no part of the system operation was hindered or enhanced. Particularly, intense focus was placed on maintaining the operational characteristics of the thermal management and lubrication system mostly by ensuring that the oil flow pattern throughout the transaxle remained unchanged. This approach avoids uncertainties associated with the losses of the high speed reduction gear, thereby providing accurate measurements of motor power output.
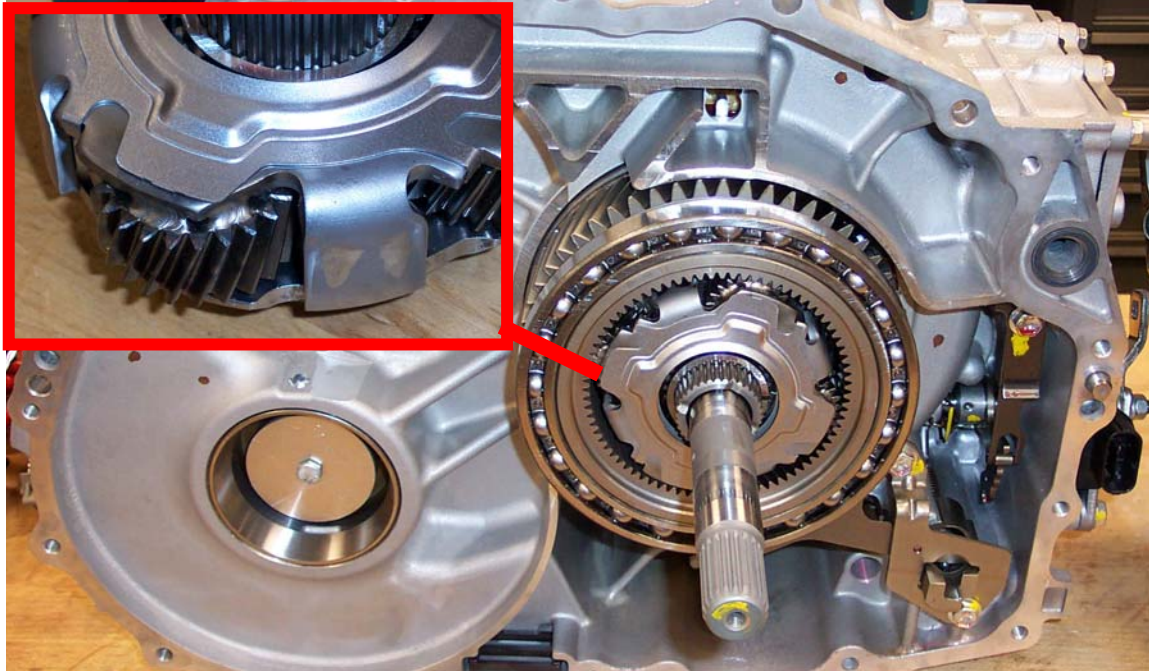
Fig. 3.1. First test setup approach with welded Camry planetary gear.
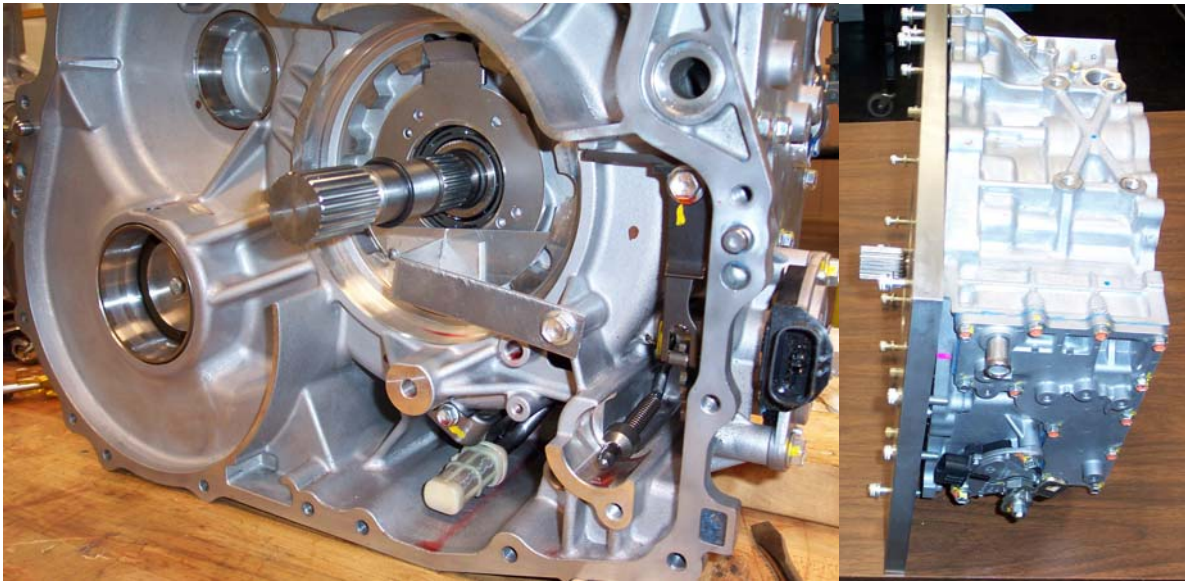
Fig. 3.2. Second test setup approach with modified motor rotor shaft.

To accommodate the high speed and power testing requirements of the Camry PMSM, the test cell was upgraded with a 400 hp dynamomter and speed reduction gearbox, as shown in Fig. 3.3. The speed reduction gearbox was required to match the speed range of the dynamometer to a speed of up to 18,000 rpm on the high speed input shaft. A high speed torque transducer (not shown) attaches to the high speed input shaft of the gearbox via a face mount support. The spline shaft output of the modified Camry rotor shaft and the fabricated faceplate mates with the input of the high speed torque transducer.
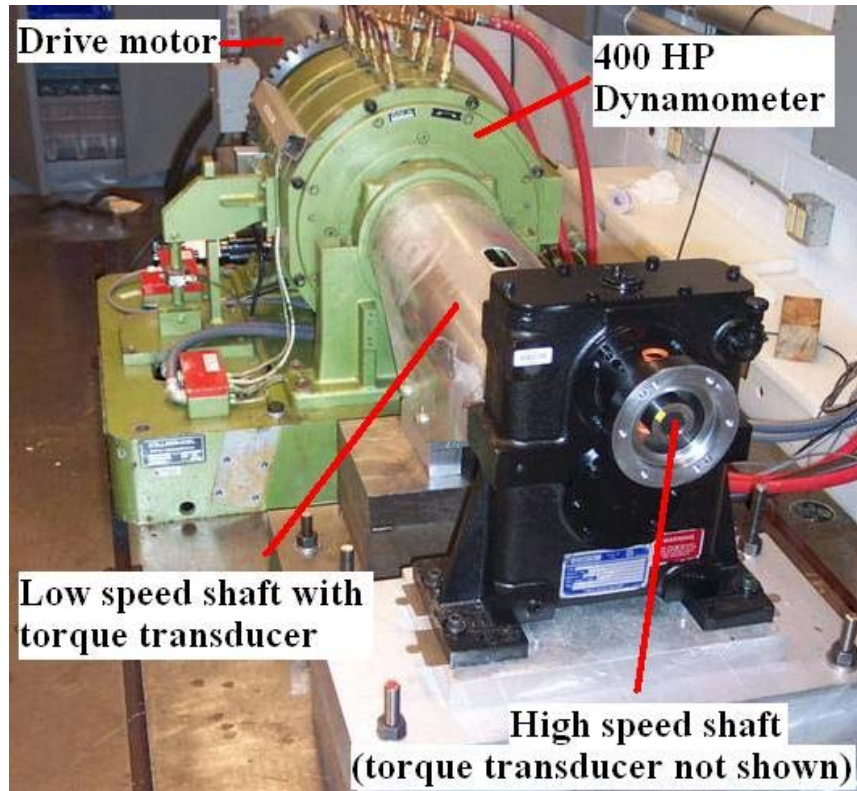
Fig. 3.3. Upgraded dynamometer test cell.

3.1.2 Instrumentation and DAQ Development

The PCU, PMSM, and transaxle were instrumented with thermistors and TCs in order to monitor and record thermal conditions and characteristics of the subsystem during various operation conditions. In preparation for performance, efficiency, and continuous duration tests in the ORNL laboratory, the motor inverter was instrumented with three TCs placed in the edges of the three power electronics heat spreaders as shown in Fig. 3.4. Two other TCs were placed in the (1) aluminum wall against the potted inductor of the buck/boost converter, and (2) edge of the heat spreader for the buck/boost converter power electronics module.
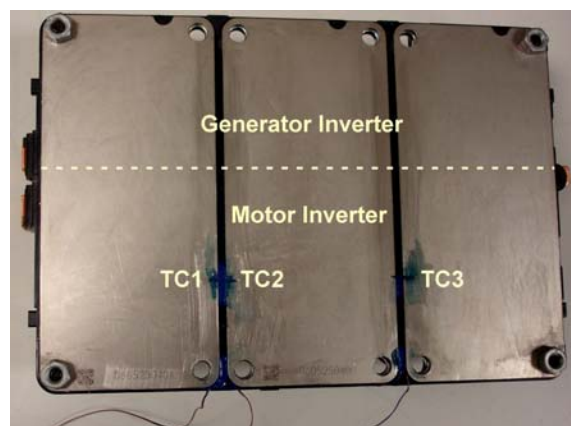
Fig. 3.4. TCs in the inverter power electronics heat spreaders.

57

Thermistors were installed in various locations on the stator windings and transaxle housing, as indicated in Fig. 3.5. Each location has a unique letter identifier and additional location information. For example, thermistor "D: ML 1" is located on the motor lead side of the stator at the 1 o'clock position indicated by the red circle. All thermistor locations on the front side of the stator are indicated by red circles and thermistor locations on the rear of the stator are marked with cyan circles. Case thermistor locations are indicated by light green circles and oil thermistor locations are indicated by orange circles. Note that thermistor "E: ML 2" is the original factory installed thermistor. The resistance of an identical thermistor was evaluated over a wide range of temperatures in order to generate a lookup table to be used with the DAQ software.
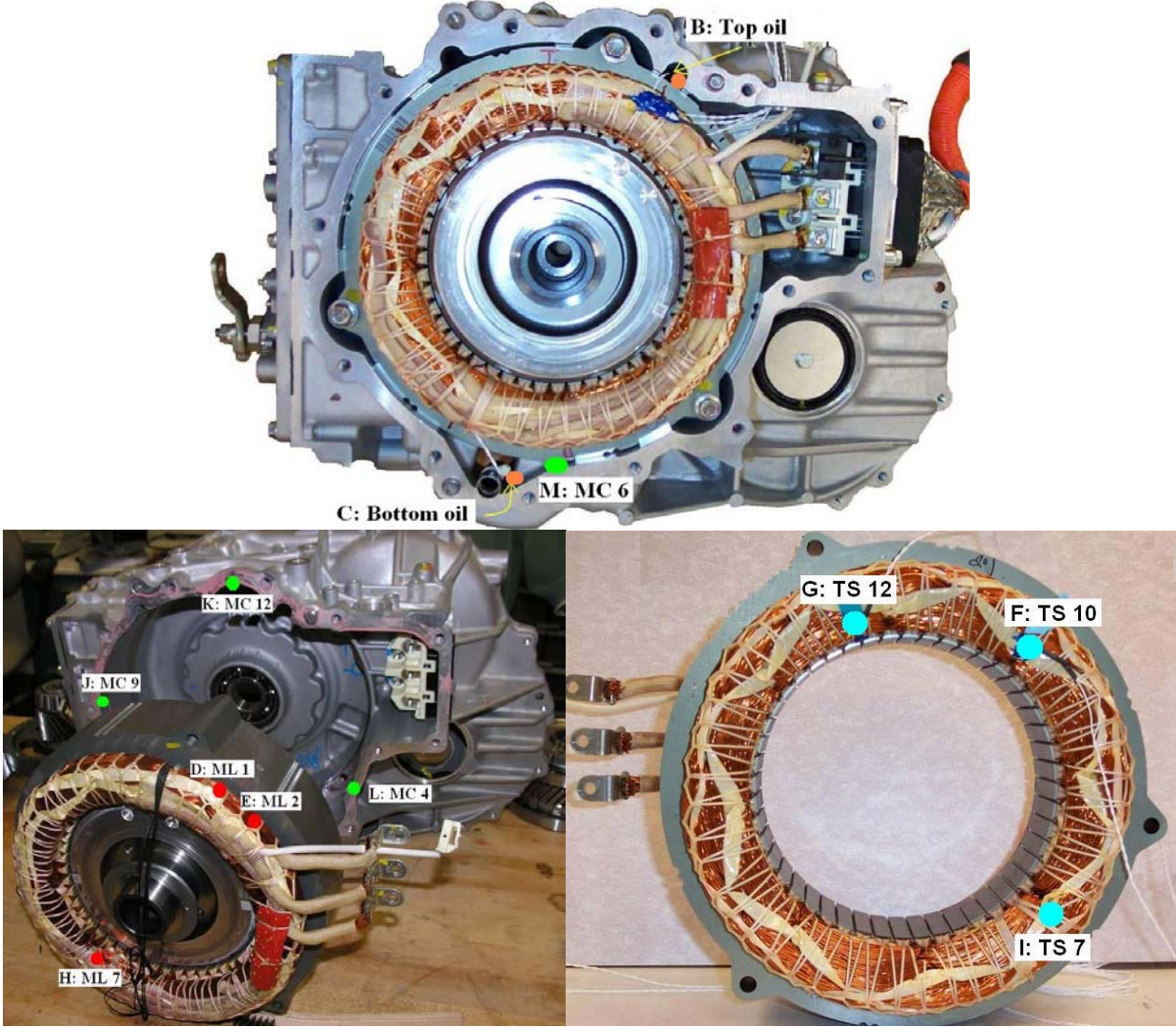
Fig. 3.5. Thermistor locations on PMSM and transaxle.

The Camry transaxle was modified to include windows and temporary viewports in the locations shown in Fig. 3.6 to facilitate observations of the oil system characteristics. These observations provided useful information regarding oil circulation and oil levels in various locations throughout the transaxle. It was especially necessary to assess these characteristics as the design, fabrication, and implementation of the second test setup approach was carried out and that these characteristics remained unchanged during

operation. It was determined that the oil reservoirs as well as the upper oil channels are nearly full when the ring gear is rotating at speeds near 1,000 rpm.
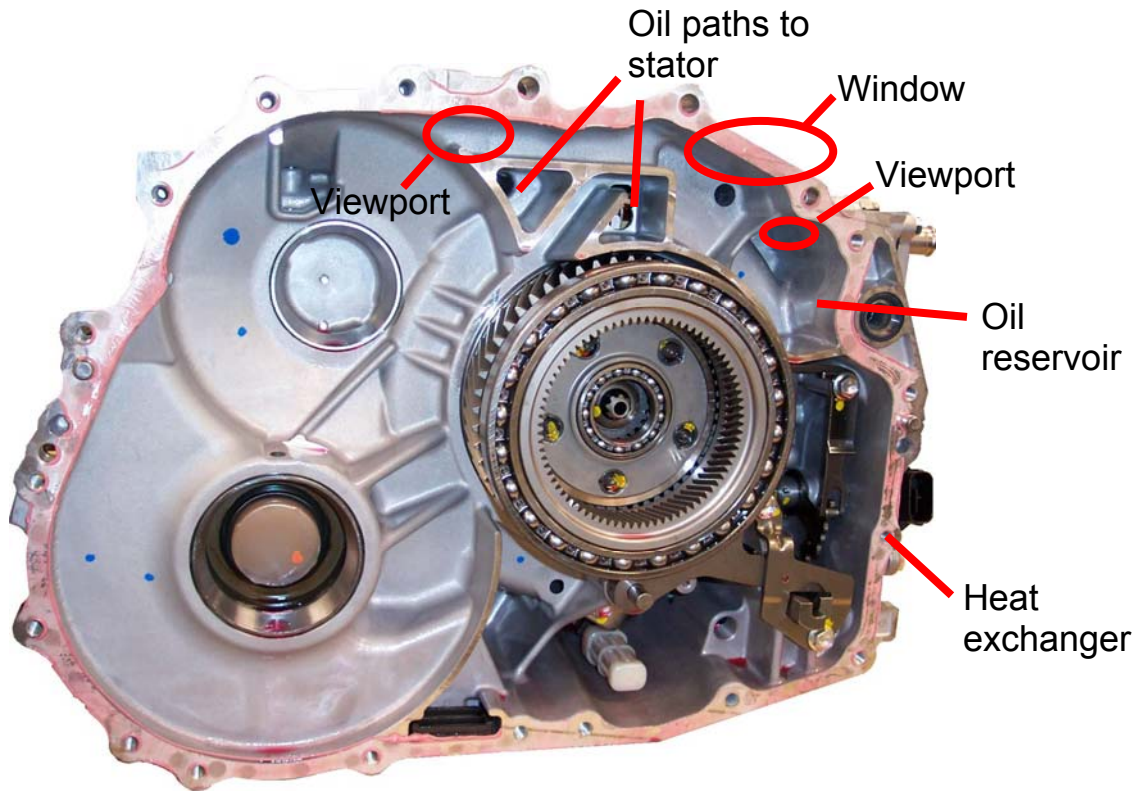
Fig. 3.6. Viewport and window locations implemented on transaxle.

A program written in the Visual Basic programming language was developed to collect data from various measurement instruments and merge the data into a convenient spreadsheet format. Torque, speed, and mechanical power were obtained using a Himmelstein torque and speed transducer. Temperature measurement signals from thermistors and TCs were collected with a Keithly 2700 acquisition unit. A Yokogawa PZ4000 power analyzer was used to carry out electrical measurements such as ac and dc rms voltage, rms current, real power, and many other properties of the waveforms.

The DAQ system was important not only for data logging, but it also served as a real time feedback system in which system conditions were monitored to ensure that operational limitations were not violated and to ensure that the system was being operated in an optimal manner. Temperature and current constraints were the primary limitations of the entire drive system. Efficiencies were calculated using the mechanical and electrical data and were used to verify that the controller operation was optimized.

3.1.3 Controller and Interface Development

The hybrid subsystems of the 2007 Toyota Camry were evaluated for performance and efficiency characteristics such as peak and continuous power ratings and motor/inverter efficiency. Continuous operational capabilities are greatly affected by the heat transfer characteristics of the motor, which is cooled through oil circulation and an ethylene-glycol coolant loop. The hybrid subsystems were operated over a broad torque-speed range in order to collect and analyze thermal and electrical data at a multitude of operation points. For each operation point during efficiency evaluations, the system was held in steady state for at least 20 seconds as a minimum of 5 data samples were taken.

ORNL's dynamometer test cell and Opal-RT-based speed and current feedback controller were adapted to provide the torque needed at each reference speed. Thus, as the applied torque from the dynamometer was varied manually, the controller regulated the torque producing current appropriately. The current controller consists of two standard proportional-integral (PI) controllers for the direct and quadrature currents, i_d and i_q, respectively. These *d-q* components are obtained by applying the *d-q* transformation to the three-phase currents which have a fixed reference. The transformation converts the three-phase currents into two-phase vectors, which have a reference that rotates with the rotor. Therefore, precise rotor position feedback is used during this transformation.

The steady state torque equation for the salient PM machine is expressed by:

$$\tau_L = n_p(L_d - L_q)\,i_d i_q + n_p K i_q, \tag{1}$$

where

n_p is the number of pole pairs,
L_d is the *d-axis* inductance,
L_q is the *q-axis* inductance, and
K is the back-emf and torque-current factor.

The total torque given by Eq. (1) consists of two torque terms which are reluctance torque and PM torque, respectively. PM torque is produced only by the current component along the *q-axis*. If current is applied which results with a negative component along the *d-axis*, positive reluctance torque is developed since the difference, L_d-L_q, in the first term is negative and all remaining variables and constants are positive in the motoring region. In theory, there is an infinite amount of *d-q* current combinations that will satisfy a particular operation condition. There is an optimal *d-q* current combination in which the motor efficiency is maximized for each particular torque. It is difficult to determine the optimal current trajectories for the entire torque-speed range, as complex factors such as effects of saturation and harmonics must be considered. Therefore, the DAQ was used to monitor the system efficiency to ensure that the controller is operating optimally.

A high level diagram of the Opal-RT controller and interface system is shown in Fig. 3.7. A console personal computer (PC) is used to develop and modify control schemes in a block diagram format, which is converted and compiled to traditional programming languages (mostly C) and sent to the target nodes through an ethernet network. The target nodes execute the controller code in real time and the console PC is used to control the mode of the controller operation as well as to update various parameters if desired. While the development process is more straightforward than microprocessor programming, the PC based architecture of the target nodes introduces a significant degradation in terms of control sampling frequency. Therefore, the system resources must be utilized in an efficient manner.
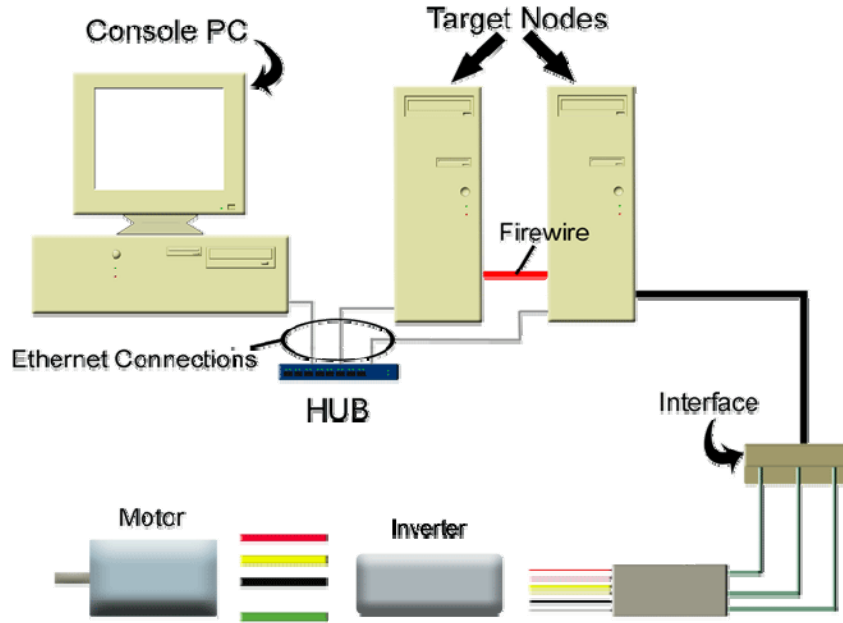
Fig. 3.7. Opal-RT controller and interface system.

3.2 BACK-EMF TEST RESULTS

The non-energized Camry PMSM was spun at various speeds over its full design range to obtain back-emf data. The shaft speed and back-emf data (line-to-neutral rms averaged for the three phases) is plotted in Fig. 3.8. This test was repeated after the performance/efficiency mapping test to verify that no magnetic strength was lost in the rotor during performance tests or extended periods of high-temperature testing. As expected, there were no significant differences in the data obtained from the second back-emf test.
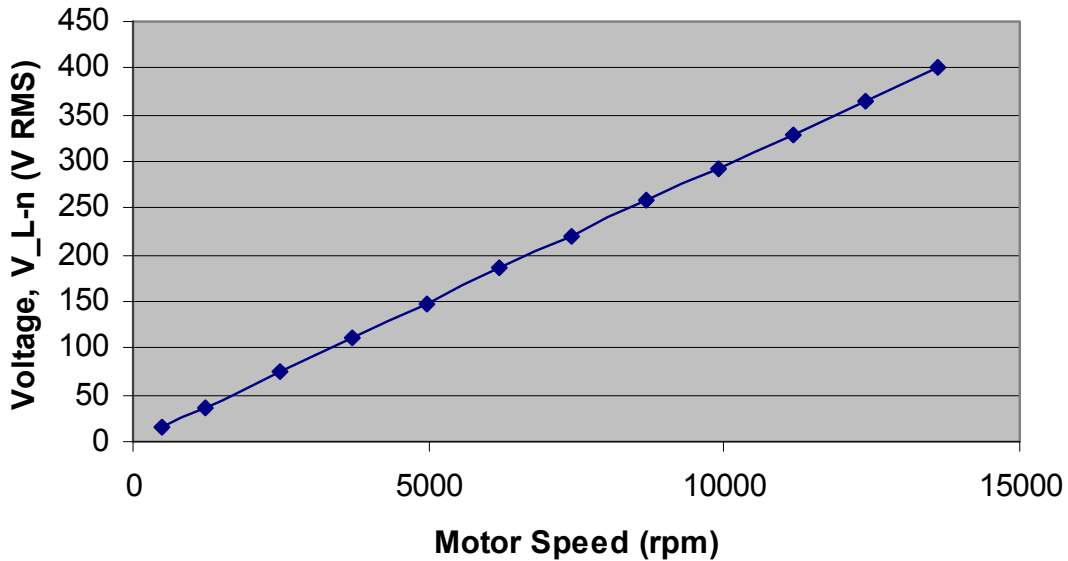
Fig. 3.8. 2007 Camry motor back-emf test results.

61

A plot containing the line-to-neutral back-emf voltage measurements observed during benchmarking evaluations of the Prius is shown in Fig. 3.9. A comparison of Figs. 3.8 and 3.9 indicates that the volts-per-hertz ratio of the Prius back-emf is higher. However, the maximum back-emf voltage of the Camry, observed at a shaft speed of 14,000 rpm is much higher than the maximum back-emf voltage of the Prius at 6,000 rpm. Note that the ratio of these maximum voltages is approximately equal to the ratio of the maximum dc-link voltages, which is 650/500.
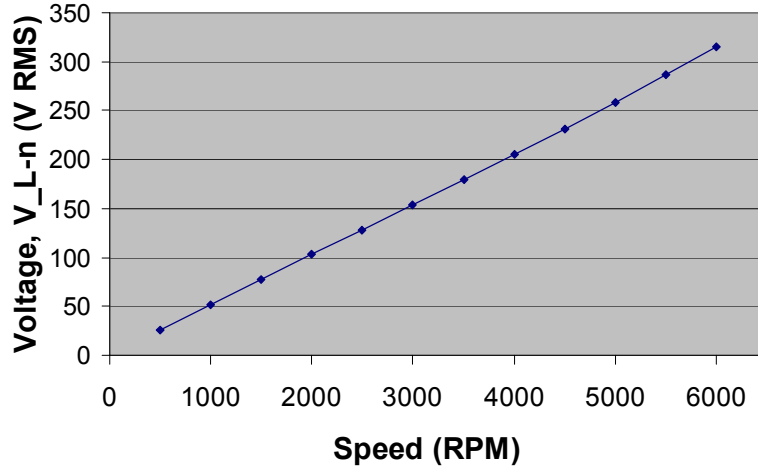
Fig. 3.9. 2004 Prius motor back-emf test results.

3.3 ROTATIONAL LOSS ASSESSMENTS

The rotational losses of the entire gear train and the Camry motor alone were evaluated by rotating the input shafts with an external drive motor. Gear train loss assessments began with the entire gear system installed, which includes the drive gears and planetary gears. The generator and motor rotor were removed in order to assess only the gear losses and motor core loss assessments were conducted at a later time. Torque and power measurements were measured and plotted versus ring gear speed as shown in Figs. 3.10 and 3.11, respectively. The average oil temperature was slightly higher than room temperature during these tests. Note the maximum speed shown in this plot is 5,500 rpm and since the speed reduction gear ratio is 2.47, the corresponding motor speed is 13,585 rpm and the vehicle speed associated with this extreme condition is approximately 113 miles per hour.
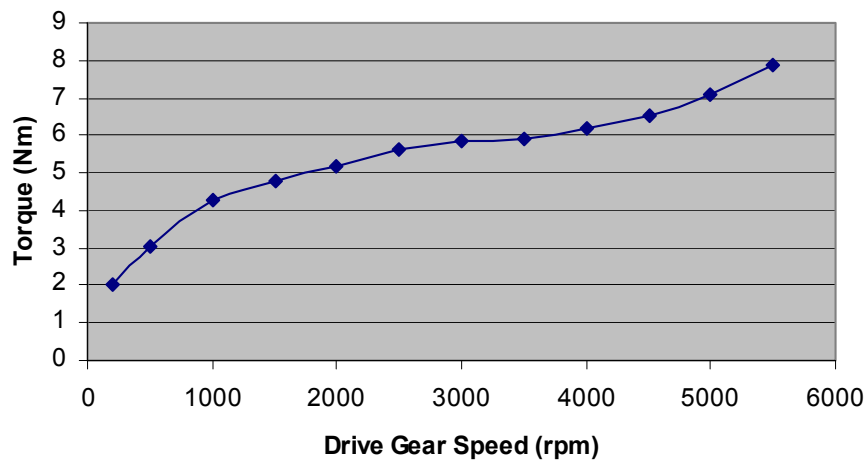
Fig. 3.10. 2007 Camry gear train rotational torque.
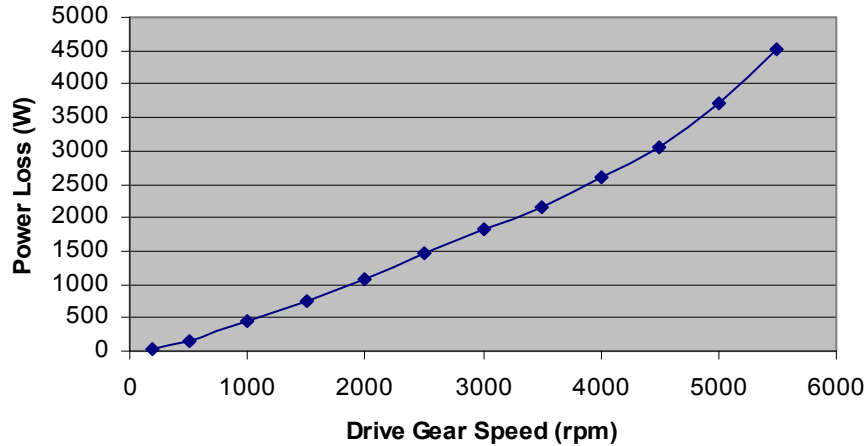
Fig. 3.11. 2007 Camry gear train rotational losses.

Results from the rotational loss tests conducted with the shaft connected directly to the motor rotor are shown in Fig. 3.12. These losses are mostly comprised of core (or iron) losses, which are associated with eddy currents and hysteresis effects. In combining the gear losses shown in Fig. 3.11 and the core losses shown in Fig. 3.12, it is inferred that a significant amount of losses are associated with the rotational motion of the drive system. Nonetheless, these losses are exceptionally low when compared to that of a conventional automatic transmission, which includes multiple planetary gears and clutching mechanisms.
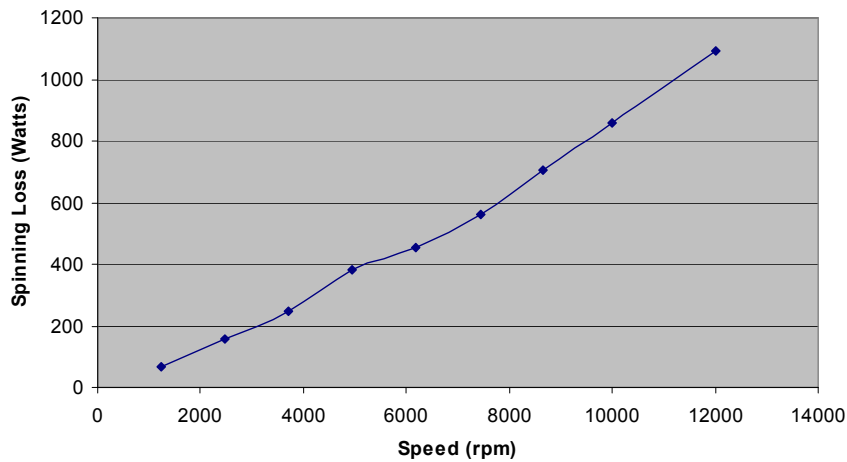
Fig. 3.12. 2007 Camry motor rotational losses.

Further gear loss assessments were conducted to obtain information which more specifically describes the losses associated with each component, as well as the influence of oil temperature upon the gear losses. The first test was conducted with all gears installed and the motor rotor removed and the oil temperature initially low. The Bay-Voltex external coolant temperature regulator was used to increase the oil temperature in order to observe the effects of increasing oil temperature as the rotor speed was held constant. These tests were conducted at ring gear speeds of 2000, 3500, and 5000 rpm. A gear system was removed after each test was conducted, and therefore the associated losses of the removed gear system can be assessed. The results from these tests are shown in Fig. 3.13, with the 2000, 3500, and 5000 rpm traces shown in shades of blue, green, and red, respectively. After tests were conducted with no motor rotor, the drive gears were removed, then the planetary gears were removed. Losses of the entire gear train tend to decrease with increasing oil temperature due to deceasing oil viscosity and losses are minimal near the common operation temperatures of the transaxle, namely 50–80ºC. Extended tests at

3500 rpm reveal that the gear losses increase beyond a temperature of 90ºC. In comparing the loss difference of each of the tests, the drive gears have the highest amount of losses associated with spinning motor and the planetary gears contribute only a small amount.
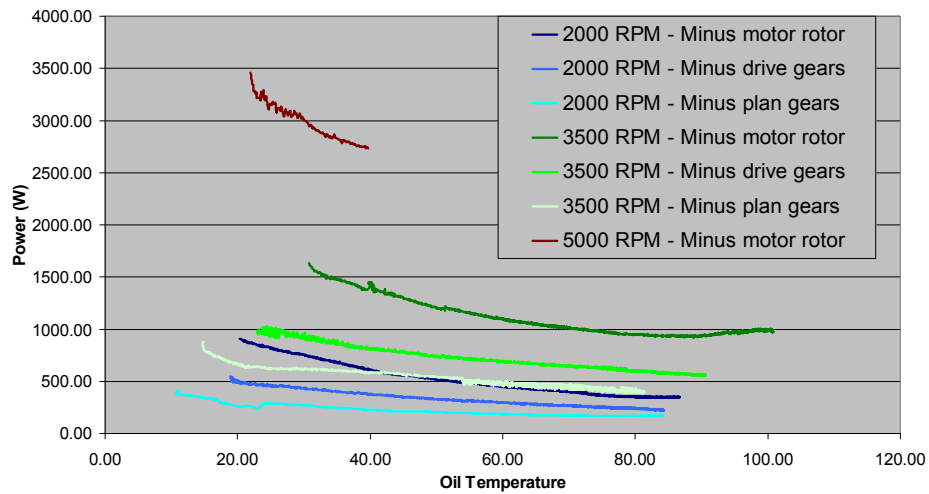
Fig. 3.13. 2007 Camry gear losses vs. oil temperature at various ring gear speeds.

3.4 LOCKED ROTOR TEST

A series of locked rotor tests were performed to determine the torque-producing behavior of the PMSM motor. During locked rotor tests, the rotor is rotated throughout an electrical cycle and the shaft is rigidly locked at each position as dc current is applied. Torque values were obtained from an in-line shaft torque sensor when the motor windings were energized. The resulting data was used to produce torque versus electrical position plots, which are shown in Fig. 3.14 for various current levels. These tests were not conducted at extremely high dc currents to avoid high temperatures which could potentially damage the stator windings or rotor magnets. The peak torque for each current level was chosen and is indicated by the blue trace in Fig. 3.15. Peak locked rotor torques for the Prius are also included in the figure, and are much larger than that of the Camry. However, the equivalent torque of the Camry motor on the low speed side of the speed reduction gear is much higher, as indicated by the yellow trace in Fig. 3.15.
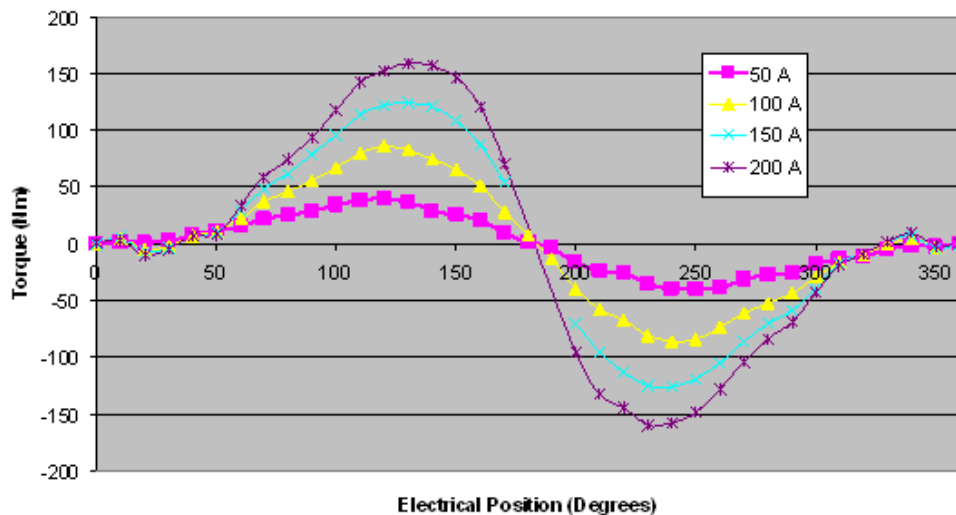
Fig. 3.14. 2007 Camry locked rotor torque vs. position for various dc currents.

64

Fig. 3.15. 2007 Camry and Prius peak locked rotor torque vs. dc current.

Interior PM motors have two torque components and there is an optimal current angle at which the two torque components produce the maximum torque per current. Figure 3.16 shows the PM torque, reluctance torque, and the total sum of the two torque components for a constant exemplar current magnitude. Although the maximum PM torque is produced at a current angle of zero electrical degrees and the maximum reluctance torque is produced at 45 electrical degrees, the maximum total torque is produced at about 35 electrical degrees. This optimal current angle varies with many conditions such as current magnitude and speed.
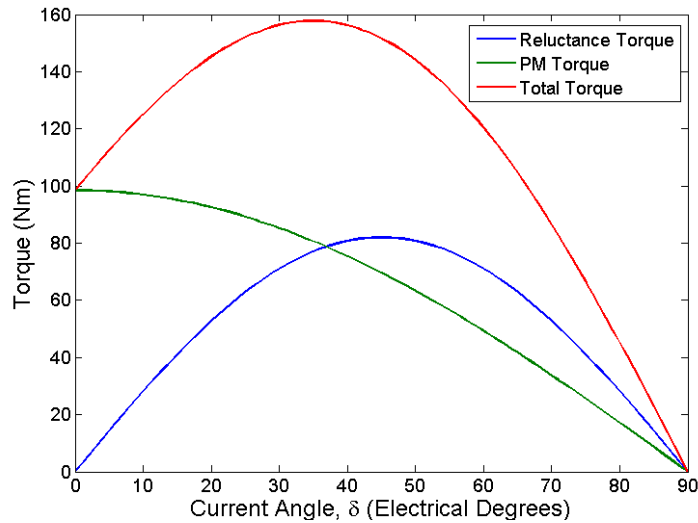
Fig. 3.16. 2007 Camry and Prius peak locked rotor torque vs. dc current.

3.5 PERFORMANCE AND EFFICIENCY EVALUATIONS

This section provides information about the performance and efficiency evaluations of the 2007 Camry hybrid subsystem components. The motor and inverter characteristics were evaluated simultaneously with power provided directly to the dc link as opposed to the power being supplied through the boost converter. Therefore, the 33 kW power rating of the inverter did not limit the capabilities of the motor and

65

inverter during the performance and efficiency assessment process. The dc-link voltage was maintained at 650 Vdc and a switching frequency of 10 kHz was used. Motor efficiency was measured throughout most of the entire torque-speed range in which the motor is capable of operating. For each operation point, the motor was controlled in steady state for at least 20 seconds and at least 5 data points were averaged to generate the efficiency map in Fig. 3.17.
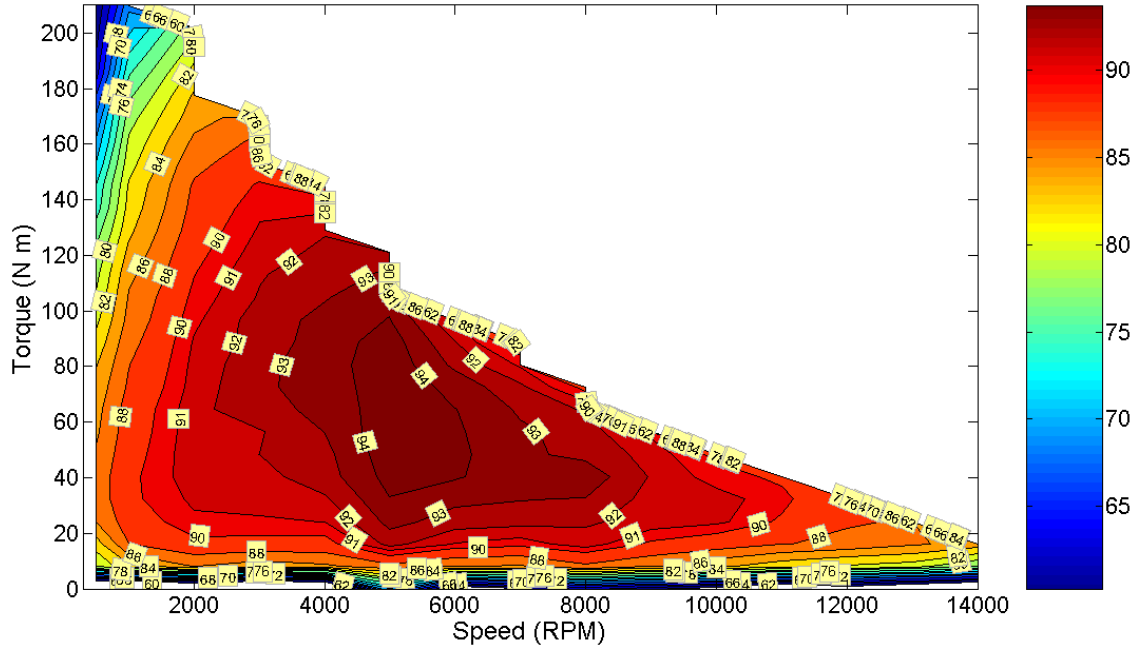
Fig. 3.17. 2007 Camry motor efficiency contours.

Efficiencies of the Camry motor are above 90% for a large portion of the torque-speed operation region. The high speed or high torque regions tend to incorporate lower operation efficiencies. To provide a straightforward comparison with the Prius motor efficiency map, the torque and speeds were scaled by 2.47 appropriately, as shown in Fig. 3.18. A comparison of the scaled Camry efficiency map and the Prius efficiency map in Fig. 3.19 reveals that the Camry has higher efficiencies for much of the map. Similar scales, axis limitations, percentage ranges, and color schemes are used to further ease the comparison. Note that a portion of the Camry high torque region is not visible. The most significant improvement over the Prius is observed at low speeds, where the Prius efficiencies drop quickly as torque increases and speed approaches zero. This region is frequented often since the electric motor is utilized to develop the torque required to accelerate the vehicle at low speeds or from standstill.
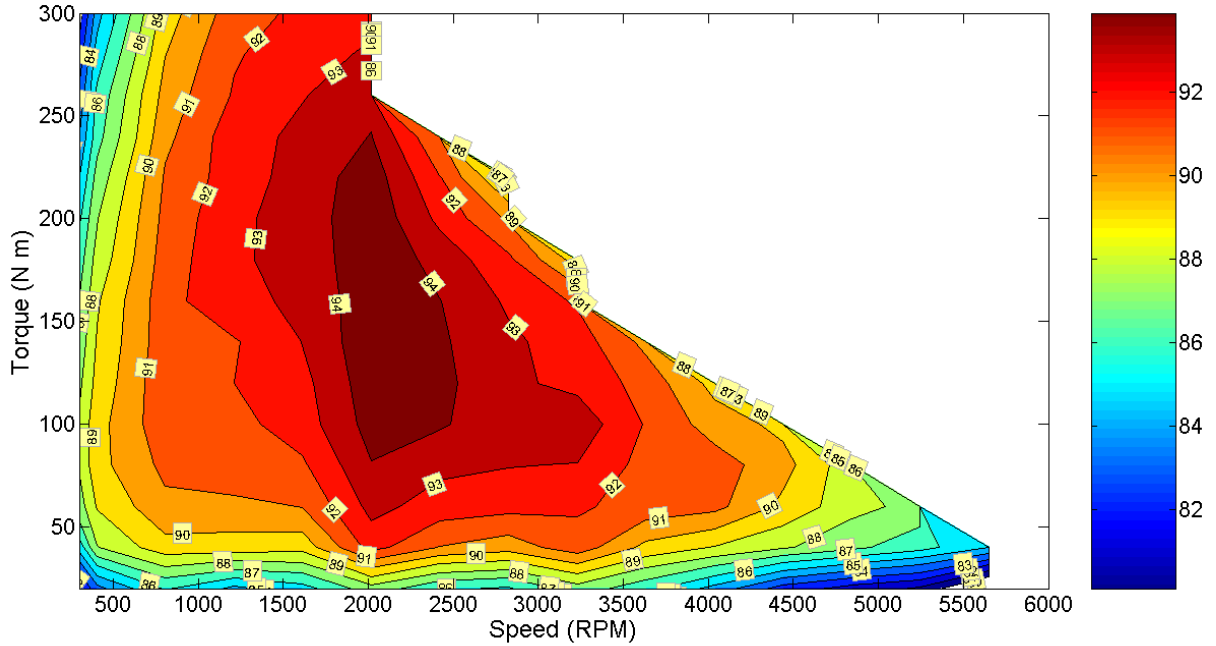
Fig. 3.18. 2007 Camry motor efficiency contours scaled by 2.47.
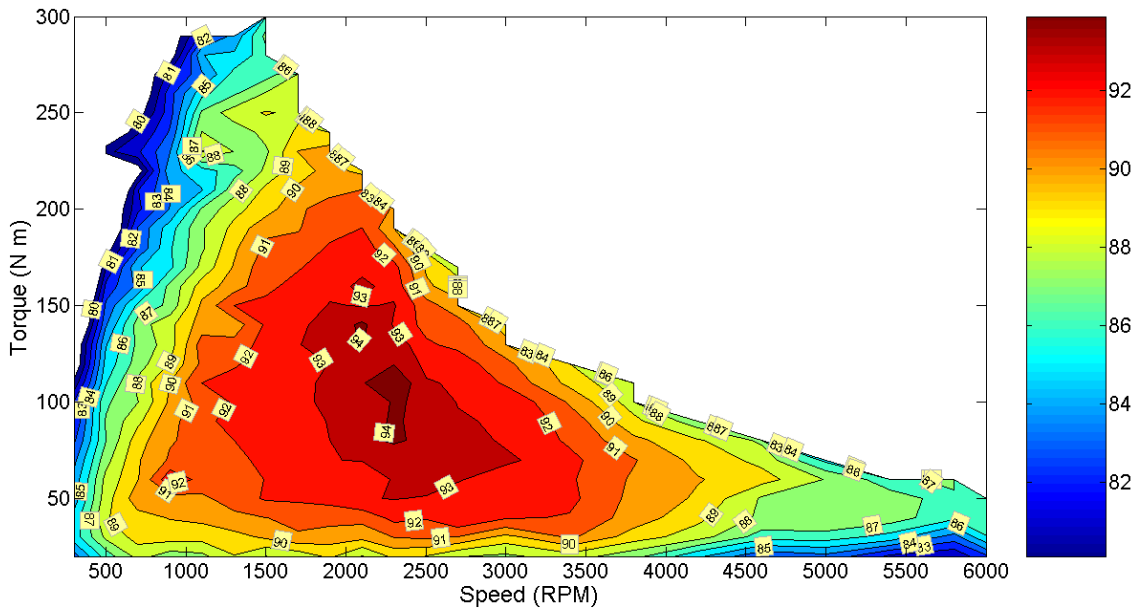
Fig. 3.19. 2004 Prius motor efficiency contours.

Thermal limitations hindered the extent of the Camry motor evaluations at low speeds and high torques, where steady state testing was limited to about 210 Nm in order to prevent over-temperature conditions. It has been verified through dynamic, short duration tests that the motor is capable of producing the published rated torque of 270 Nm, yet for only a very short time duration of a few seconds. According to the Camry service manual, the operation temperature of the motor is typically below 90ºC. With this limitation, the extent of maximum torque of 270 Nm is much shorter as temperature limitations were set at about 150ºC during the tests. The maximum power capability is limited by voltage constraints to about

67

70 kW at 4500 rpm. This matches the expected power rating based on the size of the generator inverter and boost converter. Estimated power rating techniques based on properties such as the mass, volume, speed, and thermal characteristics also result in similar power ratings for this motor. It is assumed that the published 105 kW power rating of the transaxle is the sum of the motor and generator power ratings as no rating is published for the generator.

Similar to the process used with the Camry motor efficiency contours, the Camry inverter efficiency contours were generated and scaled by the high speed gear ratio of 2.47 in order to provide a straightforward comparison with the Prius. A comparison of the inverter efficiency maps, shown in Figs. 3.20 and 3.21, indicates that the efficiency of the Camry inverter is somewhat lower than the efficiency of the Prius inverter for speeds below 2000 rpm. Similar scales, axis limitations, percentage ranges, and color schemes are used in these efficiency maps to further ease the comparison. The low speed, high torque capabilities of the Camry inverter appear to be greater than that of the Prius inverter as the speed reduction gear facilitates the use of a much lower current to generate the same amount of equivalent torque on the low speed side of the speed reduction gear. For low torques above 2000 rpm, the Camry inverter efficiency contours indicate that the efficiency decreases slightly as the torque approaches zero, whereas the Prius inverter efficiency remains consistent beyond 2000 pm. Higher losses of the Camry inverter is possibly due to the 30% increase of the dc-link voltage and the 50% increase in the number of power electronic devices when compared to that of the Prius.
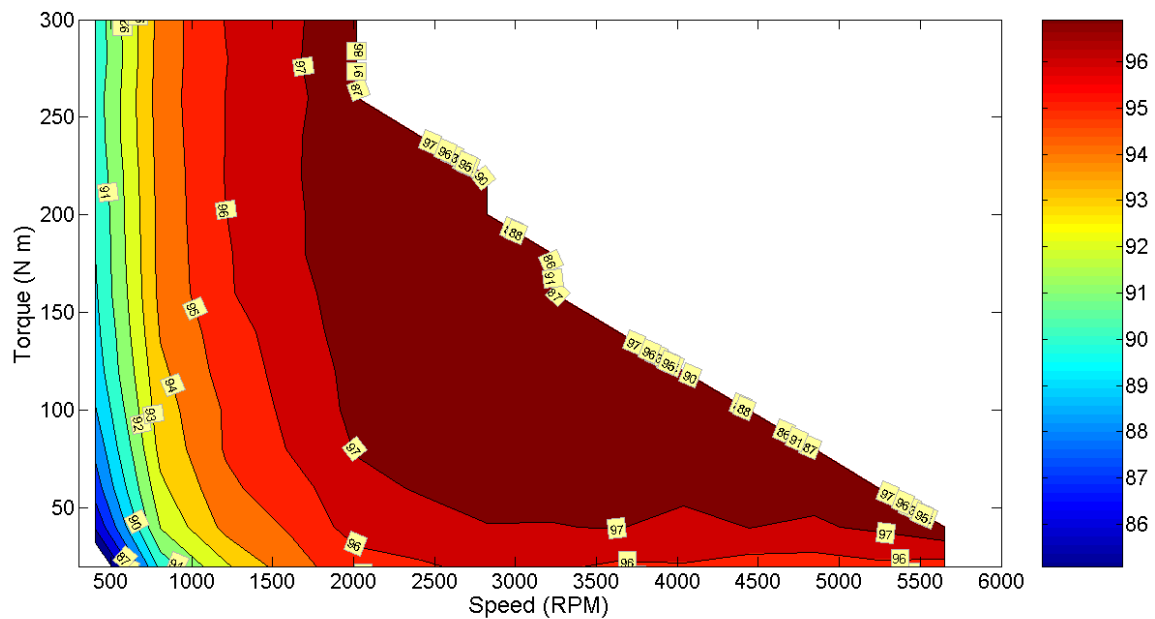
Fig. 3.20. 2007 Camry inverter efficiency contours scaled by 2.47.
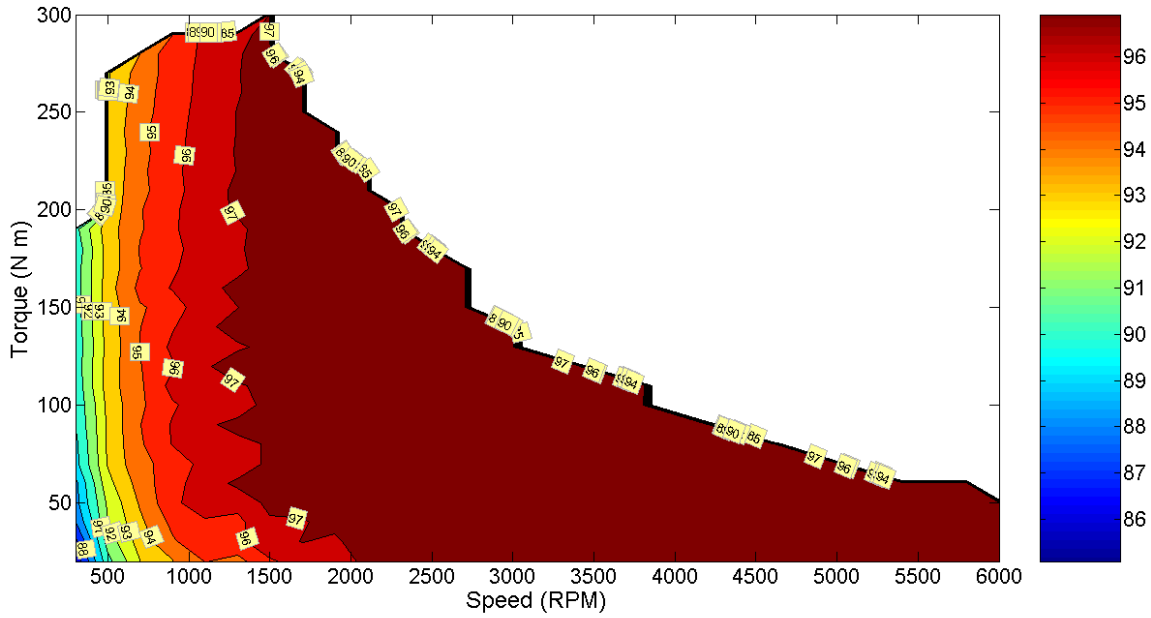
Fig. 3.21. 2004 Prius inverter efficiency contours.

The lower inverter efficiencies of the Camry cause the combined motor/inverter efficiencies to be somewhat closer than the motor efficiencies alone, as indicated in Figs. 3.22 and 3.23. Although there are striking similarities between the two efficiency contour maps, benefits of the high speed motor in the Camry are evident for the low speed, high torque regions.
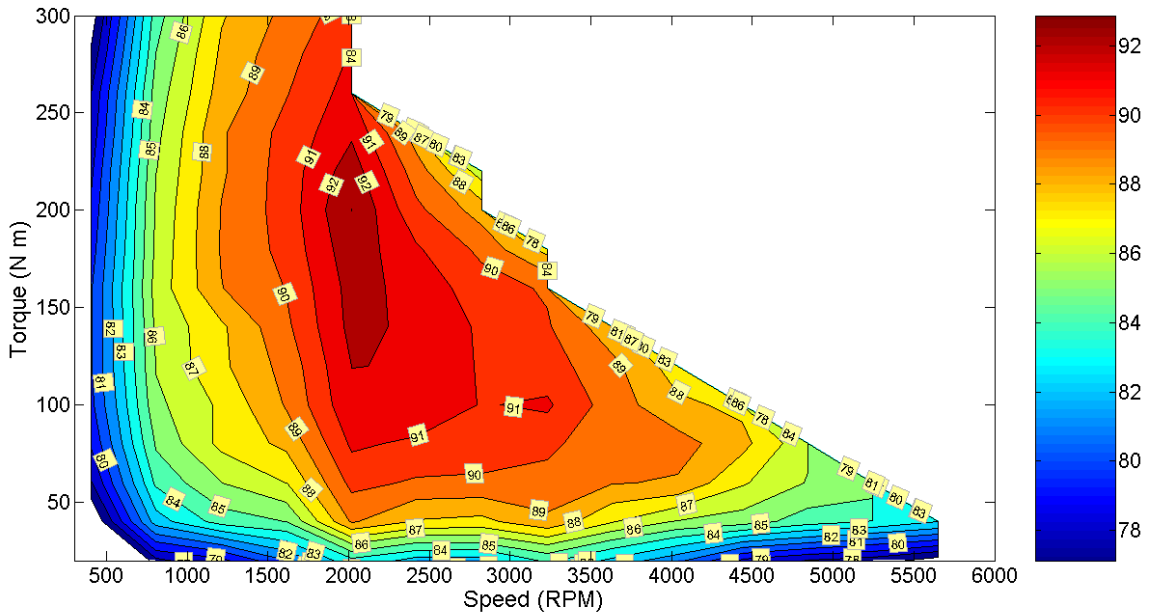
Fig. 3.22. 2007 Camry motor/inverter efficiency contours.
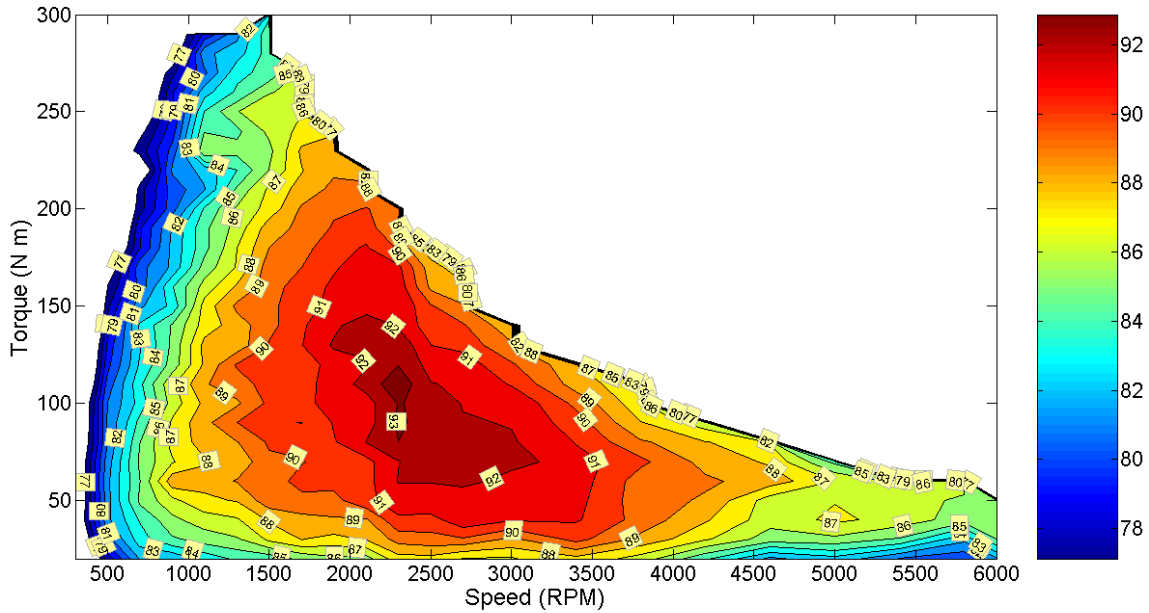
Fig. 3.23. 2004 Prius motor/inverter efficiency contours.

To further explore the various influences on inverter efficiency, tests were conducted with various dc-link voltages and inverter switching frequencies. In Fig. 3.24, a constant operation condition at 1000 rpm and 80 Nm was maintained throughout the tests. As expected, the inverter efficiency decreases with increasing dc-link voltage and increasing switching frequency. The Camry controller can operate at switching frequencies of 1.25 kHz, 2.5 kHz, 5 kHz, and 10 kHz, yet it operates at 5 kHz for much of the time when controlled by the MG ECU in vehicle. The impact of these parameters is lower for some operation conditions and high dc-link voltages are unavoidable at high speed, high torque conditions wherein back-emf voltages demand a high supply voltage.
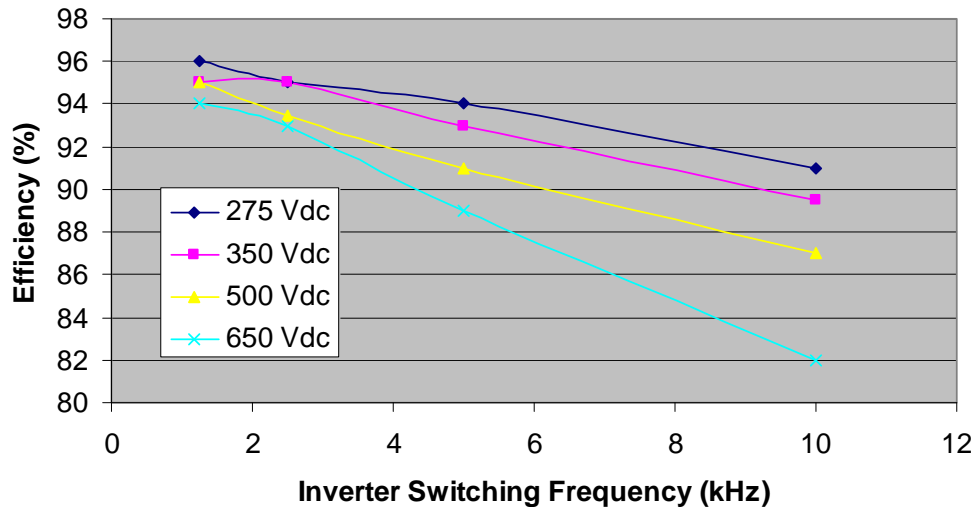
Fig. 3.24. 2007 Camry inverter efficiency vs. switching frequency for various dc-link voltages.

Boost converter efficiency assessments were conducted with various dc-link voltage and current output levels. The evaluations were conducted as the boost converter supplied the motor inverter, both of which

70

were operated at 5 kHz. The motor speed was maintained at 1000 rpm as the torque was increased to increase the boost converter current. According to the data from full vehicle tests conducted at ANL, the input voltage to the boost converter is commonly near 275 Vdc. Camry and Prius boost converter efficiencies are plotted versus boost converter input current in Figs. 3.25 and 3.26. Curve characteristics are undoubtedly different between the two, and the Prius boost converter has a slightly higher efficiency for much of the operation range. Low dc-current limitations were set for initial tests to prevent potential failures from preventing completion of general tests. Nonetheless, a failure occurred with an output voltage of 500 Vdc and input current of about 70 A and anticipated tests at 650 Vdc as well as a second series of tests at 10 kHz were not conducted. The failure was associated with an extremely high ripple current and the Toyota controller likely uses a switching frequency of 10 kHz in these conditions.
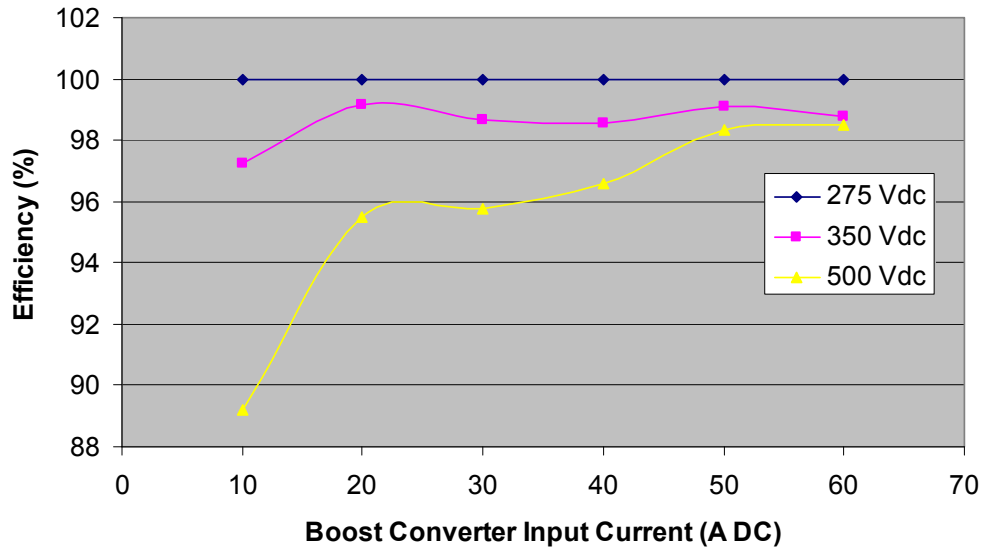

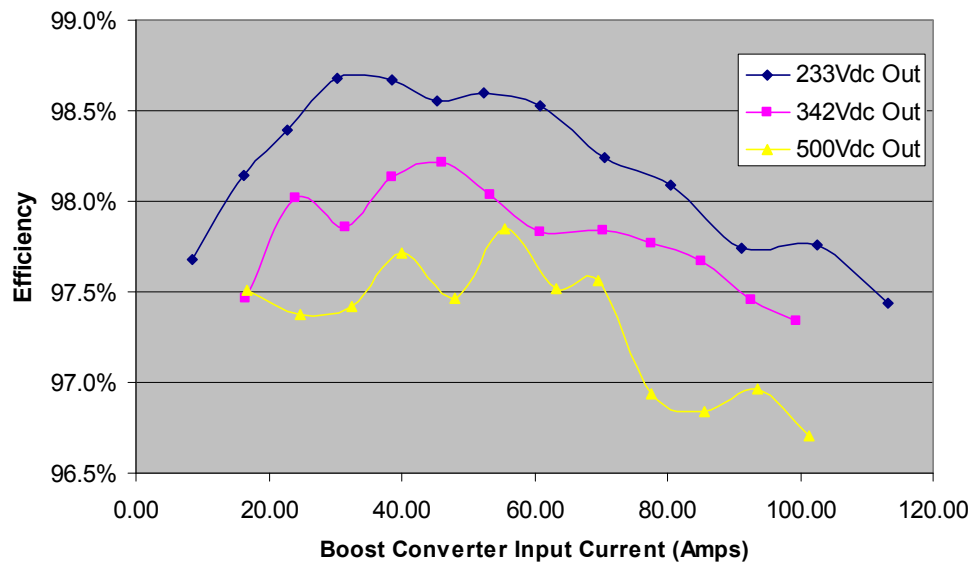Fig. 3.25. 2007 Camry boost converter efficiency vs. input current for various dc-link voltages.

Fig. 3.26. Prius boost converter efficiency vs. input current for various dc-link voltages.

71

3.6 CONTINOUS LOAD DURATION TESTS

The Camry motor was operated at continuous power levels for different speeds and coolant temperatures to observe the continuous capability of the motor under various conditions. Continuous tests were conducted at 25, 33.5, and 50 kW at 3000, 5000, and 7000 rpm with coolant temperatures of 20, 25, 50, and 65ºC. For each case, motor temperatures were allowed to stabilize prior to initiating the continuous tests and the Bay-Voltex coolant temperature regulation unit was used to regulate the coolant at a desired temperature.

TCs and thermistors were installed in various locations throughout the transaxle and PCU with locations indicated in Fig. 3.5. Coolant temperatures are indicated by the traces labeled "To Camry" and "From Cam." A thermistor labeled "D: ML 1" was installed within close proximity of the factory thermistor of the Camry, which is labeled "E: ML 2". Additionally stator, internal/external case, and inverter temperatures were monitored and recorded.

Figure 3.27 shows the continuous test results conducted at a power level of 50 kW, a motor speed of 5000 rpm, and a coolant temperature of 50ºC. The traces are labeled and identified by color in the key provided on the left. Mechanical power, "Pmech," is represented by a blue trace. The symbol at each datapoint is not distinguishable in the figure since the time scale is so large and the datapoints are close together. A table indicates the time duration for the associated stator temperature limitation in the upper left corner of the figure. For example, with a coolant temperature of 50ºC, the motor can operate at 50 kW for about 8:05 (minutes:seconds) prior to reaching a stator temperature of 130ºC. If the stator temperature limit is raised to 140ºC, the motor can operate for about 10:18 under these conditions. Thus, the extent of continuous operation capabilities depends greatly upon stator temperature limitations.
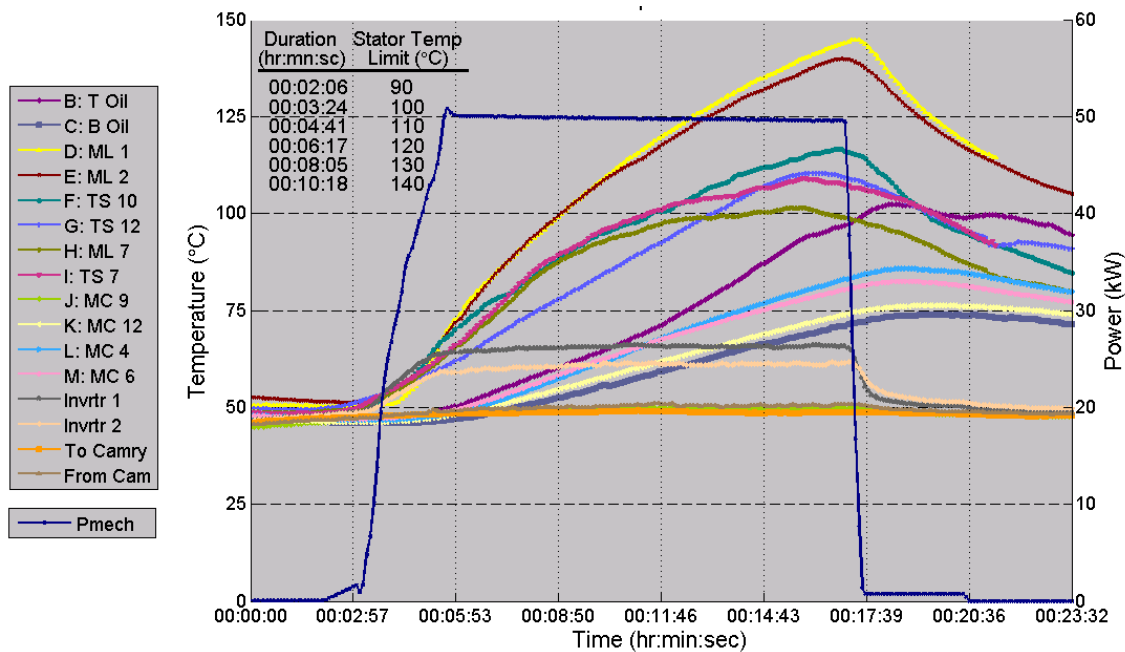
Fig. 3.27. Camry 50 kW continuous duration test at 5000 rpm with 50ºC coolant.

Stator temperature limitations are set to prevent potential damage within the stator windings and to prevent demagnetization of the PMs. Long term effects which affect the life of the PMSM must also be considered when choosing a stator temperature limitation. According to full vehicle tests at ANL, the Camry stator temperature is generally kept well below 90ºC. The temperatures of the original Camry

thermistor and the installed thermistor remained close during the continuous duration tests. Results show that the original Camry thermistor, "E: ML 2," is placed in one of the hottest locations of the motor. Figures 3.28 and 3.29 show the plots from tests conducted with a coolant temperature of 65ºC at power levels of 50 kW and 25 kW and 7000 rpm and 5000 rpm, respectively. Note that in the latter test the coolant temperature was reduced after thermal steady state was reached, as indicated in Fig. 3.29.
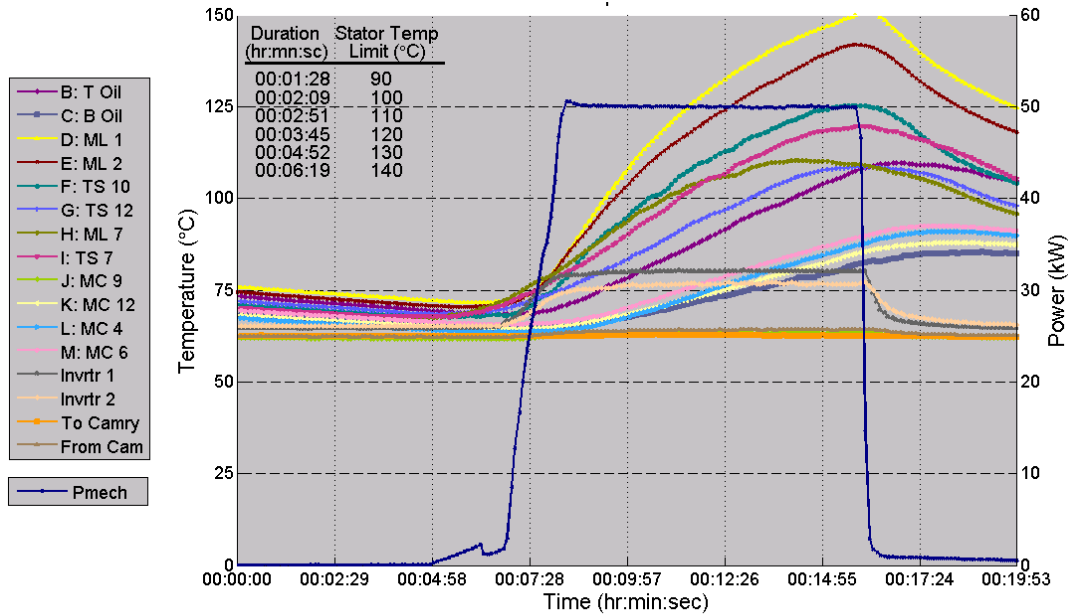
Fig. 3.28. Camry 50 kW continuous duration test at 7000 rpm with 65ºC coolant.
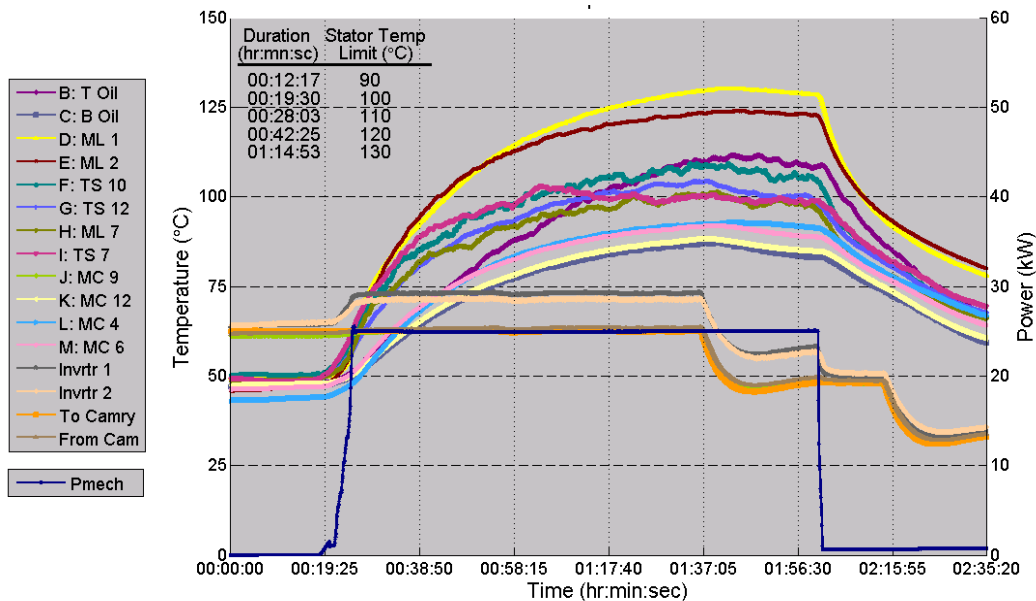
Fig. 3.29. Camry 25 kW continuous duration test at 5000 rpm with 65ºC coolant.

As expected, a comparison of Figs. 3.27 and 3.28 shows that the time extent of operation at 50 kW decreases as the test speed changes from 5000–7000 rpm and coolant temperature increases from 50–65ºC. All tests conducted at 5000 rpm produced the most efficient operation and thus the longest duration of operation at any power level when compared to test results obtained while operating at other

speeds and a similar coolant temperature. The highest temperatures stabilized near 130ºC in Fig. 3.29 at 5000 rpm and 25 kW. Note that it took over an hour to reach this temperature. Another continuous duration graph from tests conducted at 3000 rpm and 33.5 kW with a coolant temperature of 65ºC is shown in Fig. 3.30.
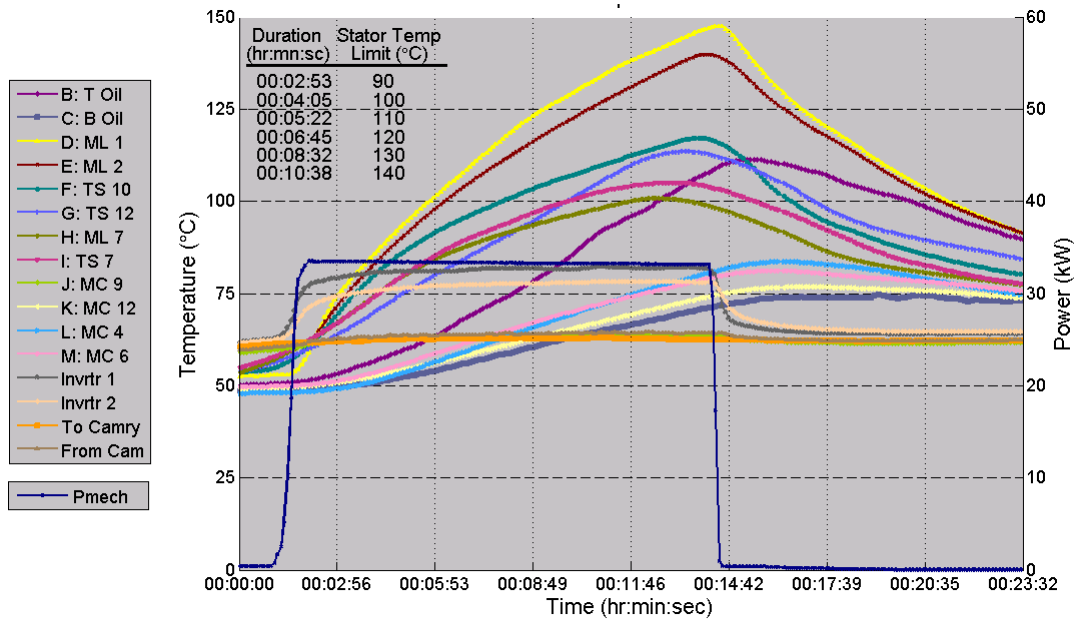
Fig. 3.30. Camry 33.5 kW continuous duration test at 3000 rpm with 65ºC coolant.

Graphs similar to Fig. 3.30 were generated for each test condition and while they are informative, it is difficult to fully study the impact of various power levels, motor speeds, coolant temperatures, and stator temperature limitations upon the extent of time at which the motor can operate under these conditions. Therefore, the duration times shown in the upper left corner of the previous figures were used to produce graphs which provide more meaningful comparisons. In Fig. 3.31, the time durations associated with operation at 25 kW with a 65ºC coolant temperature is graphed versus speed. Each trace represents the time durations which correlate to a particular stator temperature limit. Through inspection of this graph, it is more evident that the duration of operation is greater at 5000 rpm than for any other speed. Note again that in this case, the stator temperature stabilized near 130ºC at 5000 rpm, which is represented by the upper most trace. Thus, the trace for a temperature of 150ºC would theoretically have a data point that approaches infinity. Also note that tests under these conditions were discontinued after 30 minutes of operation at 7000 rpm and therefore stator temperatures did not reach higher than 120ºC.

Similar graphs are shown in Fig. 3.32 for a power level of 33.5 kW and a coolant temperature of 35ºC. At 5000 rpm, the motor operated for over 30 minutes before reaching a stator temperature of 125ºC. For low stator temperature limits, the duration capability does not change significantly as the motor speed increases from 5000–7000 rpm.

74

Fig. 3.31. Camry 25 kW continuous duration vs. speed with 65ºC coolant.
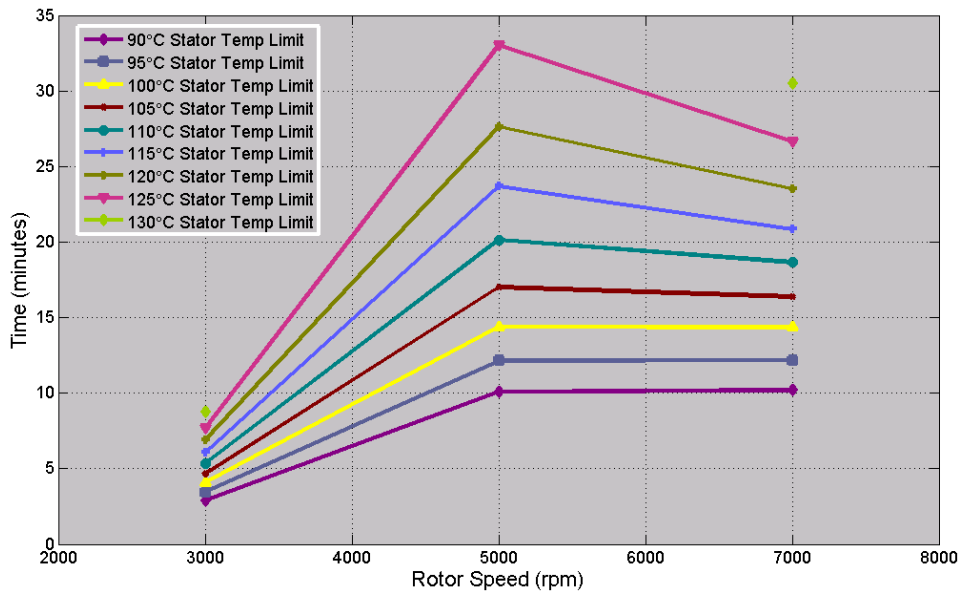
Fig. 3.32. Camry 33.5 kW continuous duration vs. speed with 35ºC coolant.

Similar graphs are shown in Figs. 3.33 and 3. 34 for continuous tests conducted at 50 kW with coolant temperatures of 35ºC and 65ºC, respectively. The trace color and stator temperature limitation correlations are consistent for all of the graphs to provide ease in comparisons. The impact of coolant temperature is quite visible as the time for stator temperatures to reach 135ºC at 5000 rpm is about 13 minutes with a 35ºC coolant temperature versus about 8 minutes with a 65ºC coolant temperature.
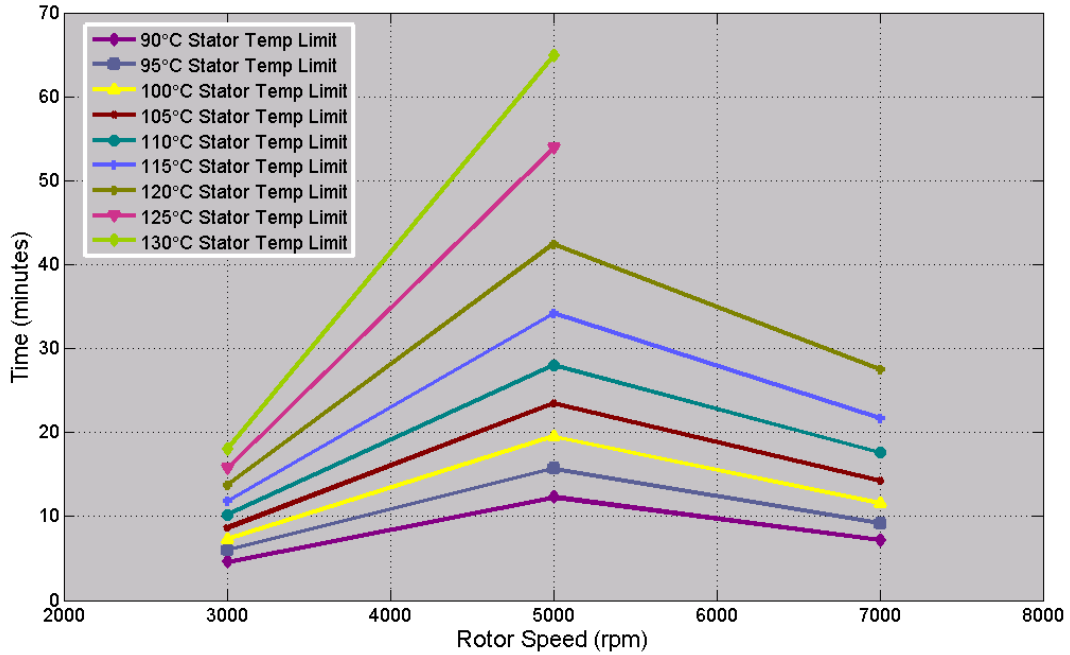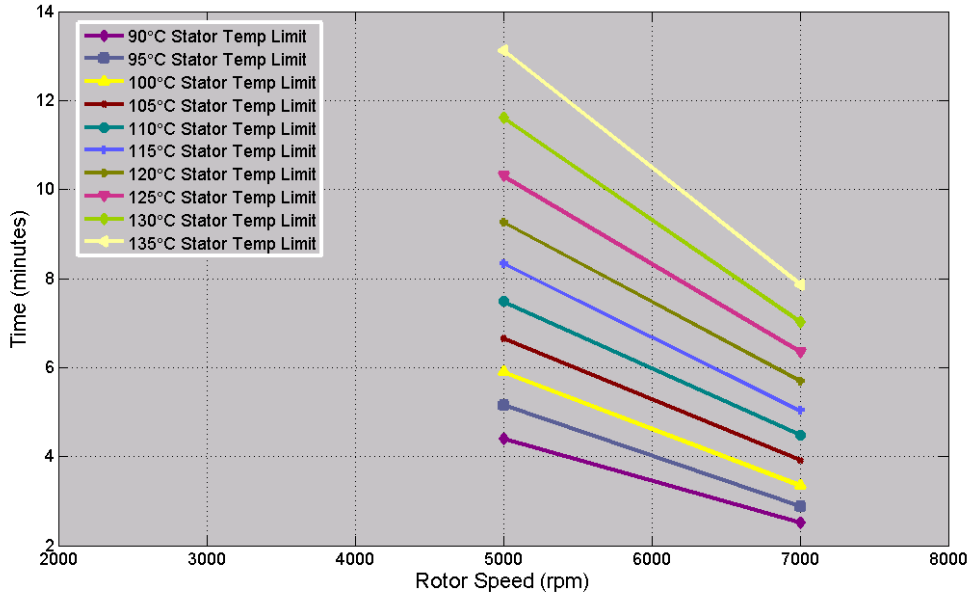
Fig. 3.33. Camry 50 kW continuous duration vs. speed with 35ºC coolant.
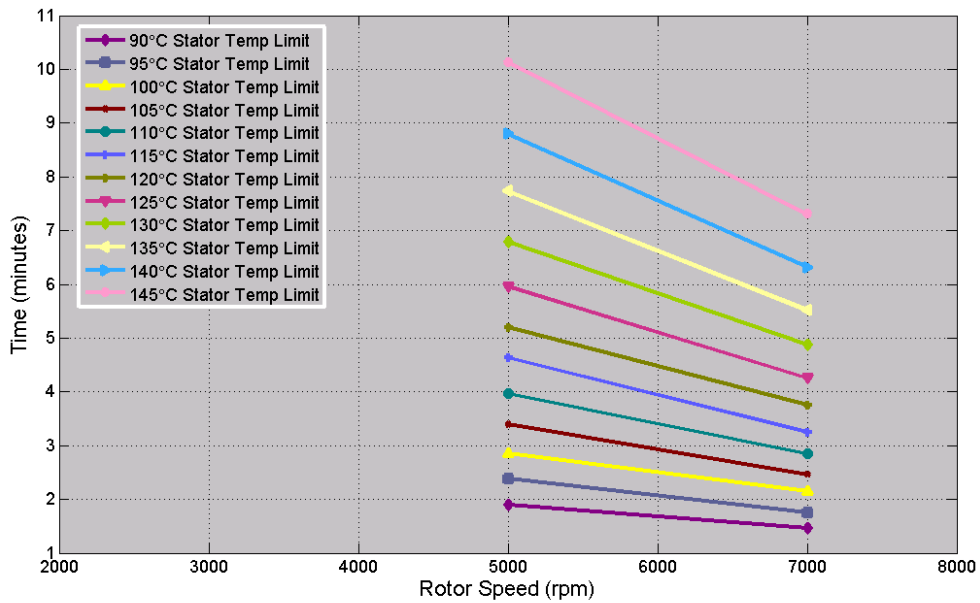
Fig. 3.34. Camry 50 kW continuous duration vs. speed with 65ºC coolant.

The previous graphs provided a clear indication of the influence of speed and coolant temperature upon duration capabilities. To provide a more clear assessment of the impact of stator temperature limitations and coolant temperature upon duration capability, duration time is plotted versus the stator temperature limit in Fig. 3.35 for operations at 3000 rpm. Each trace represents a particular power level and coolant temperature combination. In studying the figure, it is evident that coolant temperature does not affect operation duration greatly at 33.5 kW, yet coolant temperature greatly affects operation duration at a power level of 25 kW.
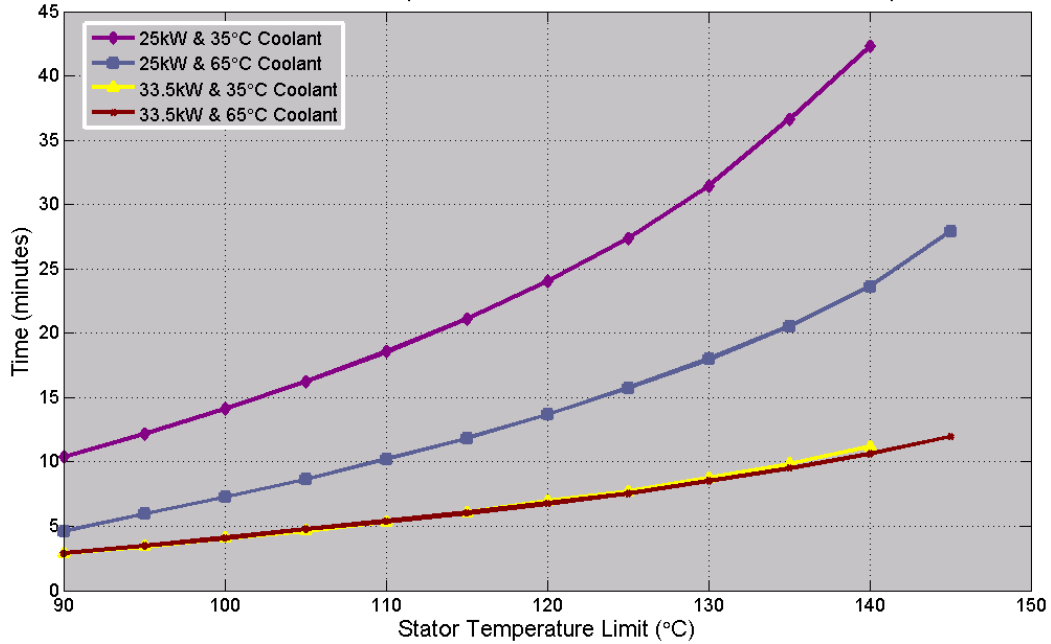
Fig. 3.35. Camry continuous duration at 3000 rpm with various power levels and coolant temperatures.

Characteristics similar to what are observed in Fig. 3.35 are observed in Fig. 3.36 where duration time is plotted versus stator temperature limit at 5000 rpm for various power and coolant temperature combinations. As the power level increases, the impact of coolant temperature upon duration decreases. For tests wherein thermal steady state was nearly reached, the curves approach a vertical asymptote which is located at the steady state stator temperature.

Fig. 3.36. Camry continuous duration at 5000 rpm with various power levels and coolant temperatures.

A graph of duration versus stator temperature limit at 7000 rpm with various power and coolant temperature combinations is shown in Fig. 3.37. Again, with increasing power, coolant temperature has a decreasing effect upon the duration of motor operation under these conditions. Note that all power-coolant temperature combinations and color correlations do not remain the same among Figs. 3.35, 3.36, and 3.37. A comparison of these figures indicates that coolant temperature has a greater impact upon the duration of operation at higher speeds. For example, the duration of operation is influenced more by coolant temperature at 7000 rpm and 25 kW than it is for 25 kW power levels at 3000 rpm and 5000 rpm.
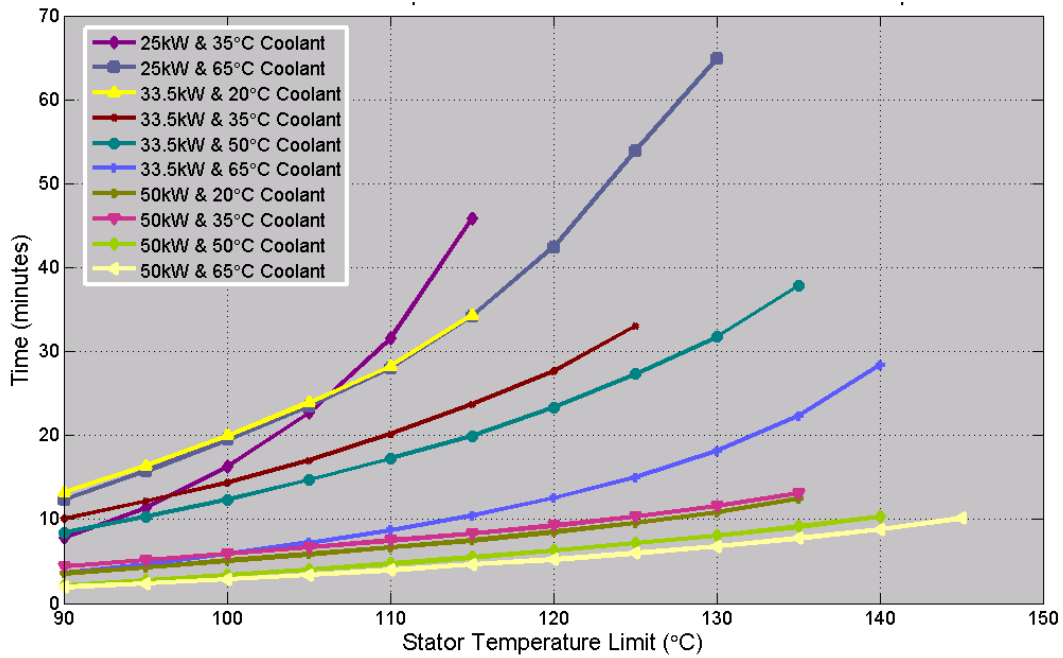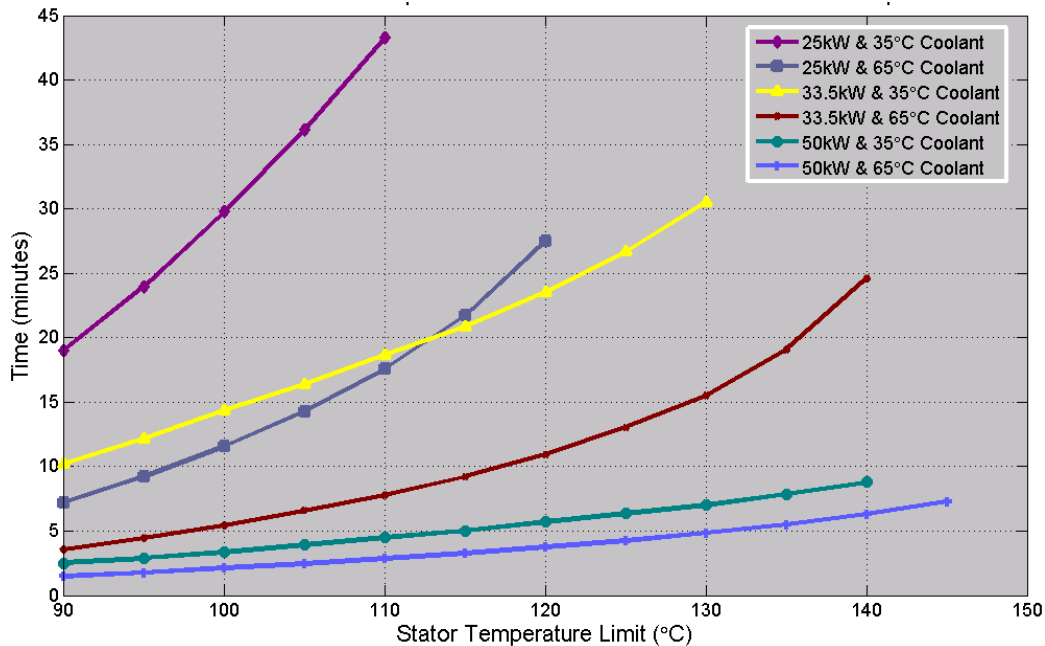

Fig. 3.37. Camry continuous duration at 7000 rpm with various power levels and coolant temperatures.

Note that in some of the tests in which lower coolant temperatures were used, the duration of operation was longer than that of a lower power level with a higher coolant level. This occurred because system temperatures were allowed to stabilize at each coolant temperature. For example, the duration of the 33.5 kW and 35ºC coolant temperature test condition is longer than that with the 25 kW and 65ºC coolant temperature test conditions if the stator temperature limitation is set at a low temperature. However, if the stator temperature limitation is set at a high level, the motor can operate longer at the 25 kW and 65ºC coolant temperature test condition. Thus, with 33.5 kW operation and a 35ºC coolant temperature, the entire system begins at a cooler temperature, yet the entire system temperature increases more quickly and eventually becomes hotter than if the system were operating at 25 kW operation with 65ºC, even though the system begins at a higher temperature (65ºC).

It is clear that defining the continuous operation capability of a motor depends on many variables, which even includes the definition of continuous operation. For example, continuous operation could be defined to be operation at a particular power level for an infinite amount of time, or a particular time restraint could be included in the definition. For some HEV applications, it is crucial that the motor is capable of operating continuously within particular power levels. For example, the Camry hybrid system requires torque from the motor and generator for the engine to supply power to the drive wheels. Many aspects must be considered for these conditions, and if properly designed, the volume and mass of the electric drive system can be optimized to match the demands of the system.

4. SUMMARY AND CONCLUSIONS

The 2007 Camry HEV subsystem assemblies were physically evaluated and comprehensively tested in the laboratory to fully assess their performance, efficiency, design, and packaging characteristics. The laboratory evaluations included back-emf, rotational loss, locked rotor, efficiency mapping, and extended-duration load tests. Overall, the Camry motor outperformed the Prius motor in terms of efficiency and equivalent torque and power, while the mass and volume of the system decreased significantly. Increased operation speed of the motor is the primary factor which provides the enhanced characteristics of the hybrid system. Additionally, the improved packaging and trench gate structure used in the PCU IGBTs led to a higher power density of the PCU components. The Camry inverter efficiencies are slightly lower than those of the Prius, yet the combined motor and inverter efficiencies of the Camry are still higher, especially for the low speed, high torque operation region. The lower motor efficiencies of the Prius have a much higher impact on the combined motor and inverter efficiencies than the impact of the slightly lower efficiencies of the Camry inverter.

Evaluations illustrate the benefits of moving to a high speed motor through improved packaging, higher efficiencies, increased performance, and improved continuous operation test results. Motor efficiencies are above 90% for a great portion of the operation range. Low speed efficiencies of the Camry are much higher than those of the Prius, which is particularly noticeable when the speed reduction gear ratio of 2.47 is applied to the efficiency map, and therefore the resulting torque is increased significantly. The peak power of the primary Camry motor is about 70 kW at 5000 rpm, which is much lower that the published rating of 105 kW. There are no specifications published for the generator and the published power rating may be for both the motor and generator. Simulations of this motor and a comparison of specific power characteristics with other high speed motors also suggest that the power rating is near 70 kW.

Continuous duration varies significantly with speed, specified stator temperature limit, and coolant temperature. A power level of 33.5 kW was maintained at 5000 rpm for about 30 minutes with 65°C coolant, at which a stator temperature of 140°C was reached. There is no standard for establishing continuous or peak power rating specifications for motors designed for HEV applications such as the hybrid Camry and Prius motors. For example, the Camry PMSM is able to sustain a power level of 50 kW at 5000 rpm for about 13 minutes with a stator temperature limit of 135ºC and coolant temperature of 35ºC; however, the duration is only about 8 minutes if a coolant temperature of 65ºC is applied. In addition to the unexpectedly low motor power rating, this highlights a very important reason for performing benchmarking tests on HEV subsystems – current technology must be verified objectively under consistent operating parameters before the results are used by the FCVT program and researchers. The influence of HEV specifications on technical goals and program planning would be drastically different if unclear published specifications of HEV systems were used as a baseline.

Among the vast amount of information obtained during benchmarking efforts, the significant findings are summarized in Table 4.1. Some of the information obtained from the Prius and Camry benchmarking studies has been and will be used by researchers to improve/verify analytical models. As a next step in the benchmarking efforts at ORNL, focus will be placed on an HEV system with improved power capabilities. These efforts are expected to be performed in FY2008 and will focus on the Lexus LS 600h hybrid subsystems, which are expected to include significant design improvements. Technological advances which facilitate higher power capability, power density, specific power, efficiency, and cost effectiveness of HEV components are essential as HEVs become increasingly dependant upon the electrical portion of the drive system and as the electric vehicle (EV) and HEV market continues to expand in the future.

Table 4.1. 2007 Camry/2004 Prius design comparison highlights

Parameter	Camry	Prius	Comments
Transaxle			
Motor power rating.	70 kW	50 kW	Published Camry power rating is likely a combination of motor and generator ratings.
Motor lamination stack length.	6.07 cm (2.39″)	8.40 cm (3.3″)	Reduced by 2.33 cm (0.91″).
Motor mass.	41.7 kg	45.0 kg	7.3% reduction.
Motor volume.	14.8 L	15.4 L	3.9% reduction.
Motor specific power.	1.68 kW/kg	1.11 kW/kg	Improved by a factor of 1.5.
Motor power density.	4.73 kW/L	3.25 kW/L	Improved by a factor of 1.5.
Equivalent torque rating.	667 Nm	400 Nm	Camry torque value from speed reduction gear (short duration).
Motor speed rating.	14,000 rpm	6,000 rpm	
Motor winding configuration.	Parallel	Series	
Power split.			
PCU			
Nominal battery voltage.	244.8 V	201.6 V	Up to 20% higher during operation.
Maximum dc-link voltage.	650 Vdc	500Vdc	
Boost converter power rating.	30 kW	20 kW	
Filter capacitor (battery level).	500 Vdc, 378 μF	600 Vdc, 282 μF	
Smoothing capacitor (boosted level).	750 Vdc, 2098 μF	600 Vdc, 1,130 μF	
Entire PCU mass.	17.86 kg	21.2 kg	15.8% reduction.
Entire PCU volume.	11.7 L	17.8 L	Prius PCU includes 12V dc-dc and compressor inverter, Camry PCU does not.
Motor inverter mass.	7.5 kg	8.8 kg	14.7% reduction.
Motor inverter volume.	~6 L	8.7 L	31% reduction.
Motor inverter specific power.	9.3 kW/kg	5.7 kW/kg	Improved by a factor of 1.6.
Motor inverter power density.	11.7 kW/L	5.7 kW/L	Improved by a factor of 2.1.
Boost converter mass.	6.6 kg	4.8 kg	37.5% increase.
Boost converter volume.	3.5 L	5.1 L	31.3% reduction.
Boost converter specific power.	4.5 kW/ kg	4.2 kW/kg	Improved by 7%.
Boost converter power density.	8.6 kW/L	3.9 kW/L	Improved by a factor of 2.21.

REFERENCES

1. Source: http://www.eere.energy.gov/vehiclesandfuels/technologies/systems/index.shtml.

2. J. S. Hsu, S. C. Nelson, P. A. Jallouk, C. W. Ayers, R. H. Wiles, S. L. Campbell, C. L. Coomer, K. T. Lowe, and T. A. Burress, *Report on Toyota Prius Motor Thermal Management*, ORNL/TM-2005/33, UT-Battelle, LLC, Oak Ridge National Laboratory, Oak Ridge, Tennessee, February 2005.

3. R. H. Staunton, C. W. Ayers, J. Chiasson, T. A. Burress, and L. D. Marlino, *Evaluation of 2004 Toyota Prius Hybrid Electric Drive System,* ORNL/TM-2006-423, UT-Battelle, LLC, Oak Ridge National Laboratory, Oak Ridge, Tennessee, May 16, 2006.

4. R. H. Staunton, T. A. Burress, and L. D. Marlino, *Evaluation of 2005 Honda Accord Hybrid Electric Drive System,* ORNL/TM-2006-535, UT-Battelle, LLC, Oak Ridge National Laboratory, Oak Ridge, Tennessee, September 2006.

5. *Camry Hybrid Vehicle New Car Features 2007*, Toyota Motor Corporation, March 2006.

APPENDIX A: 2004 PRIUS POWER CONVERTER UNIT PACKAGING ASSESSMENTS

2004 Prius Motor Inverter Mass and Volume Assessment

Total Volume of PCU casing is **17.8 L** as depicted in Fig. A.1.
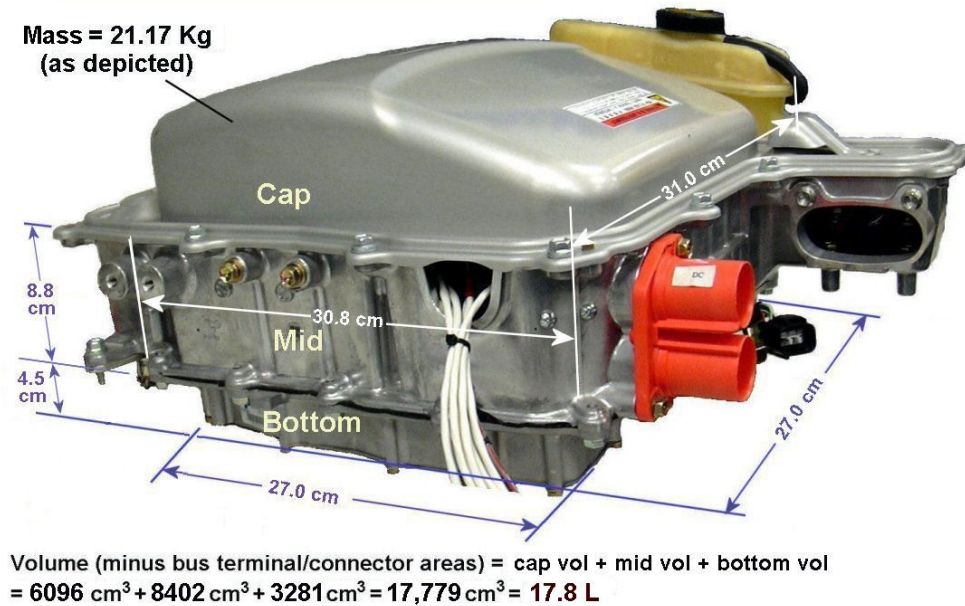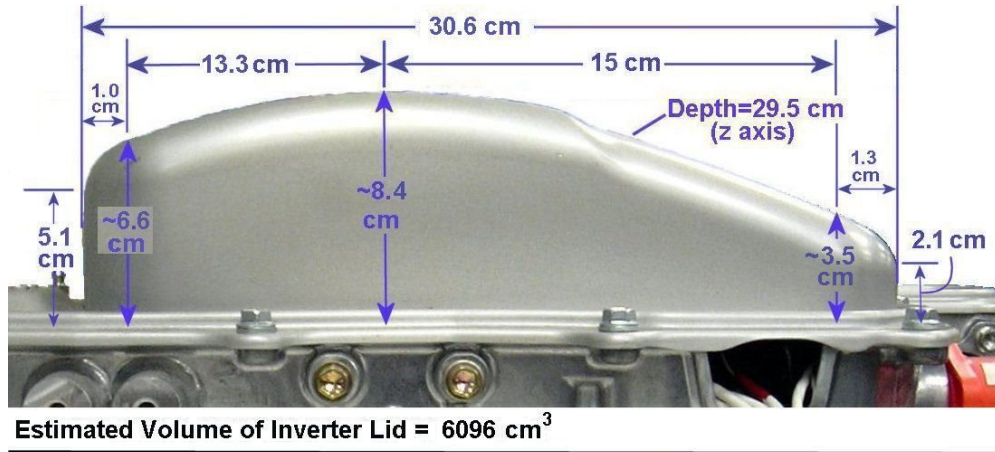
Fig. A.1. Volume of entire Prius PCU assembly.

Total volume of "inverter *only*" is **8.7 L** and is derived as follows:

- Mid section volume is reduced by 55% after the exclusion of the volume associated with the converter components, the generator portion of the inverter board (a 1/2 reduction), the generator portion of the power module (a 1/3 reduction) and the corresponding portion of the cold plate (a 60% reduction). See Fig. A.2 as an aid in visualization.
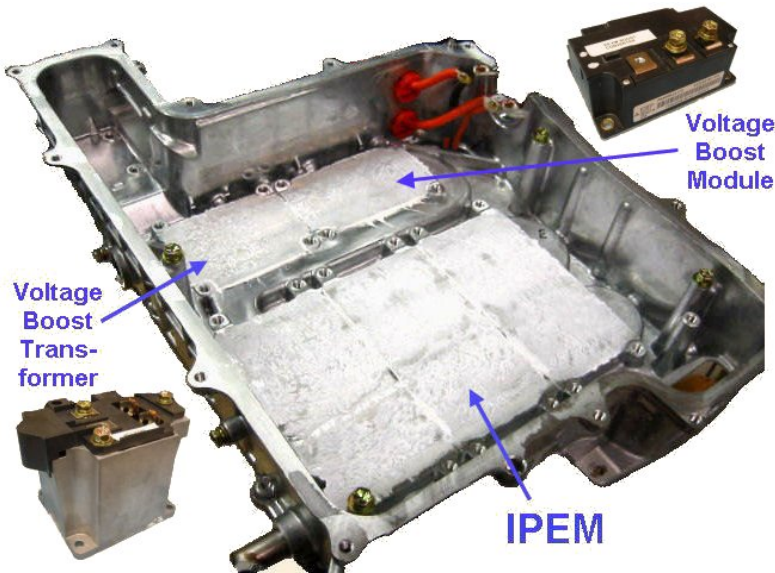
Fig. A.2. Empty inverter/converter housing showing cold plate surfaces.

- It is also reduced by the deletion of the bottom compartment (unrelated circuitry).
- The lid and capacitor volume, although not optimized, is scaled by a factor of 1130 µF/(282 µF + 1130 µF) = 4/5 to account for the separation of the boost converter and inverter capacitors.

Total mass of PCU casing as depicted in Fig. A.1 is **21.2 kg**.
Total mass of "inverter *only*" is **8.8 kg** and is derived in a similar manner that volume was derived (80% of capacitor mass, 45% of mid-section mass, and 0% of bottom section mass). The reduction of mid-section mass is actually more severe than the "45%" suggests since the high-mass converter transformer and converter power module were first fully excluded.

2004 Prius Bi-Directional Boost Converter Mass and Volume Assessment

The general circuit diagram for the converter is shown in Fig. A.3, showing that the converter topology is that of a conventional bidirectional boost converter. The figure also supplies mass and volume figures of the inductor and IPM.
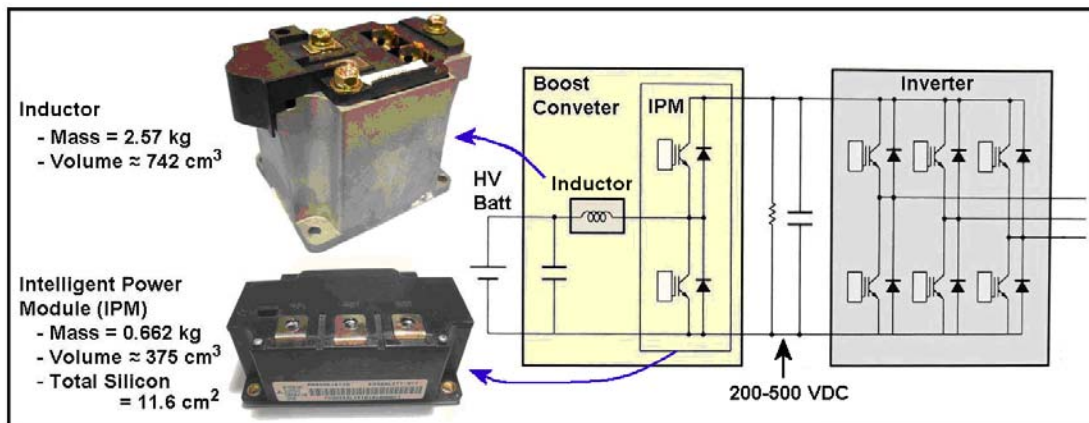

Fig. A.3. General circuit schematic of the Prius inverter.

During periods of maximum power demand from the driver, the converter provides up to ~20 kW to the inverter/motor system and the vehicle generator supplies up to ~30 kW. This power split allows a reduction in size of the high-cost HV battery and the converter, while the extent of fully electric operation is compromised.

Excluding the cold plate, the volume and mass totals for the ~20 kW boost converter IPM and inductor are ~1.12 L and 3.23 kg, respectively.

<u>Volume calculation approach A:</u> The volume of the cold plate under the 2 converter components (including adjacent mounting holes) is 19 mm × 100 mm × 250 mm = 0.48 L. However, this approach ignores the space enclosed by the converter portion of the casing.

<u>Volume calculation approach B:</u> It is more pertinent to consider the entire volume that includes the cold plate, items mounted on it, and surrounding space enclosed in the casing. This volume is 335 mm × 100 mm × 140 mm = 4.7 L.

It is estimated that 15% of the casing mass is dedicated to the bidirectional converter. Since the casing shell is 6.45 kg, the mass reduction is ~1 kg.

<u>Capcitor:</u> The entire capacitor volume is 1.8 L. The volume associated with the boost converter is approximately 1.8 × 282 μF/(282 μF + 1130 μF) = 1.8/5 = 0.36 L. The capacitor mass is approximately 2.79 kg /5 = 0.56 kg.

<u>Conclusions:</u> Accounting for the inductor, IPM, casing, and capacitor the converter system volume is **5.1 L** and the mass is **4.8 kg**.

APPENDIX B: PRIUS AND CAMRY CAPACITOR TEST RESULTS
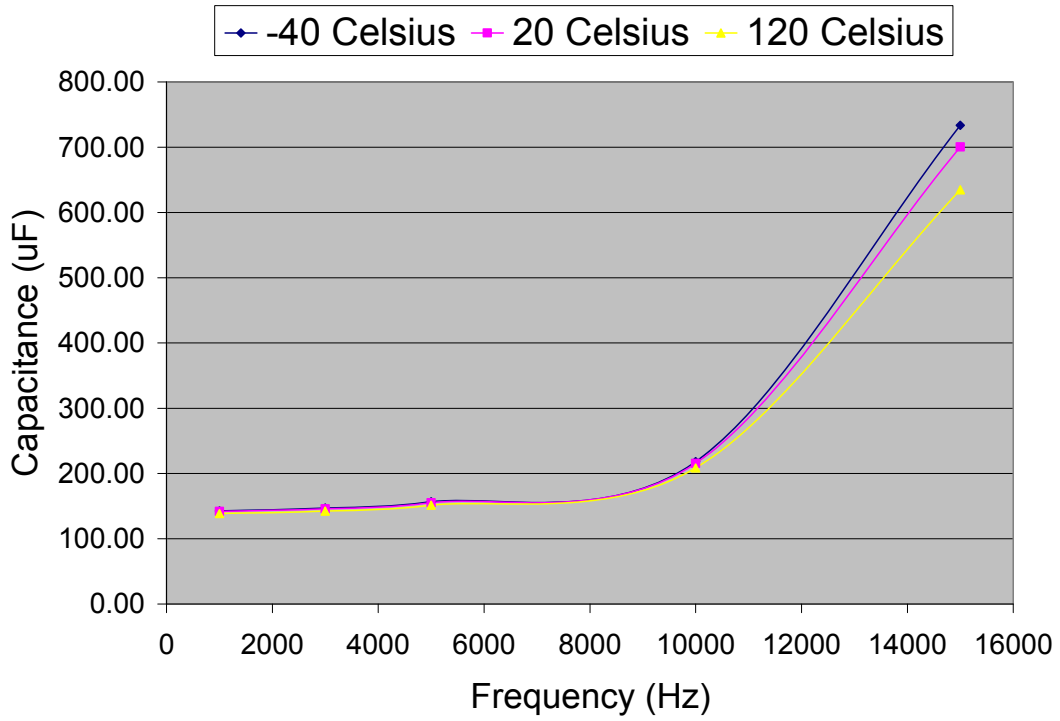
Fig. B.1. Prius single 141 µF capacitor from 1,130 µF module, capacitance vs. frequency.
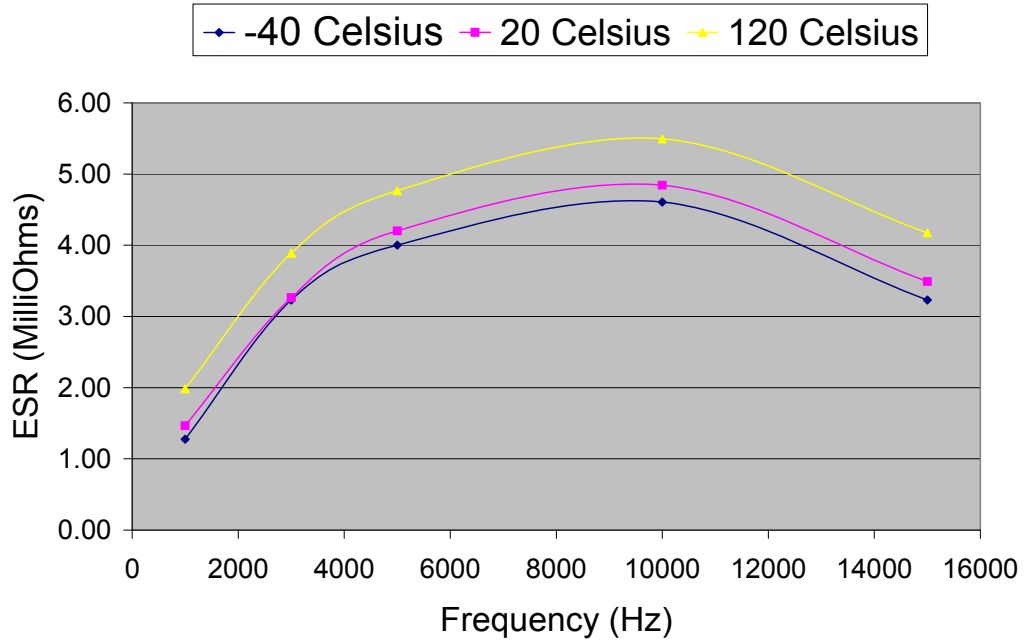
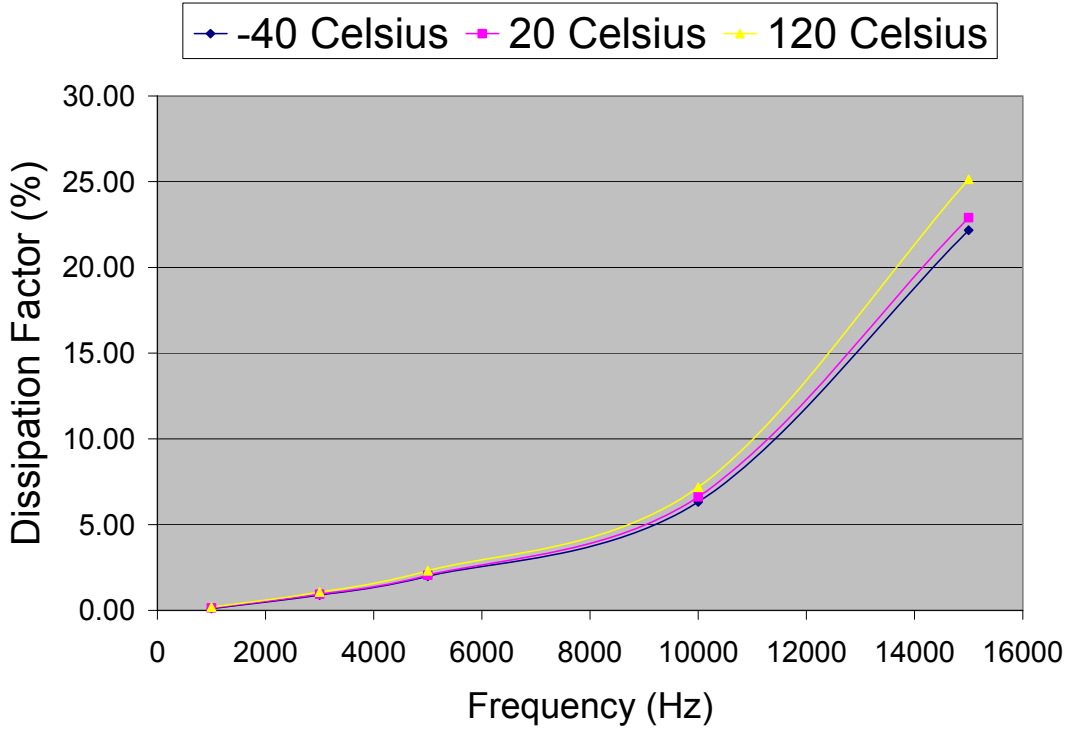Fig. B.2. Prius single 141 µF capacitor from 1,130 µF module, ESR vs. frequency.

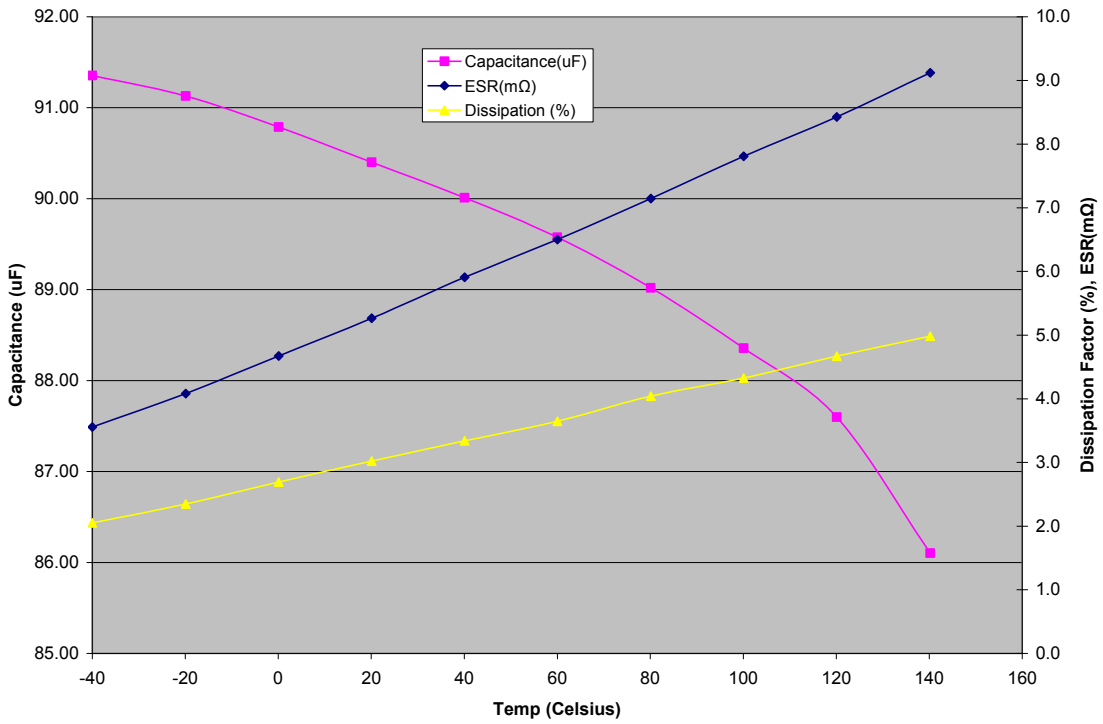**Fig. B.3. Prius single 141 µF capacitor from 1,130 µF module, DF vs. frequency.**

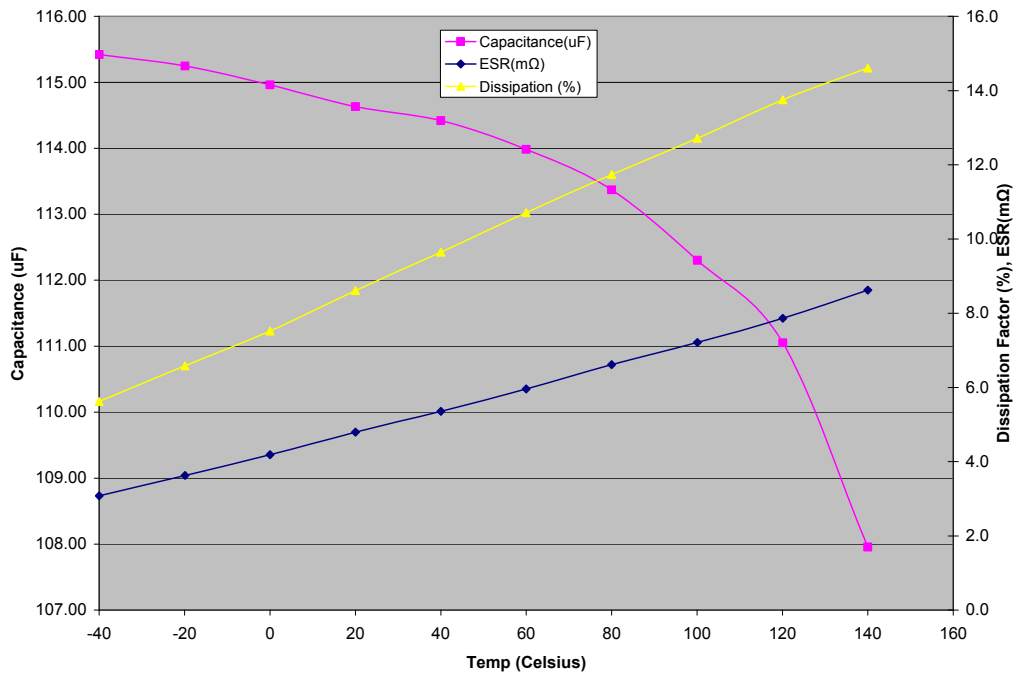**Fig. B.4. Camry single 86 µF capacitor, capacitance, ESR, and DF vs. temperature at 10 kHz.**

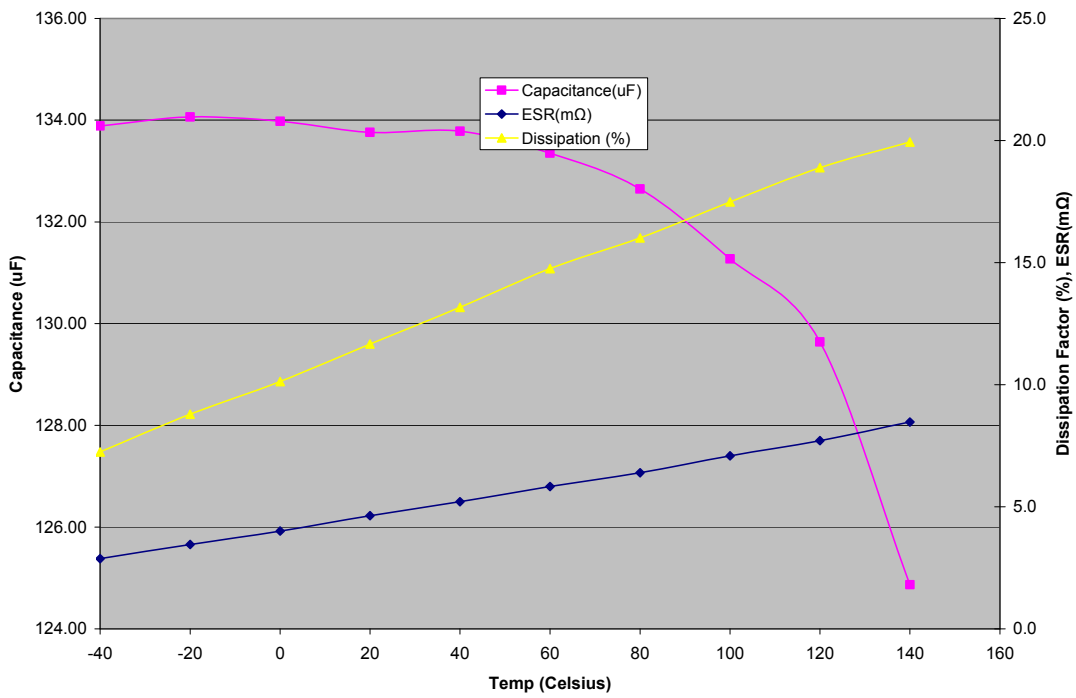**Fig. B.5. Camry single 86 µF capacitor, capacitance, ESR, and DF vs. temperature at 25 kHz.**

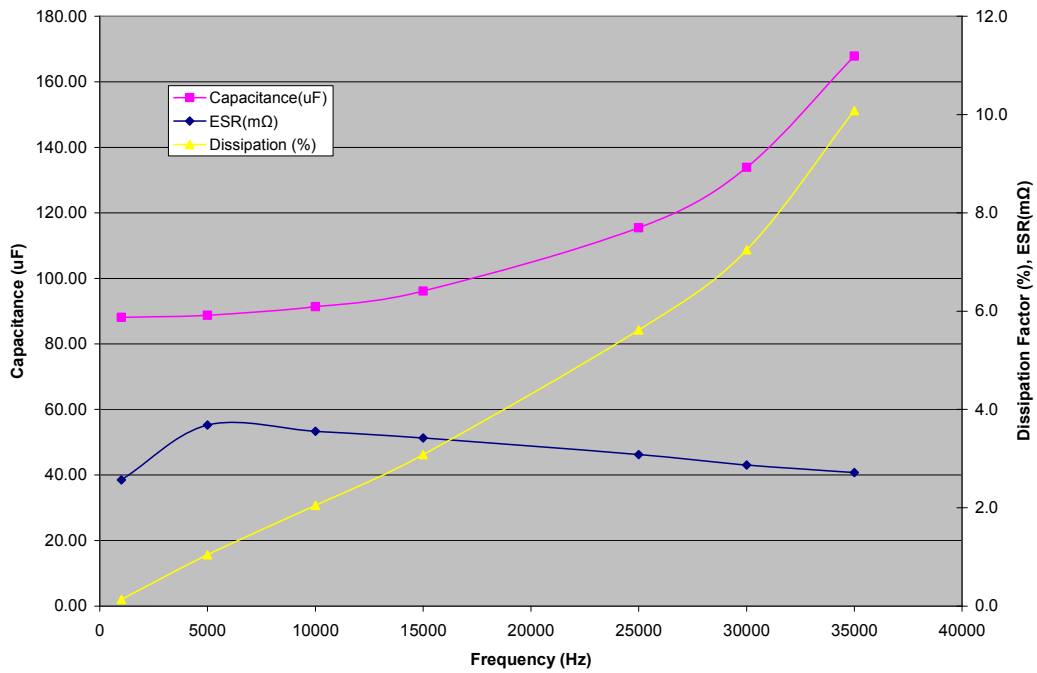**Fig. B.6. Camry single 86 µF capacitor, capacitance, ESR, and DF vs. temperature at 30 kHz.**

Fig. B.7. Camry single 86 µF capacitor, capacitance, ESR, and DF vs. frequency at -40ºC.

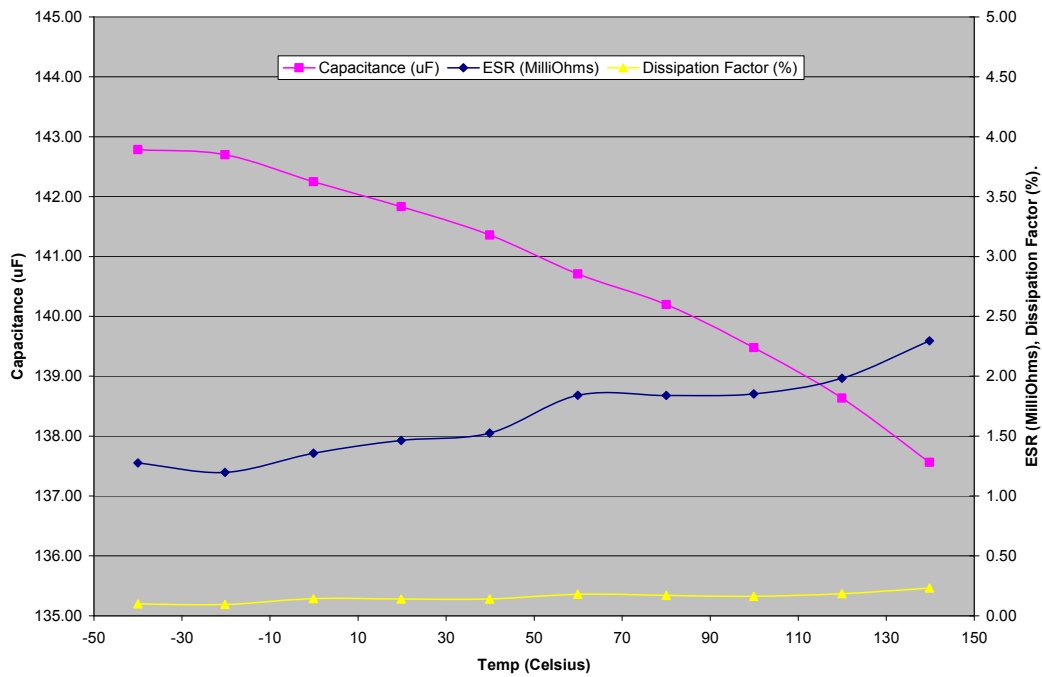**Fig. B.8. Prius single 141 µF capacitor, capacitance, ESR, and DF vs. temperature at 1 kHz.**

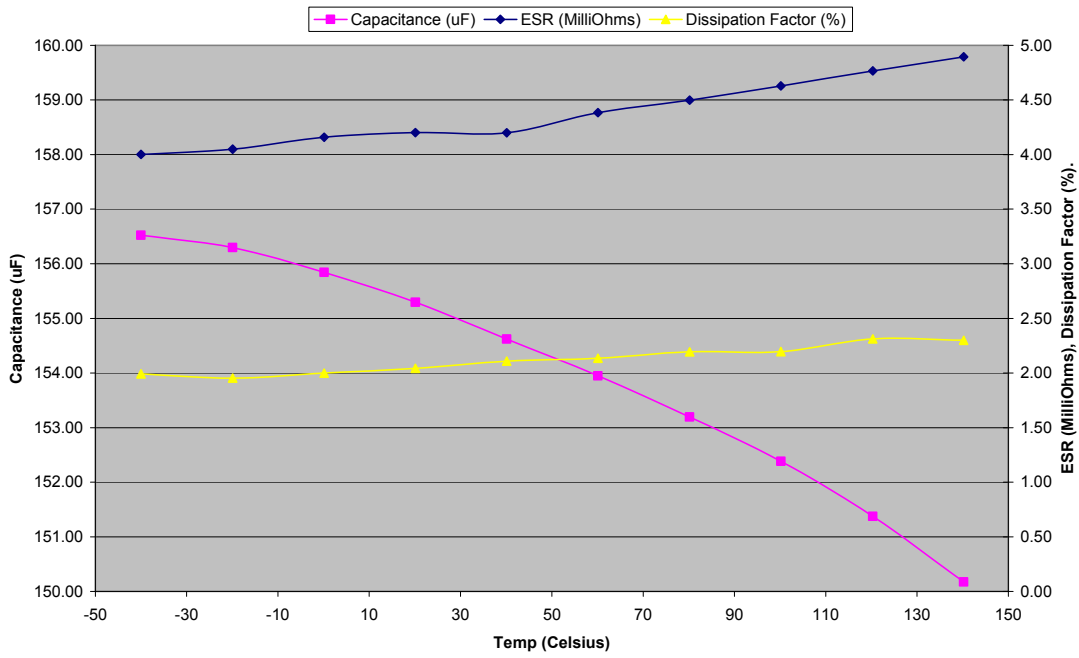**Fig. B.9. Prius single 141 μF capacitor, capacitance, ESR, and DF vs. temperature at 5 kHz.**

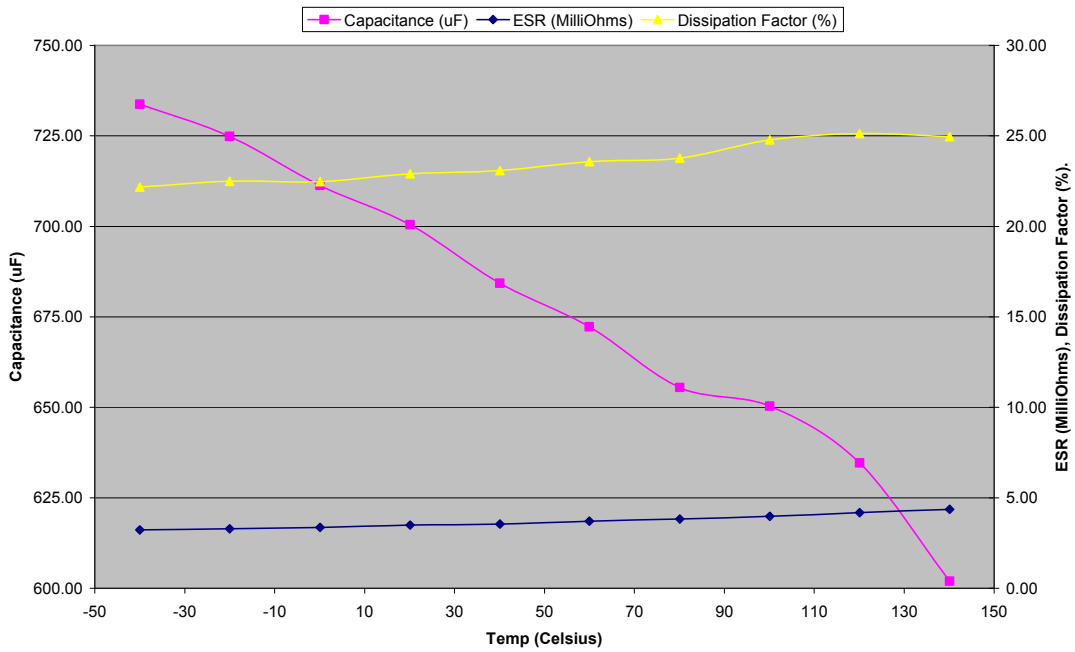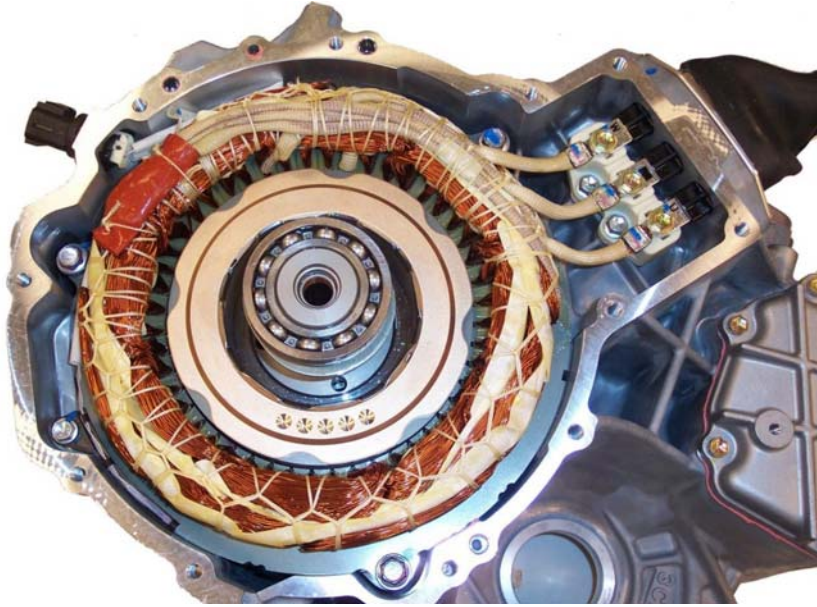**Fig. B.10. Prius single 141 μF capacitor, capacitance, ESR, and DF vs. temperature at 15 kHz.**

APPENDIX C: 2004 PRIUS TRANSAXLE PACKAGING ASSESSMENTS

2004 Prius Motor Mass and Volume Assessment

The configuration of the motor rotor and stator are shown in Fig. C.1.

Fig. C.1. 2004 Prius motor rotor and stator.

Figure C.1 shows three views of the PMSM housing with selected dimensions called out. As indicated, about 3/4th of the casing houses the PMSM rotor and stator and the remainder encloses part of the gearbox. The portion of the casing that houses the PMSM is roughly cylindrical and that is the geometry used for the purposes of estimating the PMSM casing volume. Based on the average of 3 measurements of casing diameter, the cylinder diameter can be assumed to be ~29.9 cm. The depth of the PMSM housing extending from the end plate to the surface identified in the upper left photo in Fig. C.2 is 20.5 cm. This results in a volume of 14,400 cm^3 excluding the three-phase terminal block housing and the cooling passages that protrude from the surface of the casing. Including all 3 volumes results in a total of 15,400 cm^3 (15.4 L). This volume and the 50 kW peak power specification result in a peak power density of 3.25 kW/L.

The mass of the PMSM was determined in order to estimate the specific power. The masses of the components of the Prius PMSM are:

Stator:	25.9 kg
Rotor:	10.2 kg
Case:	6.36 kg (machined – see below)
Case cover:	2.49 kg
Total mass of motor:	**44.95 kg**

The casing for the PMSM has (1) a portion that encloses one end of the gear box, and (2) compartments that enclose the gear-shift-lever-to-shift-plunger linkages. These areas are unrelated to the PMSM and were therefore machined off of the structure to obtain a new 6.36 kg mass (the original casing mass was 13.9 kg). The resulting specific power for the PMSM is 1.11 kW/kg.
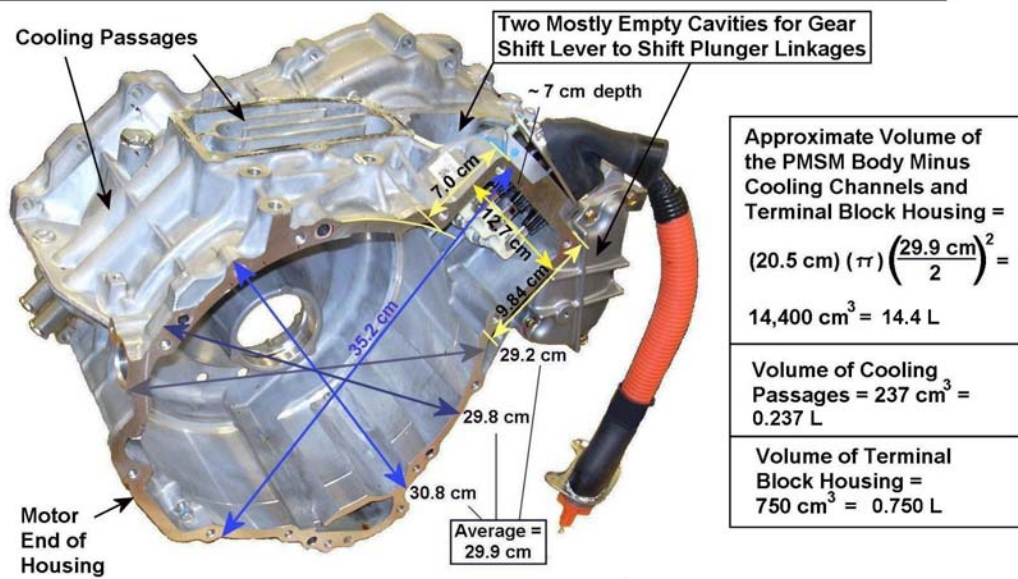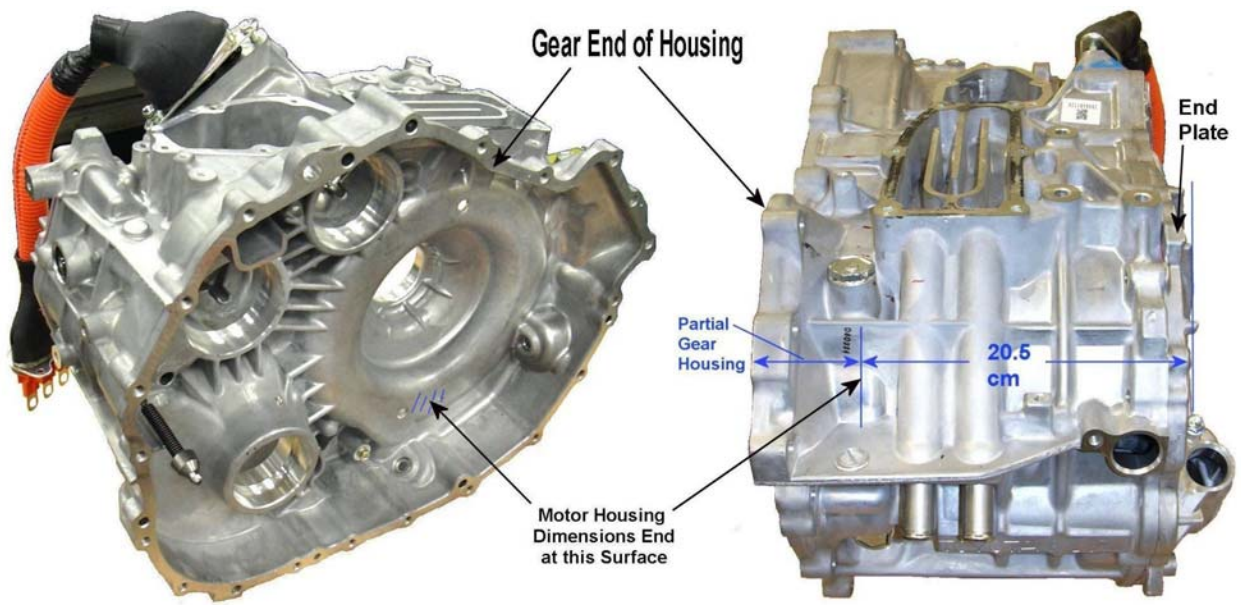
Fig. C.2. Casing of the 2004 Prius PMSM with dimensions and volume calculations.

DISTRIBUTION

Internal

1. D. J. Adams
2. T. A. Burress
3. S. L. Campbell
4. C. L. Coomer
5. J. P. Cunningham
6. E. C. Fox
7. K. P. Gambrell
8. J. S. Hsu
9. L. D. Marlino
10. M. Olszewski
11. L. E. Seiber
12. R. H. Staunton
13. Laboratory Records

External

14. F. D. Barlow III, University of Idaho, Department of Electrical & Computer Engineering, Buchanan Engineering Laboratory, Rm. 211, 607 Urquhart Avenue, Moscow, ID 83844-1023, fbarlow@uidaho.edu.
15. R. Al-Attar, DCX, raa9@dcx.com.
16. S. J. Boyd, U.S. Department of Energy, EE-2G/Forrestal Building, 1000 Independence Avenue, S.W., Washington, D.C. 20585.
17. T. Q. Duong, U.S. Department of Energy, EE-2G/Forrestal Building, 1000 Independence Avenue, S.W., Washington, D.C. 20585.
18. R. R. Fessler, BIZTEK Consulting, Inc., 820 Roslyn Place, Evanston, Illinois 60201-1724.
19. G. Hagey, Sentech, Inc., 501 Randolph St., Williamsburg, Virginia 23185.
20. E. Jih, Ford Motor Company, Scientific Research Laboratory, 2101 Village Road, MD-1170, Rm. 2331, Dearborn, Michigan 48121.
21. K. J. Kelly, National Renewable Energy Laboratory, 1617 Cole Boulevard, Golden, Colorado 80401.
22. A. Lee, Daimler Chrysler, CIMS 484-08-06, 800 Chrysler Drive, Auburn Hills, Michigan 48326-2757.
23. F. Leonardi, Ford Motor Company, 15050 Commerce Drive, North, Dearborn, Michigan 48120-1261.
24. F. Liang, Ford Motor Company, Scientific Research Laboratory, 2101 Village Road, MD1170, Rm. 2331/SRL, Dearborn, Michigan 48121.
25. M. W. Lloyd, Energetics, Inc., 7164 Columbia Gateway Drive, Columbia, Maryland 21046.
26. J. Maquire, General Motors Advanced Technology Center, 3050 Lomita Boulevard, Torrance, California 90505.
27. M. Mehall, Ford Motor Company, Scientific Research Laboratory, 2101 Village Road, MD-2247, Rm. 3317, Dearborn, Michigan 48124-2053.
28. J. A. Montemarano, Naval Surface Warfare Center, Carderock Division; Code 642, NSWD, 9500 MacArthur Boulevard; West Bethesday, Maryland 20817.
29. N. Olds, United States Council for Automotive Research (USCAR), nolds@uscar.org
30. S. A. Rogers, U.S. Department of Energy, EE-2G/Forrestal Building, 1000 Independence Avenue, S.W., Washington, D.C. 20585.
31. G. S. Smith, General Motors Advanced Technology Center, 3050 Lomita Boulevard, Torrance, California 90505.
32. E. J. Wall, U.S. Department of Energy, EE-2G/Forrestal Building, 1000 Independence Avenue, S.W., Washington, D.C. 20585.
33. B. Welchko, General Motors Advanced Technology Center, 3050 Lomita Boulevard, Torrance, California 90505.
34. P. G. Yoshida, U.S. Department of Energy, EE-2G/Forrestal Building, 1000 Independence Avenue, S.W., Washington, D.C. 20585.